The Role of Evolution and Its Impact on the Efficacy of Molecular Targeted Cancer Therapy

Inaugural-Dissertation
zur
Erlangung des Doktorgrades
der Mathematisch-Naturwissenschaftlichen Fakultät
der Universität zu Köln

vorgelegt von
Ulrich Peer Friese
aus Köln

Angenommen im Jahr 2025

Abstract

Targeted cancer therapy leverages our understanding of genetic driver mutations in tumors to select appropriate drugs that disrupt the specific molecular abnormalities driving tumor growth. While these therapies can initially induce significant tumor shrinkage, their effectiveness is often short-lived as resistance mechanisms frequently emerge, limiting their therapeutic long-term success.

From a population dynamics perspective, the failure of targeted monotherapy is anticipated: within the inherently heterogeneous population of tumor cells, some cells naturally harbor mutations that confer resistance, reflecting the tumor's genetic diversity. As treatment progresses, selective pressure favors these resistant cells, driving tumor evolution toward a population that is unaffected by the initial therapy. Additionally, an alternative, epigenetic-based mechanism—the drug-tolerant persister state—allows cancer cells to endure extended treatment periods. If therapy is halted early, these DTPs can reignite tumor evolution, leading to recurrence of the disease.

Effective targeted cancer therapies must address both: genetic resistance and persistence mechanisms. To demonstrate this principle, we analyzed the EGFR-driven non-small cell lung cancer cell line PC9, expanded our understanding of resistance mechanisms and strategies to treat them. We further studied the drug-tolerant persisters in this cell line and developed three strategies to eliminate them.

Successful targeting of both resistant cells and persisters requires either a polytherapy or an alternating therapy schedule using subsets of drugs sequentially. We introduce a population dynamic model to evaluate the costs associated with different therapy schedules, enabling optimization of treatment schedules for heterogeneous cell populations by balancing treatment durations. This general model allows to built upon knowledge of the evolution of heterogeneous cell population to minimize treatment duration as well as minimizing the risk of developing new resistance mechanisms.

Kurzzusammenfassung

Gezielte Krebstherapien nutzen unser Verständnis genetischer Treibermutationen in Tumoren, um spezifische Medikamente auszuwählen, welche die genetischen Mechanismen aushebeln, die das Tumorwachstum antreiben. Diese Therapien können anfänglich zu einem deutlichen Schrumpfen des Tumors führen, aber ihre Wirksamkeit ist oft nur von kurzer Dauer, da häufig Resistenzmechanismen auftreten, die den langfristigen Therapieerfolg einschränken.
Aus der Perspektive der Populationsdynamik ist das Scheitern einer gezielten Monotherapie absehbar: Innerhalb der von Natur aus heterogenen Tumorzellpopulation tragen einige Zellen von Beginn an Mutationen, die ihnen eine Resistenz gegen die Therapie verleihen. Mit fortschreitender Behandlung werden diese resistenten Zellen durch den Selektionsdruck bevorzugt, was die Tumorentwicklung in Richtung einer resistenten Population lenkt, die von der ursprünglichen Therapie nicht betroffen ist. Darüber hinaus ermöglicht ein alternativer, epigenetisch basierter Mechanismus – der Zustand der therapietoleranten Persistenzzellen – den Krebszellen, lange Behandlungszeiträume zu überdauern. Wird die Therapie vorzeitig beendet, können diese DTPs die Tumorevolution neu entfachen und so zu einem Rückfall führen.
Eine wirksame gezielte Krebstherapie muss daher sowohl genetische Resistenz- als auch Persistenzmechanismen adressieren. Um dieses Prinzip zu demonstrieren, analysierten wir die EGFR-getriebene nicht-kleinzellige Lungenkrebs-Zelllinie PC9 und erweitern unser Verständnis von Resistenzmechanismen sowie effektive Strategien zu deren Bekämpfung. Zusätzlich untersuchten wir die therapietoleranten Persistenzzellen in dieser Zelllinie und entwickelten drei Strategien, um sie zu eliminieren.
Um sowohl resistente Zellen als auch Persistenzzellen erfolgreich zu bekämpfen, ist entweder eine Polytherapie oder ein alternierender Therapieplan erforderlich, bei dem einzelne Medikamente sequentiell verabreicht werden. Wir stellen ein allgemeines Modell vor, das die Kosten verschiedener Therapiepläne bewertet und die Optimierung von Behandlungsplänen für heterogene Zellpopulationen ermöglicht, indem die Behandlungsdauern der einzelnen Shritte anpasst. Dieses Modell nutzt das Wissen über die Evolution heterogener Zellpopulationen, um sowohl die Gesamtbehandlungsdauer zu minimieren als auch das Risiko neuer Resistenzbildungen zu verringern.

Contents

Chapter 1

Biology of cancer

"*The Emperor of All Maladies*" is the title of a Pulitzer Prize-winning book by Siddhartha Mukherjee [1], which fittingly describes cancer as the most formidable of diseases. Cancer has been a pervasive presence throughout history, with its recognition spanning millennia. The term 'cancer' originally arose from the observation of malignant growths clinging to vital organs like the claws of a crab. Over time, our understanding of cancer has deepened, shifting from these early descriptive associations to a more nuanced genetic comprehension, as we continue to unravel its complex underlying causes.
Today, many diseases and causes of death that were once untreatable have become manageable or have been largely eradicated. This shift has placed cancer at the forefront of global health challenges, as it remains largely untreatable and is now the second leading cause of death worldwide, with 9.89 million deaths annually as of 2021 [2]. This increasing burden is mirrored by a growing trend in research and funding aimed at combating this relentless disease. This thesis aims to add some strings to the web of knowledge around cancer.

1.1 Cancer in the Human Body

The human body is an intricate and complex system composed of numerous components, each playing a vital role in maintaining overall health and ensuring survival [3]. At the highest level, it is organized into systems of organs, each with specific functions. These organs are composed of various types of tissue, such as muscle, connective, epithelial, and nervous tissues, which provide structure and support, facilitate movement, and regulate body processes.
At the most fundamental level, these tissues are made up of single cells, the basic units of life. Each cell contains the same heritable genetic information in the form of deoxyribonucleic acid *DNA*, housed within the nucleus. However, gene expression in these cells varies according to their specific roles, leading to their differentiation into distinct specialized types. This differentiation allows cells to adopt the specific shapes and structures necessary to perform their unique functions within the body, from muscle contraction to nerve signal transmission.
Evolutionarily, the human body has developed multiple mechanisms to maintain a functioning

and stable internal environment. However, cells can become damaged and cease to function properly. External factors can damage or alter the DNA, disrupting the gene regulatory networks essential for normal cell function. While the body has mechanisms to repair or remove these damaged cells, sometimes these processes fail. When such alterations lead to uncontrolled cell growth, the result is the formation of *neoplastic cells* or *tumors*. This condition, known as cancer, is characterized by the specific organ or cell type that has morphed into tumors, such as in brain, breast, colon, or lung cancer. The progression of cancer is categorized into stages, which indicate the extent of disease spread:

1. Stage I: Cancers are localized to one part of the body.

2. Stage II: Cancers are early locally advanced.

3. Stage III: Cancers are late locally advanced.

4. Stage IV: Cancers have spread to other organs and have metastasized.

This staging helps in determining the appropriate treatment approach and prognosis for the patient see also in [4, 5].

Cancer is a complex disease with a variety of underlying causes that can be broadly categorized into environmental, infectious, and genetic factors. Environmental factors include exposure to ionizing radiation, such as gamma rays and X-rays, as well as non-ionizing UV radiation from the sun. These forms of radiation can cause DNA damage, leading to mutations that may result in cancer. Infectious agents also play a significant role in cancer development. For example, Helicobacter pylori infection is a major risk factor for stomach cancer [6]. Similarly, infections with the human papillomavirus (HPV) are strongly linked to various cancers, particularly cervical cancer in women. HPV can integrate its DNA into the host cell's genome, disrupting normal cellular functions and promoting cancerous growth [7]. This is further enhanced by air pollution [8].
Genetic predisposition is another critical factor in cancer risk. It is estimated that 5-10% of all cancers are primarily due to inherited genetic mutations [9]. These genetic factors can significantly increase an individual's susceptibility to cancer, often involving specific gene mutations like those in the tumor suppressor genes BRCA1 and BRCA2, which are associated with a higher risk of breast and ovarian cancers [10, 11].
Moreover, lifestyle factors such as diet, smoking, alcohol consumption, and physical inactivity can also influence cancer risk. For instance, diets high in processed meats and low in fruits and vegetables are linked to an increased risk of colorectal cancer [12]. Furthermore, smoking is well-known to be the most frequent cause of lung cancer while also the easiest avoidable risk factor [13]. Thus, understanding these diverse risk factors is crucial for effective prevention and early detection strategies.

1.2 The Hallmarks of Cancer

The hallmarks of cancer, first outlined by Douglas Hanahan and Robert Weinberg in their high impact paper in 2000 [14] and later expanded in 2011 [15], describe the essential changes in cell physiology that collectively dictate malignant growth. These hallmarks are built upon decades of research and constitute an organizing principle for understanding the complexities of the neoplastic disease. They include:

Sustaining Proliferative Signaling

Cancer cells have the ability to continuously signal themselves to proliferate. Unlike normal cells, which stay in a state of homeostasis and require external growth signals to divide, cancer cells can produce their own growth factors or activate downstream components of growth signaling pathways autonomously. This unregulated signaling leads to relentless cell division and uncontrolled tumor growth.

Evading Growth Suppressors

Normal cells are controlled by growth suppressors, which prevent unchecked proliferation. Cancer cells, however, develop mechanisms to evade these suppressive signals. They achieve this by mutating tumor suppressor genes like p53 or Rb, disrupting the cellular pathways that would normally inhibit excessive cell growth, thus facilitating uncontrolled expansion.

Activating Invasion and Metastasis

In contrast to healthy cells, which remain at their assigned position, cancer has the ability to spread through the body's blood or lymph system. Tumor cells can invade surrounding tissues and migrate to distant sites. This process is called *metastasis* and involves alterations in cell adhesion, degradation of the extracellular matrix, and the ability to survive in foreign tissue environments. The metastatic spread is what often makes cancer deadly, as it enables the formation of secondary tumors in vital organs.

Enabling Replicative Immortality

Normal cells have a finite number of divisions before they enter senescence, partly due to the shortening of the protective layer at the end of chromosomes consisting of repetitive

nucleotide sequences called *telomeres*. Cancer cells, however, activate telomerase or alternative lengthening mechanisms to maintain their telomere length, allowing them to bypass senescence and achieve limitless replicative potential, which contributes to tumor growth.

Inducing Angiogenesis

Every living cell requires a blood supply to provide oxygen and nutrients for survival. And so do cancer cells for their growth. For this purpose, cancer cells can induce a process called *angiogenesis*, the formation of new blood vessels, by releasing pro-angiogenic factors like VEGF. This neovascularization supports the expanding tumor mass and also facilitates metastasis by providing a route for tumor cells to enter the bloodstream.

Resisting Cell Death

Apoptosis, or programmed cell death, is a cells natural answer to abnormalities detected in their intracellular processes. It acts as a natural barrier to cancer development. Cancer cells can resist apoptosis by altering the balance of pro- and anti-apoptotic proteins, mutating death receptors, and disrupting apoptotic signaling pathways. This resistance allows cancer cells to survive despite genomic instability and other stresses that would normally induce cell death.

Later, in 2011, the list of hallmarks was expanded by two further emerging hallmarks

Deregulated Metabolism

Cancer cells exhibit altered metabolism to support their rapid growth and proliferation. They preferentially use glycolysis over oxidative phosphorylation for energy production, even in the presence of oxygen, known as the Warburg effect. Even though already known as early as 1923 [16, 17], this effect gained a renewed research interest recently. This metabolic reprogramming was long thought to be a weakness of cancer but recent research indicates that this altered metabolism creates the necessary building blocks for cell division such as amino acids, nucleotides and lipids [18].

Evading the Immune System

The immune system is essential in maintaining overall health by providing a multi-layered defense against external substances and abnormal DNA fragments that do not originate from the body. It constantly monitors for these elements, identifying and classifying cells with

mutations or foreign components as non-self. This ability enables the immune system to recognize and eliminate most emerging cancer cells and nascent tumors, thereby preventing their progression [19].
However, cancer cells have evolved various strategies to evade immune detection and destruction. These include downregulating antigen presentation, secreting immunosuppressive molecules, and creating an immunosuppressive tumor microenvironment. These mechanisms allow cancer cells to bypass the body's natural defenses and proliferate unchecked [20]. An increased incidence of malignancies in individuals with immunodeficiencies further underscores the importance of the immune system in controlling cancer [21].

The updated hallmark paper also identified two characteristics which act as necessary conditions for the development of hallmarks that allow cancer cells to survive, proliferate, and disseminate. Hence they are named *enabling characteristics* and consist of

Tumor-Promoting-Inflammation

Chronic inflammation is associated with an increased risk of cancer. Inflammatory cells in the tumor microenvironment can produce growth factors, survival factors, and pro-angiogenic molecules that promote tumor development and progression. Moreover, the inflammatory response can lead to the release of chemicals that are actively mutagenic, thereby damaging DNA and promoting genetic instability in cancer cells [22].

Genomic Instability

Cancer cells exhibit high levels of genomic instability, leading to higher rates of mutations, chromosomal rearrangements, and aneuploidy as compared to normal cells. This instability results from defects in DNA repair mechanisms and cell cycle checkpoints [23]. It generates genetic diversity within the tumor, enabling cancer cells to adapt to changing environments and resist therapies. This is a crucial characteristics and the heterogeneity introduced by mutations plays an important role in all of the following chapters.

1.3 Treatment Perspective

It typically takes a long period of time between the initial formation of a single malignant cell and the final, macroscopic, clinically detectable tumor. During this latent period, the patient may not experience any noticeable symptoms. Once the tumor reaches a size that causes medical complaints, the patient is prompted to visit a doctor. Following a series of tests and evaluations, the patient is then referred to a specialized oncologist for further examination.

After additional diagnostic tests, the oncologist confirms the diagnosis of cancer, providing details about the type and stage of the disease. Along with the diagnosis, the oncologist will propose a comprehensive treatment plan that may include one or a combination of the following treatments [24]:

1.3.1 Classical Treatment Options

Surgery

For much of history, surgical removal was the only known treatment option for tumors. Performed even in ancient times, these surgeries often had high mortality rates. However, the success rate significantly improved with the advancements in modern medicine, anesthetics, and sterile operating environments. Today, surgery often remains the most promising treatment strategy, provided it is feasible and the tumor is located in an accessible organ. Usually surgeries are performed for cancers diagnosed in stages 1-3, whereas in stage 1 a single surgery can already be curative.
Despite its benefits, surgery presents major challenges. It is not always possible to perform a surgery in any location. Once the tumor has surpassed a certain size, cells have migrated to other sites and for metastasized tumors it is nearly impossible to eradicate all malignant cells solely through surgical means. In such cases, a combination of surgery and other treatments is essential, either with curative intent or to manage symptoms and extend the patient's life.

Radiotherapy

After the discovery of X-rays by Conrad Röntgen in 1895 and radium by Marie and Pierre Curie in 1898 [25], radiation was quickly proposed for cancer treatment [26], marking the beginning of modern cancer therapy. The key principle behind radiation therapy is the DNA-damaging property of ionizing radiation, which leads to the death of targeted cells. Early treatments faced significant challenges: X-rays of that time were of low energy and lacked the penetrative power to reach deeper cancer cells hidden behind other tissues, and radium's undirected radiation caused severe radiation sickness. These challenges were overcome with the invention of linear accelerators in the mid-20th century, which can produce well-focused, high-energy beams capable of precisely targeting cancer cells at various depths utilizing hadrons. They pose a great addition to surgical removal of tumors and in some instances an excellent alternative where surgical removal is no option due to the delicacy of the tumor type [27]. Figure 1.1 shows the shape of the Bragg curve for different ionizing radiations, which which describes the partial energy transfer $\frac{\partial E}{\partial r}$ from ionizing radiation while travelling through matter [28]. Heavy particles such as protons and carbon ions deposit the majority of their energy only after penetrating through several centimetres of tissue and are thereby

able to target tumors below surface. The sudden drop of energy transfer after its peak is particularly desirable to spare healthy tissue from an aggressive therapy.

Chemotherapy

The third and last classical treatment option, chemotherapy, emerged from observations during World War I, where soldiers exposed to mustard gas exhibited suppressed blood cell formation. This effect was later harnessed to treat lymphomas, which involve an overproduction of white blood cells, thereby temporarily alleviating symptoms and igniting extensive research into chemical treatments for cancer. Initially, chemotherapy referred to any cancer treatment using chemical agents. However, as various drug-related treatments for cancer emerged, the term chemotherapy was refined to describe therapies using drugs that non-specifically target all rapidly dividing cells. These drugs inhibit mitosis (cell division) or damage DNA, prompting DNA repair mechanisms to induce apoptosis to terminate the damaged cells life. Chemotherapy can be curative in some cases, but it is often administered as an adjunct therapy, known as adjuvant chemotherapy, following surgery or radiotherapy to target any remaining cancer cells or metastases. Stage IV cancers are almost always treated with chemotherapy to attack all metastasises simultaneously, including the ones that have not yet been detected. This enhances the overall treatment effect and manages the disease more effectively.

1.3.2 Targeted Therapy

Similar to chemotherapy, targeted therapy relies on pharmaceutical agents administered to the patient's body. However, the mechanism of action is quite different. Instead of broadly acting on all rapidly dividing cells, targeted therapy is specifically chosen for its ability to target certain molecules or pathways crucial to cancer cell growth and survival, hence the name *targeted therapy* or *molecularly targeted therapy* [29].
The key insight that led to the development of targeted therapy is the understanding that cancer cells are often driven by alterations of specific *driver genes* that cause uncontrolled proliferation. These driver genes, or the genes downstream in the signaling pathways they regulate, present special vulnerabilities in cancer cells [30]. They can be seen as the cancer's 'Achilles' heel. By inhibiting these driver genes or their downstream targets in the signaling pathways, targeted therapies can effectively disrupt the signaling required for cancer cells' survival and proliferation, thereby rendering the cancer cells non-malignant.
Oncogenic drivers can be understood as locks that require a specific key, the inhibitor, to be locked. The discovery of targeted therapy ignited a large-scale search for various inhibitors that could target all known oncogenic drivers. This quest has led to the development of increasingly specific molecules with each generation of inhibitors, aiming to reduce cross-reactivity and improve efficacy, often rendering previous generations of inhibitors obsolete.

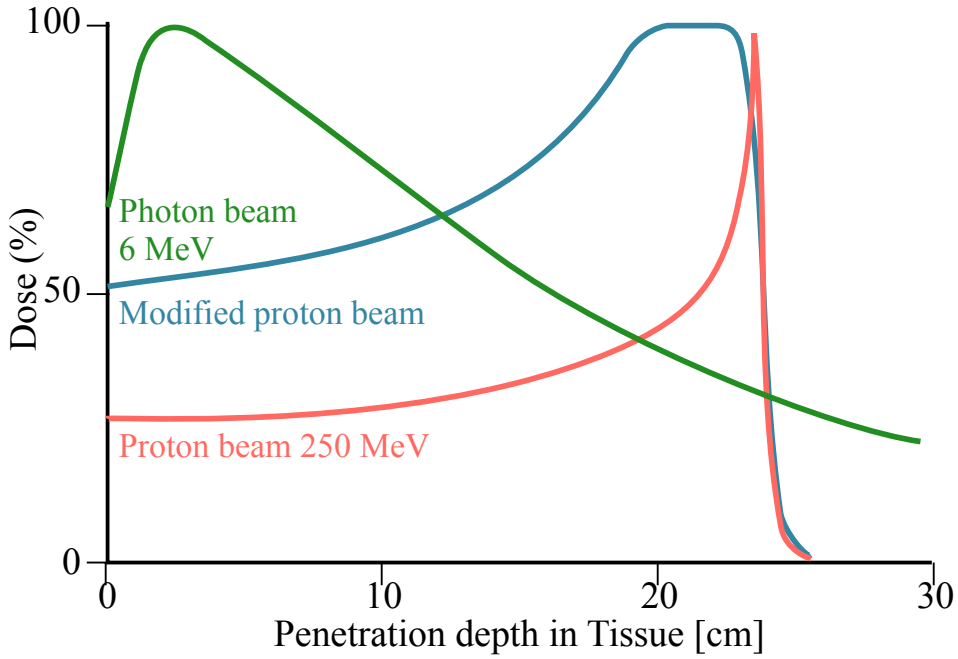

Figure 1.1: Representation of the Bragg curve for radiotherapeutically relevant beams

The curves display the characteristic Bragg peak, where energy delivery of heavy particles is maximized at a specific depth, allowing precise targeting of tumors while minimizing damage to surrounding healthy tissue. This property is essential for radiation therapy, as the rapid drop-off beyond the Bragg peak ensures that tissues beyond the tumor receive minimal radiation exposure. Furthermore the combination of protons or ions of different energies can influence the position and intensity of the Bragg peak, enabling tailored treatments for varying tumor depths.

Adapted from an image by Д.Ильин. This image is licensed under the Creative Commons CC0 1.0 Universal Public Domain Dedication, available on Wikimedia Commons. Accessed on October 24, 2024.

This approach allows for more precise treatment, potentially reducing the side effects associated with traditional chemotherapy by sparing normal, healthy cells. After an initial diagnosis, further tests are necessary to identify the specific oncogenic drivers. However, beyond this and follow-up checks, no additional hospital visits are usually required. This is a significant advantage over classical treatment options, which involve several hours of intravenous injections with severe side effects, costly time in an operating room, or access to very expensive synchrotrons that are not widely available in every hospital. Targeted therapy is solely administered through orally ingestible pills, making it a more convenient and more accessible option for patients.
On the other hand, targeted therapy presents several challenges. Targeted therapy alone is rarely curative; after an initial treatment success, cancer often goes into remission and subsequently reappears (*relapses*) [31]. The underlying reason for this is the large number of cells in a tumor at the time of detection, typically around $N \approx 10^9$ cells. Due to this vast number of cells, there is a high probability that every single point mutation in the DNA will appear by chance within the tumor. Consequently, some cells will have accumulated mutations in their genome, that confer resistance against the initial treatment before it has even started [32]. Once the susceptible cells are eradicated, these pre-existent resistant cells can divide and form secondary tumors at the former sites. The relapsed tumor is then resistant to the initial treatment and requires an alternative therapeutic strategy.

chronic myeloid leukemia

The first and most prominent success story of targeted therapy is the treatment of *chronic myeloid leukemia* (CML), a specific type of blood cancer [33]. CML originates in the bone marrow and is characterized by the uncontrolled production of myeloid cells, a type of white blood cell. The hallmark of CML is the presence of the Philadelphia chromosome, a genetic abnormality resulting from a translocation between chromosomes 9 and 22 [34]. This translocation leads to the formation of the BCR-ABL fusion gene [35, 36], which encodes an abnormal tyrosine kinase protein that is constitutively active. This constant activity drives the overproduction of abnormal white blood cells, disrupting normal blood cell production and leading to the clinical manifestations of CML.
If untreated, CML will quickly advance to acute leukemia and result in the patient's death. However, its nature makes it particularly amenable to targeted therapy. The disease is driven entirely by a single protein, BCR-ABL, which is absent in healthy human cells. Therefore, inhibiting BCR-ABL targets the disease specifically and has no effect on healthy cells in the body, resulting in minimal or manageable side effects. Furthermore, the symptoms of CML are caused by the overproduction of myeloid cells, not the cancerous stem cells. Consequently, even a small number of abnormal cells (approximately $N \approx 10^4$) can produce dramatic symptoms and can be detected early, before the cancer cells develop significant heterogeneity and resistance mechanisms against the treatment.

These insights led to the development of inhibitors targeting this specific protein, culminating in the successful creation of *Imatinib* which is sold under its brand name *Gleevec* [37–39], a drug that not only has revolutionized the treatment of CML [40] from a fatal disease to a manageable condition under continued treatment but also significantly raised the profile of targeted therapy as a whole. This breakthrough demonstrated the potential of targeted therapies to provide highly effective and specific treatment options with fewer side effects, leading to their adoption as a prominent addition to the arsenal of clinical cancer treatments [41]. Today CML acts as a textbook example and is no longer associated with the once negative prognosis. Patients diagnosed with CML have a no longer a negative prognosis but have a CML specific survival rate of $> 90\%$[42].

1.3.3 Novel Treatment Approaches

In recent years multiple different treatment options have entered an oncologists arsenal and are under research. Two of the most promising, *immune checkpoint blockade* and *personalized anti-cancer vaccine* belong under the category of immunotherapy and as such utilize the patient's own immune system to target the cancer. The immune system is usually excellent in distinguishing cells that belong into the human body, and foreign objects, such as bacteria, virus infected cells and also malicious cancer cells. However, as one of the hallmarks of cancer describes, tumors are able to develop mechanisms to evade the immune system. The following treatment options are two strategies to overcome that evasion and revert the immune systems efficiency to its intended state.

Immune checkpoint blockade

The immune system consist of different cells, among them t-cells, that detect foreign cells, which are then later neutralized by killer t-cells. They have regulatory pathways named immune checkpoints that aims to stop T cells from attacking cells from the own body from overreacting by deactivating them when triggered. This process is exploited by cancer cells by expressing the respective immune checkpoint ligands, that bind to the T cells receptors and deactivate them

· Interfering this exploitation is the key idea behind an immune checkpoint blockade therapy [43]. This is done by inhibiting for example PD-1 (Programmed Death-1) or its ligand PD-L1 (Programmed Death-1), thus reactivating the T cells recognition of cancer cells. Another possible target is TLA-4 (Cytotoxic T-Lymphocyte-Associated Protein 4) which is another checkpoint receptor that dampens T cell activity and thus often expressed by cancer cells to evade the immune system.

As the immune systems regulation is inhibited, an immune checkpoint blockade therapy typically goes along with side effects associated with an overreacting immune system such as skin rashes, fever, inflammation and other autoimmune reactions.

Personalized Anti-Cancer Vaccine

Unlike preventive vaccines, which are designed to protect against viruses that can potentially cause cancer by integrating their DNA into human cells such as those for HPV, personalized anti-cancer vaccines focus on treating cancer after it has already developed [44]. These vaccines are tailored to each individual patient's tumor, aiming to stimulate the immune system to specifically target cancer cells.
Once cancer is diagnosed, the tumor undergoes genomic profiling to identify unique mutations that give rise to neoantigens — abnormal proteins that appear on the surface of cancer cells but are absent from normal, healthy cells. These neoantigens serve as precise markers for the immune system to attack. Based on this analysis, an mRNA vaccine is created, designed to train the immune system to recognize and destroy any cells that express these neoantigens [45].
This approach is highly personalized, as each vaccine is custom-made for the patient's specific tumor profile. While this personalized strategy shows great promise and has yielded encouraging results in clinical trials, it comes with significant logistical and financial challenges. Each vaccine must be developed individually, which increases both production complexity and cost.
However, the potential benefits are substantial. Personalized vaccines can offer high specificity, reducing damage to healthy tissues and potentially providing a more effective and durable immune response than traditional treatments [46].

1.4 Cell Culture

1.4.1 Foundations and Applications in Cancer Research

Cell culture is a vital technique in biological and medical research, offering a controlled environment to study the behavior of cells isolated from tissues. This process begins with the extraction of cells from a tissue sample, typically from a biopsy or surgical removal of tumor tissue. The tissue is then enzymatically digested to separate individual cells, which are transferred to a sterile culture flask containing a growth medium designed to meet the metabolic and environmental needs of the specific cell type. The growth medium includes essential nutrients such as amino acids, glucose, vitamins, and minerals, along with growth factors that mimic in vivo conditions. Usually antibiotics and fungicides are added to the growth medium to protect the cell culture flask against contaminations. If successful, the cells adapt to their new environment, establish a population, and begin to grow.
Cancer cells are particularly advantageous for cell culture research due to their ability to divide indefinitely, a characteristic they acquire through mutations that activate the enzyme telomerase. This enzyme prevents the shortening of telomeres—repetitive nucleotide sequences at the ends of chromosomes—which in normal cells limit the number of times a cell

can divide. Healthy, non-cancerous cells usually reach a natural division limit, known as the Hayflick limit, where telomere shortening triggers programmed cell death after 50-70 divisions [47]. Cancer cells, however, bypass this limitation, rendering them "immortal" in a culture setting. This ability to proliferate without restriction makes cancer cell lines essential for studying tumor biology and therapeutic responses under laboratory conditions.
One of the earliest and most famous immortal cell lines is HeLa, derived from cervical cancer cells taken from Henrietta Lacks in 1951 [48]. While the HeLa cell line has contributed to countless scientific breakthroughs, it also raises ethical concerns as it was created without the consent of Lacks or her family. Despite this, HeLa cells have become a cornerstone of modern biological research, particularly in the development of vaccines and cancer treatments.

1.4.2 Handling and Maintenance of Cancer Cell Lines

The cultivation of cancer cell lines involves careful management to ensure their viability and consistency over extended periods [49]. Cells in culture are either grown in suspension, where they float in the growth medium, or adherently, where they attach to the surface of the culture vessel. Whether a cell line grows in suspension or adheres to a substrate depends on the specific characteristics of the cells. For example, HeLa cells can grow in suspension, while other cancer cell lines, like PC9 and HCC827, grow adherently. In adherent cultures, cells must first be detached from the surface using enzymes such as trypsin before they can be passaged or split into new flasks.
Maintaining cell cultures requires routine splitting, known as passaging, where the cell population is divided and given fresh growth medium to prevent overcrowding and depletion of nutrients. Passaging typically occurs once or twice a week, depending on the growth rate of the cells. It is crucial to keep growth conditions, such as temperature, CO_2 levels, and nutrient availability, as constant as possible to ensure reliable and reproducible experimental outcomes across different time points. Maintaining a population in exponential growth phase, where cells have abundant space and resources, minimizes stress-induced selection pressures that could skew experimental results.
As cell lines are passaged over long periods, genetic mutations can accumulate due to random errors in DNA replication. While some mutations may slow down cell growth and be naturally selected against, others might confer an advantage, such as resistance to specific drugs. This process of evolution in vitro is an important consideration for researchers, as it can influence the outcome of drug testing and the reproducibility of experiments. Monitoring for such mutations is crucial, especially in drug sensitivity studies, where even minor genetic changes can lead to resistance. This is usually overcome, by discarding the batch of cells after it reaches a certain number of passages and restarting with a new batch.

1.4.3 Applications of Cancer Cell Lines in Research

Despite certain limitations, cancer cell lines are invaluable tools for exploring the genetic and molecular underpinnings of cancer. In real tumors, cells exist within a complex microenvironment, interacting with surrounding tissues, the immune system, and the vascular system, which supplies oxygen and nutrients to the tumor. In contrast, cancer cell lines in vitro are isolated from this microenvironment, and while this simplification is advantageous for controlled experimentation, it also means that certain aspects of tumor behavior, such as immune evasion and angiogenesis, are not fully recapitulated. Furthermore, grown tumors have evolved spatially heterogeneous, meaning different parts of a tumor can behave differently depending on their genetic makeup and local environment. Cell lines, derived from a small tissue sample, might not capture this full heterogeneity.
Nonetheless, cancer cell lines serve as powerful molecular models for tumors. Since the 1990s, advances in high-throughput sequencing technologies have allowed researchers to map the genetic alterations in various cancer cell lines, identifying key driver mutations that contribute to cancer progression. These genetic insights have led to the classification of tumors not only by their tissue of origin but also by their genotype, enabling more personalized approaches to cancer therapy [50, 51].
Cancer cell lines are also instrumental in drug discovery and testing. The ease and affordability of growing these cells make it possible to screen large libraries of compounds to assess their efficacy and toxicity. By comparing the genetic profiles of cancer cell lines with their responses to different drugs, researchers can link specific genetic alterations to drug sensitivity or resistance. This systematic approach has been crucial in identifying potential targeted therapies, which aim to exploit the vulnerabilities introduced by cancer-specific mutations.

Chapter 2

Spectrum of Resistance Mechanisms in EGFR Driven Non Small Cell Lung Cancer Cell Line PC9

Our research work is on optimal, curative treatment strategies of targeted cancer therapy. In particular, the strategies are aimed at targeting the resistance mechanisms that typically undermine the efficacy of drugs. We conduct our experiments using cell culture models, utilizing the advantages of reproducibility and comparability. Our primary test model is the PC9 adenocarcinoma cell line, known for its activating EGFR mutation. In this chapter, we will explore our model organism in greater detail, examining its characteristics, potential treatment options, and determine all resistance mechanisms that are likely to develop. The results presented here have been obtained in collaboration with the Brägelmann lab and the student Nina Müller.

2.1 Cell Signaling via Tyrosine Kinase Receptors

Various cellular functions are governed by complex chemical signaling processes, which trigger consecutive reactions leading to either a desired outcome or, in the case of malignant cells, an undesired one. The signaling process is structured into layers, starting with the input layer, consisting of the receptor tyrosine kinases (RTKs) [52]. These receptors are transmembrane proteins, meaning they consist of a ligand-binding domain outside the cell and enzymatic regions inside. This allows them to detect and react to external signals. Each receptor is specifically activated by a corresponding ligand, similar to a key fitting into a lock. Ligand binding induces two receptors to bind together into a pair, or dimer, which subsequently leads to the phosphorylation of tyrosine residues on the intracellular portion of the receptors through each receptor's partner. This *autophosphorylation* creates docking sites for signaling complexes composed of cytoplasmic enzymes and adapter proteins, forming the *processing layer* of the signal transduction pathway.
Once assembled, these signaling complexes dissociate, releasing activated effector and adapter

proteins into the cytoplasm. These proteins then stimulate various signal transduction cascades, including the mitogen-activated protein kinase (MAPK) pathway, phosphoinositide 3-kinase (PI3K), the protein kinase B (AKT), and several transcriptional regulators. These pathways collectively trigger the cell's response such as adhesion, migration, growth, apoptosis or differentiation in the *output layer*.
Finally, the ligand-receptor complex undergoes endocytosis, where it is internalized by the cell and either degraded or recycled back to the cell membrane, effectively terminating the signal. This finely tuned process of signal initiation, propagation, and termination is crucial for maintaining cellular homeostasis. When this process malfunctions, it can lead to aberrant cell growth. However, these same dysfunctions present a significant vulnerability that can in principle be exploited by targeted therapies, such as tyrosine kinase inhibitors.

2.2 The Epidermal Growth Factor Receptor

Our receptor of interest is the *epidermal growth factor receptor* (EGFR), also known as ErbB1. It is part of the ErbB family of receptor tyrosine kinases (RTKs), which includes EGFR/ErbB1, HER2/ErbB2, HER3/ErbB3, and HER4/ErbB4 [53, 54]. Each of these receptors is activated by specific ligands; for EGFR, the ligand is *epidermal growth factor* (EGF). Upon ligand binding, two receptors dimerize, undergo autophosphorylation, and activate intracellular signaling cascades, see also **??**.
EGFR plays a critical role in regulating various cellular processes, including cell proliferation, differentiation, migration, and survival. It is an essential component of the cell's ability to respond to external growth signals. The receptor's activation involves dimerization, which can occur either as a *homodimer* (EGFR/EGFR) or *heterodimer* (EGFR paired with other ErbB family members such as HER2). This interaction triggers the autophosphorylation of specific tyrosine residues in the receptor's cytoplasmic domain, creating docking sites for intracellular signaling proteins. These proteins mediate downstream signaling events that regulate vital cellular functions.
Among the key signaling pathways activated by EGFR are the mitogen-activated protein kinase (MAPK) pathway [55], which includes proteins such as RAS, RAF, MEK, and ERK. This cascade is crucial for cell division and differentiation, influencing how cells grow and replicate. Disruptions in this pathway, particularly through mutations in components like RAS or RAF, can lead to uncontrolled cell proliferation, which is a hallmark of cancer development. Another significant pathway activated by EGFR is the PI3K/AKT/mTOR pathway [56], which promotes cell growth, survival, and metabolic regulation. This pathway is frequently upregulated in various cancers, enhancing cellular resistance to apoptosis, which enables cancer cells to thrive and evade normal growth controls.

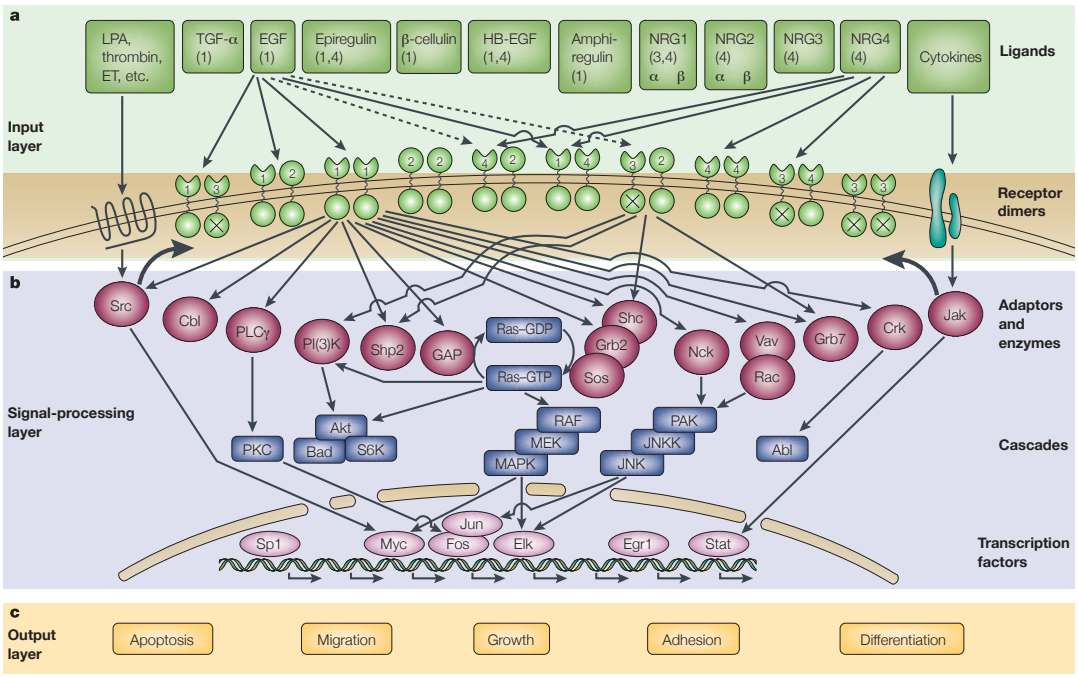

Figure 2.1: ErbB signaling network

Illustration of the ErbB signaling network structured into three primary layers: the input layer, signal processing layer, and output layer. The input layer consists of ErbB receptors that bind extracellular ligands, initiating the signaling cascade. The signal processing layer encompasses the intracellular pathways and molecular interactions that transduce and modulate the signals received, including key proteins and secondary messengers. The output layer represents the cellular responses elicited by the network, such as gene expression, proliferation, differentiation, or apoptosis.

Reproduced with Permission from Springer Nature [54]

2.3 The Cell-Line PC9

The PC-9 cell line is a well-established human lung adenocarcinoma model extensively used in cancer research, specifically in studies focusing on non-small cell lung cancer (NSCLC). Unlike small cell lung cancer (SCLC), which is its smaller counterpart, NSCLC accounts for approximately 85% of all lung cancer cases [57]. The PC-9 cell line is characterized by a deletion mutation in exon 19 of the EGFR gene [58]. This mutation disrupts the normal regulation of EGFR expression, leading to its overexpression. Hence an abundance of receptors populate the cell surface. This increases the probability of ligand binding and dimerization dramatically. As a result, the ErbB-1 signaling pathway remains constantly active, driving uncontrolled cell division and contributing to the malignant nature of these cells. Due to its driver mutation in EGFR, it is logical to treat this cell line with an EGFR tyrosine kinase inhibitor. This goes with great success initially, resulting in the death of the majority of cells. Effective EGFR inhibitors have been around for more than two decades such as gefitinib, sold under brand name Iressa, or erlotinib, sold under its brand name Tarceva [59, 60]. After these drugs oral administration, the inhibitors dissolve and are absorbed into the bloodstream, eventually reaching the tumors. Due to their small molecular size (hence the term "small molecule targeted therapy"), they can diffuse through cell membranes. Once inside the cells, the drug competes with ATP for binding to the kinase domain of the EGF receptor, effectively blocking its phosphorylation. This inhibition disrupts the signaling cascade. Thus, halts cell proliferation and reduces the number of living cancer cells.
The in-vitro treatment of a large population of PC-9 cells closely mirrors the challenges frequently encountered in cancer treatments in vivo: Initially, the treatment may seem successful, with no visible cells remaining. However, upon closer examination under a microscope, a small number of residual cells can still be detected. Over time, these cells proliferate, forming colonies that become visible to the naked eye. These regrown colonies have developed resistance to the initial treatment, rendering them no longer sensitive and necessitating the use of a different drug to effectively continue the therapeutic strategy. An alternative way to survive the treatment is the drug-tolerant persister state, which is further discussed in chapter 3.
PC-9 cells serve as our model organisms throughout this thesis, providing a proof-of-principle for results that could potentially be translated from in-vitro to in-vivo settings. Similar to patients with diagnosed NSCLC, PC-9 cells possess activating mutations that drive their indefinite division. As these cells continue to divide, additional errors or mutations can accumulate in their DNA, leading to the emergence of new genotypes. In rare cases, such alterations may confer resistance to ongoing treatments. The rate of point mutations is estimated to be on the order of magnitude $\mu \approx 10^{-8} - 10^{-9}$ per nucleotide per cell division [61]. While this may seem like an insignificant number, it becomes highly relevant given the large number of malignant cells in a patient's tumor, which typically contains $N \approx 10^8$ cells per cubic centimetre or gram. Tumors often go undetected until they grow large enough to cause symptoms, usually well beyond one cubic centimetre in size. Consequently, the expected

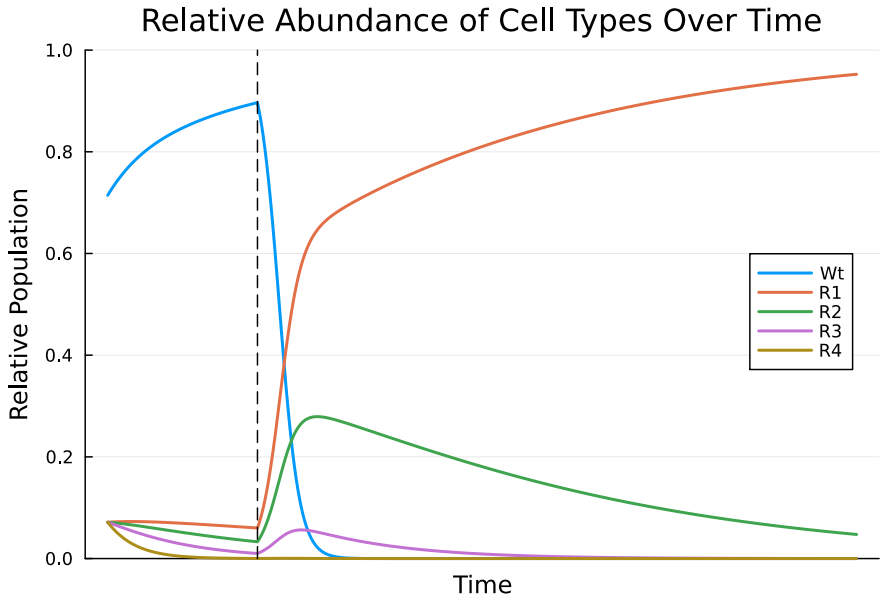

Figure 2.2: Population dynamics of a heterogeneous population under treatment
Shown are the relative cell numbers of 5 cell types with the growth rates specified in table 2.2. The vertical dashed line marks the treatment start against the parental cell type. After the treatment eradicates the parental type, all resistant cell types rapidly proliferate and compete with each other. The fittest resistant type, R1, dominates population.

number of any point mutation per generation in a tumor of this size is $\langle m \rangle = \mu N \approx 1$. In other words, within a tumor of one cubic centimetre, it is likely that every possible point mutation is already present, including those that may confer resistance to therapy. This underscores the challenge of treating tumors once they are detected, as their genetic heterogeneity is already advanced, increasing the likelihood of resistance to treatments. After the initiation of treatment targeting the bulk of the tumor, driven by EGFR activation in the so-called parental cells, all sensitive cells are quickly eradicated. This leaves space for the pre-existent resistant offsprings to proliferate and regrow a tumor in the same place the primary tumor has been eradicated. During this period different genotypes compete with each other and the fastest dividing one will take over the population, see also **??**.
In order to create a framework to model and analyse the cancer evolution, the entire spectrum of resistance mechanisms must be known.

2.4 Iterative Exhaustion of Resistance Mechanisms

2.4.1 Experimental Design

The experimental procedure to identify and isolate possible resistance mechanisms in PC9 cells is based on the following concept. A large number of parental PC9 cells are grown in a HYPERflask, a specialized cell culture flask with ten intermediate layers that provide ample surface area for cell adherence and growth. Once the flask reaches confluence, with approximately 5×10^8 cells, the culture is treated with the EGFR inhibitor erlotinib at a concentration of 500 nM, a known effective treatment for EGFR-driven NSCLC. This treatment immediately exerts its effect, eradicating the majority of the cells. However, after continuous treatment, resistant cells begin to repopulate the flask. These resistant cells are then transferred to a separate container and multiplied, split and maintained under continuous treatment to prevent reversion to the parental genotype. Potentially multiple resistance mechanisms compete for dominance in these cells, but keeping them in a continuously proliferative state of exponential growth ensures that the fastest growing resistant variant will dominate the population. These cells are designated as R1, representing the first resistance mechanism that emerges from the parental cell line. The R1 cells are subsequently multiplied, analyzed, and stored for future experiments.
This initial step is then iteratively repeated to isolate a series of resistance mechanisms. The i-th resistant variant, Ri, is exposed to a panel of drugs known to be effective against various resistance mechanisms or cancer driver mutations. If a drug is found to be effective against the Ri cell line, a new HYPERflask filled with parental PC9 cells is continuously treated with this drug in combination with all previously used drugs. By design, this treatment will eradicate all parental cells as well as all resistant cells R1,...,Ri. The treatment is continued until resistant cells again repopulate the flask. These newly created resistant cells are then again harvested, multiplied and designated as R(i+1).
The decision to always start with the parental cells ensures that each resistant cell line is created with its unique resistance mechanism, rather than progressively adding resistance mechanisms to an already resistant cell line. This approach allows for the study of each resistance mechanism in isolation. The rationale behind starting with parental cells rather than the most recent resistant variant is based on probability: the likelihood of a single resistance mechanism occurring is already low, estimated to be on the order of point mutation probabilities, $P_1 \approx 10^{-8}$. The probability of two resistance mechanisms arising simultaneously in the same cell is significantly lower, around $P_2 \approx P_1^2 \approx 10^{-16}$, which is much smaller than the inverse of the number of cells within a human body, let alone within a tumor. Hence it is unlikely to be pre-existent in an initial tumor within a patient's body.
For a more detailed analysis, these probabilities can be adjusted to account for factors such as the mutational window, gene copy number, and the total number of potential resistance mechanisms. For example, if there are n resistance mechanisms, the joint probability of two equal likely mechanisms arising together must be adjusted by a factor reflecting the number of

ways to choose 2 mechanisms from n, given by $\binom{n}{2} = \frac{n(n-1)}{2}$. However, the general argument and orders of magnitude remain valid.
This experiment has been performed by Nina Müller, who isolated all of the resistant cell types described in the following sections and characterized the mechanisms for resistance for R1-R3 before I joined the research project and participated in the experiments.

2.4.2 R1

The first observed resistant variant is sensitive to the third-line EGFR inhibitor, osimertinib. Subjecting these cells to Sanger sequencing reveals that the resistance arises from the well-known *gatekeeper* mutation T790M. This mutation involves a point mutation in exon 20 of the EGFR gene, where the 790th amino acid, threonine, is replaced by methionine [62, 63]. The amino acid substitution alters the shape of the EGFR protein, specifically in the ATP binding pocket, which has two significant consequences. First, it introduces a slight fitness disadvantage, meaning the cells have a slightly lower growth rate of $\lambda_{R_1} = 0.76 \pm 0.05 \text{day}^{-1}$ in drug free medium. Second, and more critically, it reduces the binding affinity for erlotinib, thereby negating its effect and rendering the cells resistant to the initial treatment, hence the term *gatekeeper*. Osimertinib, can covalently bind to the ATP binding pocket and effectively inhibit EGFR [64]. We estimate that the mutation rate is approximately eight times the native point mutation rate due to the elevated copy number of the EGFR gene in PC9 cells. This suggests that around 15 resistant cells carrying the T790M mutation are present in a HYPERflask (see figure 2.3). R1 cells are then selected and cultured in RPMI 1640 medium with a concentration of 500 nM erlotinib.

2.4.3 R2

Treating a large population of parental cells with erlotinib and Osimertinib eradicates parental and R1 cells and allows a resistant variant carrying a known point mutation in the NRAS gene, Q61R in exon 3, to emerge as dominant [65]. This has been confirmed via Sanger sequencing. NRAS is part of the RAS/MAPK signaling pathway, which functions downstream of several growth factor receptors, including EGFR. When NRAS is mutated at Q61R, the RAS protein becomes constitutively active, continuously signaling for cell growth and proliferation even in the absence of external growth signals. As a result, inhibition of EGFR by erlotinib or osimertinib fails to affect these cells, allowing them to proliferate uncontrollably [66]. Cells with the NRAS mutation often respond to MEK inhibition [67] and so do R2, who can be effectively treatet with trametinib. R2 cells are selected and grown in RPMI 1640 medium with a concentration of 500 nM erlotinib and 100 nM osimertinib. We determined a growth rate of $\lambda_{R_2} = 0.3 \pm 0.07 \text{ day}^{-1}$ in drug free medium and estimated the mutation rate to be 5 fold increased to the natural point mutation rate due to copy number variations, hence resulting in an expected number of 7 resistant cells in a filled HYPERflask (see figure 2.3).

2.4.4 R3

Treating a large population of parental PC9 cells with erlotinib, osimertinib and trametinib yields the third variant that emerges after the third iteration of the experiment. It exhibits heightened sensitivity to the MET inhibitor tepotinib. Whole exome sequencing revealed a focal amplification of the hepatocyte growth factor (HGF) gene, along with an overexpression of both HGF and its receptor MET which was determined with RNA-seq. It is well-established that exposure to HGF can reduce the sensitivity of EGFR-mutant cell lines to EGFR inhibitors [68]. As the ligand for MET, HGF plays a crucial role in activating this receptor, and MET amplification is a recognized mechanism of acquired resistance to EGFR inhibition. The R3 cell line demonstrates significant sensitivity to MET inhibition, especially when combined with inhibitors targeting EGFR and MEK. Additionally, this variant can be targeted by the multikinase inhibitor dasatinib.
dasatinib inhibits several kinases such as BCR-ABL, see [69] and the SRC family kinases. As it is inhibiting multiple kinases it is interfering with multiple pathways and is involved in numerous physiological processes [70], which is why dasatinib is often referred to as a "dirty" inhibitor due to its non specificity. While its use may be associated with various side effects, dasatinib presents a valuable opportunity to develop a proof-of-concept treatment panel, offering a multifaceted approach to overcoming drug resistance in this context. The R3 cells are grown in RPMI 1640 medium with 100 nM erlotinib,20 nM osimertinib and 10 nM trametinib. Their growth rate in a drug free medium is $\lambda_{R_3} = 0.67 \pm 0.07$ day^{-1}.

2.4.5 R4

Treating a large parental population pof PC9 cells with erlotinib, osimertinib, trametinib yields the fourth resistant variant. It is sensitive to the PI3K/mTOR inhibitor dactolisib but also responsive to dasatinib, which was already effective in the previous resistance case. This finding presents an intriguing treatment strategy, as a single drug proves effective against two genetically distinct resistance mechanisms. Further analysis revealed that this resistance is driven by an overexpression of the WWTR1 gene and its protein product, TAZ [71]. Overexpression of WWTR1 alone is sufficient to confer resistance to EGFR inhibition [72, 73]. Additionally, after a drug holiday, we did not observe any reversion to the previous drug-sensitive state, suggesting that the resistance is likely due to a genetic alteration rather than reversible epigenetic changes, which are often responsible for the formation of so-called drug-tolerant persisters. Given that SRC inhibition is known to suppress YAP/TAZ activity [74], dasatinib emerges as a logical choice for treating R4 cells. R4 are grown in RPMI 1640 medium with 100 nM erlotinib,20 nM osimertinib, 10 nM trametinib and 100 nM tepotinib. Their growth rate measured in a drug free medium is $\lambda_{R_4} = 0.48 \pm 0.04$ day^{-1}.

concentrations [nM]	**erlotinib**	**osimertinib**	**trametinib**	**tepotinib**
R1	500	0	0	0
R2	500	100	0	0
R3	100	20	10	0
R4	100	20	10	100

Table 2.1: Concentrations of inhibitors required for the growth of resistant PC9 cell lines

The PC9 resistant cell lines (R1-R4) are grown in RPMI 1640 medium supplemented with 10% FBS and 1% penicillin-streptomycin and the above listed concentrations of drugs. These concentrations are carefully selected to prevent reversion to previous resistance mechanisms, ensuring that only the fastest-growing variants capable of sustaining growth in the presence of these drugs will survive and dominate the cell population.

2.4.6 Drug Tolerant Persisters

After four iterations of the experiment, no further resistance mechanisms regrew from a full HYPERflask under treatment. This result has very promising consequences. It means that any potential 5th or higher resistance mechanisms appear with such a low frequency, that they are not likely to be observed in a population of $\approx 5 \times 10^8$, which is already at the limit of radiological detectability for lung adenocarcinomas. Or even more promising: any potential resistance mechanims against a combined treatment of erlotinib, osimertinib, trametinib and dasatinib (EOTD) is so unlikely to develop, that it does not occur in vivo tumors of patients. However, after a drug withdrawal, fast proliferating colonies emerge from isolated cells that persisted the combination treatment. so called drug tolerant persisters (DTP), which will be discussed in greater depth in chapter 3.

2.5 Expected Number of Mutants

We estimate the expected number of mutated cells, C, in a population of size N with a mutation rate from wild-type cells to a specific mutant variant μ based on an evolutionary model derived in [75] as

$$C = -\frac{\mu}{1-\mu}\frac{N}{\beta}\log\left(1-\frac{\beta}{\delta}\right). \tag{2.1}$$

The model incorporates the stochastic emergence of mutations that can grow exponentially after their birth until the population reaches a finite carrying capacity. Here, δ represents the relative death rate of resistant cells compared to wild-type cells. Since we do not have precise estimates for the death rates of the resistant variants, we assume them to be equal to

the wild-type death rate, $d_{\mathrm{wt}} = 0.06$, hence $\delta = 1$ On the other hand, β denotes the relative birth rate of the resistant variant, b_{R_x}, to the growth rate of wild-type cells, b_{wt}. We do observe significant deviations in these rates. The relative birth rates can be extracted as $\beta = \frac{b_{\mathrm{R}_x}}{b_{\mathrm{wt}}} = \frac{\lambda_{\mathrm{R}_x}+d_{\mathrm{R}_x}}{\lambda_{\mathrm{wt}}+d_{\mathrm{wt}}}$ where the respective growth rates $\lambda = b - d$ are easily observable in an exponential growth experiment. A population of known size, well below its capacity limit, is maintained in a cell culture flask under standard growth medium and conditions. This setup is crucial because many drugs can impose stress on the cells, reducing their division rate—a factor we aim to avoid at this stage. In newly diagnosed tumors or freshly initiated cell culture experiments (as described in Section 2.4.1), cells can grow without stress. Therefore, it is essential to determine each cell variant's stress-free growth rate to accurately estimate the number of pre-existing mutant cells.
However, this requirement poses a challenge when incubating resistant cells, as they must be maintained under the same panel of drugs that were used to select them from wild-type cells, as summarized in Table 2.1. To address this, we implemented a compromise by giving the resistant cells a drug holiday of at least 2 weeks before beginning the determination of growth rates. The drug holiday is kept under 2 weeks to prevent any significant reversion of the cells to the wild-type.
To avoid overcrowding effects, such as cell-cell contact inhibition, nutrient depletion, or the accumulation of waste products, the cell number is counted and diluted bi-weekly [76, 77]. The resulting cell numbers are then fitted to an exponential growth curve:

$$N(t) = N_0 \mathrm{e}^{-\lambda t} \tag{2.2}$$

and the resulting rates are averaged over each measurement. The resulting growth rates and estimates are summarized in table 2.2. The large deviations in the expected number of resistant cells can be attributed to a well-known phenomenon observed already by Luria and Delbrück in their famous hallmark experiment regarding the number of pre-existing resistant mutants in bacterial populations. Their finding of resistance against antibacterial drugs can be translated to pre-existent cells that are resistant against targeted cancer therapies. The timing of the initial resistance mutation significantly impacts the final number of resistant cells at the end of the growth period. If the mutation occurs early, the resistant progeny have more time to divide and to exponentially increase their population.

2.6 Toxicity of the EOTD Combination Treatment

The combination of four drugs, erlotinib, osimertinib, trametinib, and dasatinib, can inhibit a sufficient number of proteins across multiple signaling pathways, leading to the effective shutdown of survival mechanisms in PC9 cells. While each drug is approved individually for treatment, their combined use has not been tested yet. The danger of such broad inhibition lies in the potential for cross-reactivity, where healthy human cells are also unable to tolerate the treatment, leading to severe side effects. This phenomenon is seen with drugs like

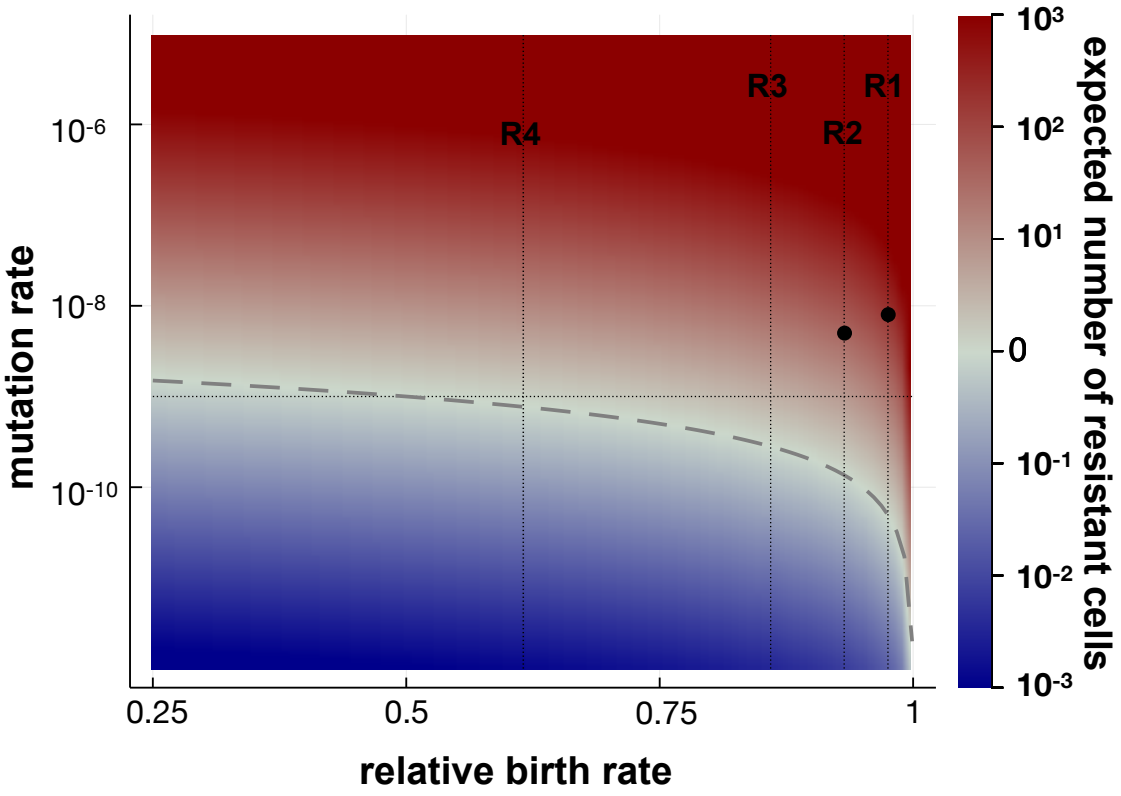

Figure 2.3: Expected number of resistant cells

The expected number of resistant mutants cells increases as a function of their birth rate (relative to the parental cells) and their mutation rate as specified in model (2.1). Red hues indicate an expected number of resistant cells higher than one, indicating parameters where resistant cells typically exist in a population of size 5×10^8 prior to therapy. Vertical lines correspond to the measured growth rates for R1–R4, black dots indicate estimates of mutation rates for the respective resistance mechanism as summarized in table 2.2. The horizontal line indicates base-line rate of point mutations of 10^{-9} per nucleotide and cell division.

PC9 variant	Growth rate	Eexpected number of mutants C
Wt	$\lambda_{\mathrm{WT}} = 0.78 \pm 0.06\mathrm{day}^{-1}$	N/A
R1	$\lambda_{\mathrm{R}_1} = 0.76 \pm 0.05\mathrm{day}^{-1}$	14.5
R2	$\lambda_{\mathrm{R}_2} = 0,73 \pm 0.07\mathrm{day}^{-1}$	7.7
R3	$\lambda_{\mathrm{R}_3} = 0.67 \pm 0.07\mathrm{day}^{-1}$	2.3
R4	$\lambda_{\mathrm{R}_4} = 0.48 \pm 0.04\mathrm{day}^{-1}$	1.6

Table 2.2: Growth rates of PC9 wild type and expected number of resistant cells under drug free medium
The growth rates were measured in drug-free medium following a drug holiday lasting between 2 and 4 weeks, ensuring sufficient time for cellular recovery while minimizing the risk of reversion to the wild-type phenotype. The estimates of resistant cells within a population of $N = 5 \times 10^8$ were calculated using equation (2.1). Due to the absence of more precise data, we used the simple point mutation rate as the mutation rate μ for both the R3 and R4 cell line.

staurosporine, which inhibits too many kinases that it kills both cancerous and healthy cells indiscriminately.
Testing the safety of such combination treatments in living organisms (mice or humans) is beyond the scope of this study. However, we assessed cell viability in vitro using HEK293T and mouse embryonic fibroblast (MEF) cells, which do not rely on the pathways inhibited by erlotinib, osimertinib, trametinib or dasatinib. These cells serve as indicators of human cell tolerance and help assess the feasibility of using these drug combinations in therapy.

The results, shown in Figure 2.4, indicate no dramatic viability loss in healthy cells treated with the drug combination over a one-week period compared to untreated controls. The experiment was replicated three times and yielded consistent results, suggesting that this combined treatment approach may effectively target resistant cells while minimizing harm to healthy tissue.

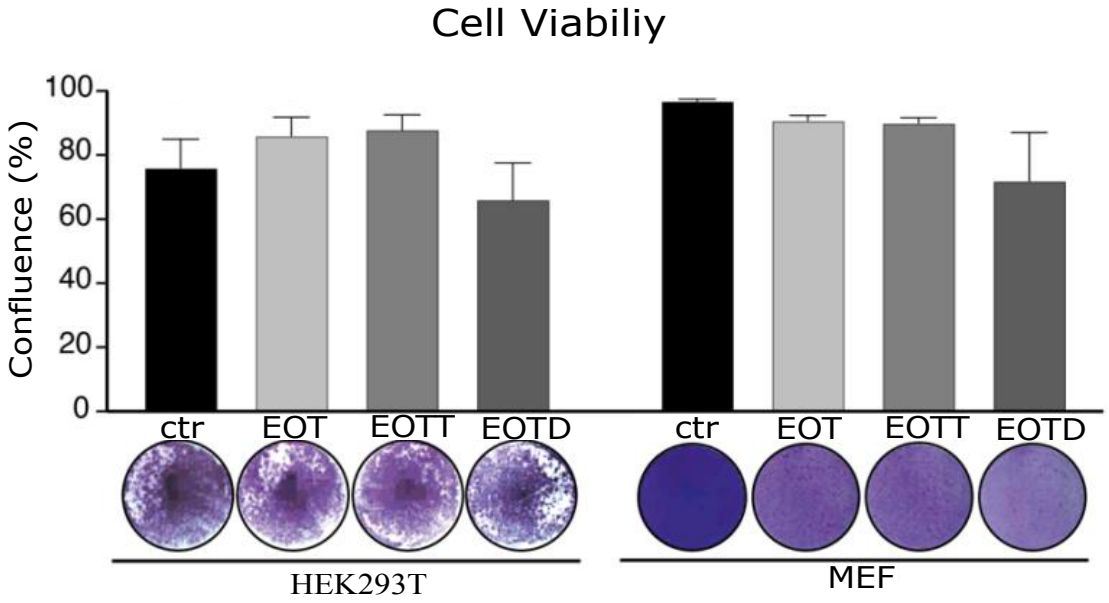

Figure 2.4: Cell viability under varying treatments

Plotted is the confluence of HEK293T and mouse embryonic fibroblast (MEF) cells under the according combination treatments {EOT, EOTT, EOTD}. Height of the bar indicates the mean over 3 runs and error bar indicates the standard deviation. In comparison to a DMSO control, we observe no significant loss in viability. This experiment was collaboratively planned, with the experimental work and visualization conducted by the Brägelmann lab.

Chapter 3

Drug Tolerant Persisters

3.1 Overview

Targeted cancer therapies, as administered today, are generally not expected to be fully curative. For instance, patients with advanced EGFR-driven NSCLC undergoing first-line treatment with erlotinib have a median progression-free survival of 11.7 months [78]. This period reflects the median time between tumor remission and the tumor relapse, half of the patients experience relapse later , while the other half experiences the relapse even sooner. In chapter 2, we examined the key reasons behind this: Large heterogeneous tumors consisting of many cells that cover a wide spectrum of mutations, and some of which confer resistance to the initial therapy. We characterized the spectrum of resistance mechanisms in the PC9 cell line for EGFR-targeted therapy and proposed a treatment panel combining erlotinib, osimertinib, trametinib, and dasatinib. This combination successfully targeted both wild type cells and all potential resistance mechanisms, with no new resistant variants emerging during continued treatment. Targeting all resistance mechanisms is crucial for achieving a curative outcome.
However, while most wild type and resistant cells die quickly under this treatment, a small subpopulation of cells manages to persist, as described in Chapter 2.4.6. These cells, known as *drug tolerant persisters* (DTPs) or *drug tolerant cells* (DTCs), survive a continued treatment without any mutations in their genome that confer resistance against this treatment. In this chapter, we will explore the nature of these persister cells and their ability to withstand therapies. We will discuss their relevance in therapeutic applications, investigate their epigenetic principle that allows them to persist under treatment. We discovered three strategies to treat them effectively. An open question that has a serious impact is whether these DTPs can divide and thus take an active part in tumor evolution as opposed to non dividing, dormant cells that just accompany a tumor without any dynamic properties.

3.1.1 DTP Cells Survive Targeted Therapy treatment

Drug-tolerant persisters (DTPs) are a common challenge in targeted cancer therapies. Across various treatment strategies (E, EO, EOT, EOTD), we consistently observed that some cells

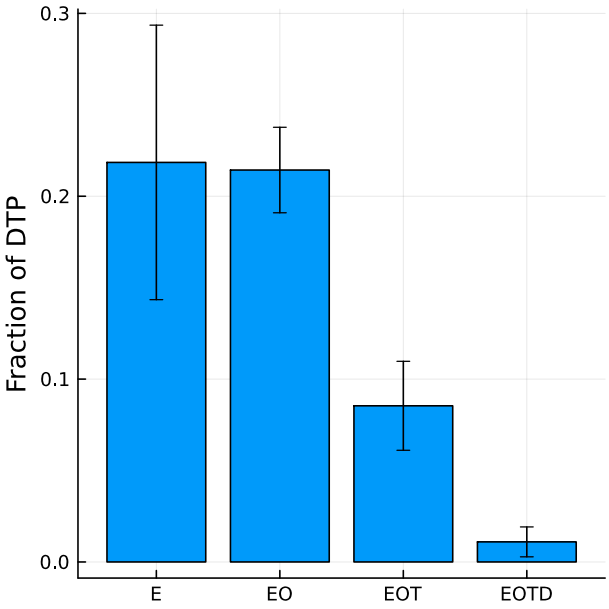

Figure 3.1: Fraction of surviving DTP after 4 days of continued treatment
Bar plot illustrating the fraction of surviving persister cells under the treatment conditions E, EO, EOT, and EOTD. Each bar represents the mean value from three independent experiments, and the error bars indicate the standard deviation.

survived, though adding more drugs progressively reduced the number of surviving DTPs. We define DTPs as cells that survive for more than four days under treatment targeting their driver mutation without those that carry a resistacne conferring mutation as described in chapter 2. PC9 parental cells, driven by EGFR, are highly sensitive to EGFR-targeted therapies, yet survival was observed after all treatments. Specifically, 21.8% of cells survived after four days of erlotinib treatment. We measure a similar rate, namely 21.3%, with the erlotinib-osimertinib (EO) combination, it dropped to 8.5% with erlotinib, osimertinib, and trametinib (EOT), and further decreased to 1.1% with the full EOTD (erlotinib, osimertinib, trametinib, dasatinib) combination.

This indicates that there might exist an entire spectrum of persisters, similar to the resistant cells in 2 and adding more drugs to the treatment panel reduces the number of cells able to persist under the treatment. This hypothesis explains the similarity of numbers in E-, and EO-persisters, as they are simply the same, EGFR-inhibition tolerating persisters.
The four-day time frame is chosen to ensure that any resistant cells cannot divide fast enough to artificially inflate the survival percentages. Without this time restriction, resistant cells could quickly dominate the population, as they do under prolonged erlotinib treatment, which mirrors the conditions used to generate the respective resistant cell lines in chapter 2.

3.1.2 DTP State Is Reversible of Epigenetic Nature

Following a treatment withdrawal, the persister cells start to proliferate again. This enables us to regrow each of the surviving cells into colonies of offsprings and count these colonies at low densities instead of individual cells. This process happens quickly within $1-3$ weeks. This rapid expansion allows to regrow them in sufficient numbers to study these persisters in depth. These newly grown cells, named exEOTD-DTP or exE-DTP respectively after the type of persister cells that they originate from, are again highly sensitive against EGFR inhibition and die as quick as the parental PC9 cells. We analysed the gene expression via RNA-seq and compared the expression patterns with a cluster analysis which compared similarities between different cell strains [79]. We found that exEOTD-DTP cluster together with parental cells, as opposed to EOTD-DTP and E-DTP itself, meaning they have similar gene expression patterns. Furthermore we found in the RNA-seq analysis several up and down regulated Key genes compared to parental PC9 cells such as HMOX1, HMOX2 and most importantly *Glutathione peroxidase 4* (GPX4) as an upregulated gene. GPX4 has already been observed as an potential target to treat DTP [80, 81], and we investigate the treatment options in further detail in chapter 3.2.3. The results of the analysis are published in [75, 82].
We conclude, that our drug tolerant persisters are not genotypically different from parental cells, but just have an epigenetic alteration, that allows them to adapt to treatment with an EGFR or combination inhibition more efficiently on short time scale and revert their state back to the original[83–85]. This is backed up by the time scale of state changes, which can occur within days as opposed from entire generations. This aligns with findings from other researchers who link DTPs to epigenetic aberrations [86]. The word epigenetic changes stems from Greek and means *beyond genetic*, to emphasize that epigenetic changes do not require a change of the DNA sequence inside a cell. They can for instance stem from conformational changes of the DNA, resulting in blocking or promotion of certain genes. Conformational changes can for example result due to the addition of methyl groups into the promoter region and therefore blocking the binding of DNA polymerase to the promoter and down regulating the respective gene.

3.1.3 DTP Are a Challange for Treatments

Studying DTP in vitro is challenging. Due to the heterogeneity of large populations DTP are mostly accompanied by resistant cells that divide faster and eventually interfere with experiments. To prevent the emergence of resistant cells, two strategies are effective: using a broader drug panel like EOTD to target all resistance mechanisms or employing a method similar to that of Hata et al. [87]. In their approach, wild type PC9 cells were divided into multi-well plates and treated with the EGFR inhibitor gefitinib. The wells could be separated into either of two categories. First, the wells which contain pre-existent resistant variants, that divided rapidly and quickly reached confluency. These wells were discarded. Second,

wells that housed a small but stable population of persister cells after the initial treatment. These wells containing only persister cells were continiously treated with the EGFR inhibitor gefitinib to prevent growth. After several weeks, new resistant variants emerged in the wells and quickly took over the population. Genetic testing confirmed that the cells had acquired mutations conferring resistance to gefitinib. This experiment highlights a key insight: resistance is not only pre-existing but can also develop de novo. However, while the emergence of de novo resistance from DTPs may seem concerning for in vivo treatments [88], the number of DTPs is typically much smaller than the initial number of parental cells in an untreated tumor. Assuming the mutation rate, μ, is the same for both wild type and persister cells, the expected number of cells with de novo resistance arising from DTPs is negligible compared to the pre-existing resistant cells originating from the parental cells, which have grown over multiple generations within the tumor. Moreover, pre-existing resistant cells emerge earlier and must be targeted regardless, making de novo resistant cells a less pressing concern under this aspect of targeted cancer therapy.
Another effective method to study DTP without the distortion from emerging resistant cells, is to use the EOTD drug panel. While the number of initial EOTD-DTP is smaller than E-DTP after an erlotinib treatment, as depicted in figure 3.1, the number of surviving DTP after longer periods only shrinks with longer treatment intervals. This is an important difference, as E-DTP manage to grow slowly. The number of DTP shrinks immediately below a critical threshold and can no longer be detected from a classical cell counter within its usual error tolerance of about ± 2000 cells per cell culture flask, but an alternative strategy enables us to count them. The persister state is reversible and after a drug withdrawal, the surviving persister cells will proliferate and form isolated colonies where the isolated cells have been. This enables us to count surviving cells at low densities with an exact resolution.

The ability of DTPs to persist over extended treatment periods and regrow rapidly upon drug withdrawal poses a major threat to the success of cancer therapies. Similar to resistant cells, a single surviving DTP can proliferate exponentially after the end of treatment, potentially leading to tumor relapse. This makes DTPs an important factor in tumor evolution, and they must be specifically targeted, as their persistence threatens the efficacy of curative therapies.

3.2 Eradication Treatment Options

An EGFR monotherapy is insufficient to effectively eradicate large populations of EGFR-driven NSCLC cells, such as our parental PC9 cells. Pre-existing resistant cells can quickly take over and repopulate the tumor. Even when attempts are made to address this issue—whether through a brief period of combined EOTD (erlotinib, osimertinib, trametinib, and dasatinib) treatment followed by continued erlotinib monotherapy, or by separation experiments similar to 3.1.3 where resistant cells are isolated and discarded —the monotherapy is still destined to

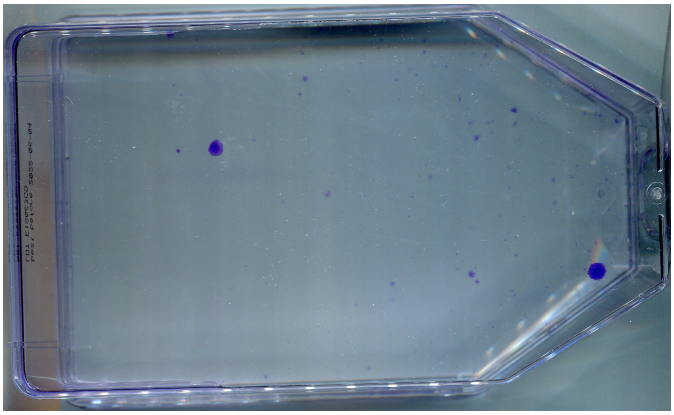

Figure 3.2: CV stained persisters after 6 Weeks of continued EOTD treatment
10^6 parental PC9 cells were seeded into a T175 cell culture flask. After one day of attachment, they were continuously treated with EOTD for six weeks. By the end of the treatment, no macroscopic colonies were visible. The surviving cells were given a two-week drug holiday to allow any remaining cells to proliferate. The outgrown colonies that emerged during this period are CV stained and shown here.

fail. This failure is due to drug-tolerant persister cells (E-DTPs), which can survive the initial treatment and slowly proliferate, regrowing the population over time. Additionally, these persisters may accumulate mutations, leading to the emergence of de novo resistant cells.
To combat this, we identified three treatment options that not only tackle these problems but also provide promising in vitro results that could potentially be translated into in vivo treatment strategies.

3.2.1 EOTD Combined Therapy Leads to Exponential Drop of Persisters

The combination of EOTD not only inhibits the development of all known resistant cell variants but also effectively suppresses the growth of persister cells. Regardless of treatment duration, we did not observe any proliferating cells in our cell culture experiments. The treatment is so potent against persisters that a two-week course is sufficient to reduce the number of surviving persisters below the threshold detectable by conventional cell counters. Instead, to precisely quantify the remaining persisters, we employed the aforementioned method involving a fixed treatment duration followed by a drug holiday of 1.5–2.5 weeks, allowing any surviving cells to form visible colonies, which were then counted manually. The results show a clear exponential decay of surviving persisters outgrowing into colonies, described by the equation

$$N(t) = N_0 e^{-\lambda t}, \tag{3.1}$$

with a decay rate of $\lambda = 0.79 \pm 0.17$ weeks^{-1}, or equivalently, a half-life of $T_{\frac{1}{2}} = 1.13 \pm 0.24$ weeks.
This outcome is promising as it implies that EOTD treatment alone is sufficient not only to suppress resistance mechanisms but also to target and eliminate drug tolerant persisters. However, since DTPs act as a reservoir for potential tumor regrowth if not eradicated, it is critical to ensure that all persister cells are eliminated before discontinuing treatment. Even with the exponential decline in cell numbers, the complete eradication of persisters may take an extended period. To illustrate the order of magnitudes, at detection a tumor of 1 cm^3 contains about $\approx 10^8$ cells, as determined in chapter 3.1 1.1% of these survive as EOTD-DTP, and it would take ≈ 23 weeks of continued treatment for this number to drop down to one single cell. These ≈ 23 weeks can be seen as lower threshold for a treatment duration, and in therapeutic applications a hypothetical patient would be treated for a longer period to ensure the eradication of the last persister cell. During this time, this hypothetical patient would require constant treatment and endure potential side effects. Although the combined effects of the four inhibitors are unknown, it is reasonable to expect that the side effects would be at least as significant as those associated with each individual inhibitor [89–91]. Therefore, it is desirable to find drugs or a combination of drugs to specifically target the DTP.

3.2.2 Bcl-2 and Bcl-xl Inhibition Effectively Eradicates Persisters in PC9 Cells

Inspired by the results of Hata et al. [87], we tested our persisters against a dual inhibition of Bcl-2 and Bcl-xl with the drug navitoclax, also known as ABT-263. The Bcl-2 and Bcl-xl proteins are both anti apoptotic proteins which are often expressed in cancer cells to evade apoptosis. Hence, an inhibition of these two proteins is one possible strategy to restore apoptosis.
We seeded four T175 cell culture bottles with parental PC9 cells and let them grow until the cells reached confluence, with $\approx 5 \times 10^7$ cells and divided the experiment into different branches. Half of the bottles are treated for two weeks with erlotinib, and the other half with EOTD. One bottle of each branch is additionally treated with 1 μM of navitoclax during the second week. In the end, the treatment is followed by two weeks of drug holiday, to let surviving cells outgrow into colonies.
We find that the bottles treated only with erlotinib are covered with a dense layer of cells and the additional treatment with navitoclax only showed a minor effect in the final result. This is largely due to surviving resistant cells that were able to grow throughout the entire duration of the experiment. This hypothesis is backed up by the growth rates that we measured in table 2.2. a single PC9 R1 cell is able to divide ≈ 25 times during the duration of the experiment, hence having the opportunity to repopulate the entire flask after four weeks. The navitoclax targeted only persister cells and slightly thinned the forming layer of resistant cells from persisters.

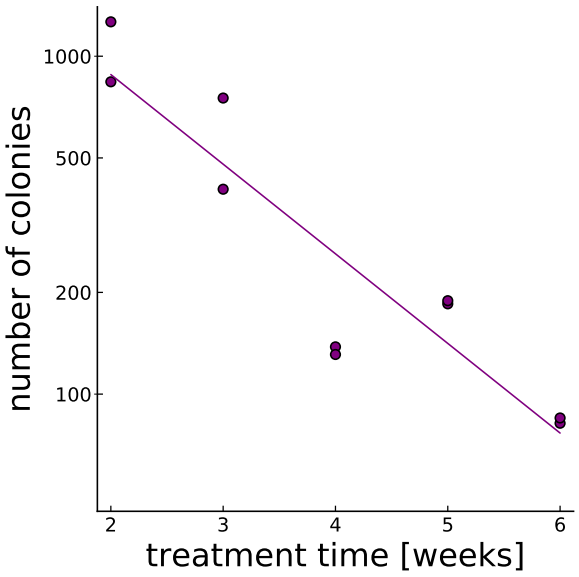

Figure 3.3: Exponential decay of DTP under continued EOTD treatment
10^6 parental PC9 cells were seeded into T175 cell culture flasks. After one day of attachment, they were continuously treated with EOTD for varying durations, as indicated. By the end of the treatment, no macroscopic colonies were visible. The surviving cells were given a two-week drug holiday to allow any remaining cells to proliferate. The outgrown colonies that emerged during this period are CV stained and counted and the resulting number is plotted here against time. The curve follows an exponential fit of (3.1) with parameters $N_0 = 2993$ and $\lambda = 0.79 \pm 0.17$ weeks^{-1}

The flasks treated by EOTD showed hundreds of isolated colonies at the positions where drug tolerant persisters survived throughout the treatment and regrew into colonies. This result was to be expected, similar to the result displayed in figure 3.3. Co-treating the cells with EOTD as well as navitoclax during the second week eradicated all cells and even after longer drug holiday no colonies regrow.
This result is displayed in figure 3.4 and we find consistent results over three replicates. Navitoclax has already been tested in patient studies in combination with EGFR inhibition [92, 93] and MEK inhibition [94]. It showed tolerable side effects and is a promising treatment addition to enhance the efficacy of EOTD from resistant cells to DTP as well. We repeated the experiment with HCC827 cells, also an EGFR driven NSCLC cell line with an exon 19 deletion, that grows slower than PC9 cells and is more robust against an EOTD treatment. While no (fast growing) resistant cells emerge during EOTD treatment, persisters survive in greater numbers than in PC9 and survive even prolonged treatments of more than eight weeks. An additional navitoclax treatment did not show any meaningful effect here.

3.2.3 GPX4 Inhibition Against Persisters

Through RNA-seq analysis, we identified *Glutathione Peroxidase 4* (GPX4) as a significantly upregulated gene, highlighting its potential role in the cellular response mechanism. GPX4 is an enzyme that helps protect cells from oxidative damage by reducing lipid hydroperoxides, which are highly reactive molecules that can destroy cellular membranes. GPX4 utilizes glutathione to convert these lipid peroxides into non-toxic forms, preventing lipid peroxidation and thus preserving cell integrity. Its function is crucial in blocking a form of regulated cell death called ferroptosis [95], which is triggered when lipid peroxides accumulate, leading to cell membrane damage. Ferroptosis is distinct from other types of cell death like apoptosis and is iron-dependent, relying on iron-catalyzed reactive oxygen species (ROS) to initiate lipid peroxidation. GPX4 plays a vital role in countering this oxidative process, hence allowing cells to evade ferroptosis. Inhibiting GPX4 is one way to restore the possibility for cells to die via programmed cell death.
Treating PC9 for one week of EOTD followed by one week of EOTD accompanied by 1 μM of the GPX4 inhibitor RSL3 can effectively eradicate all cells and we observed no cells regrow after a drug holiday of two weeks. Inspired by the success we employ a different treatment tactic. Instead of treating all type of cells simultaneously, this treatment is supposed to target different types of cells subsequently, while using fewer drugs at the same time. This proof-of-concept aims to mimic a potential transfer to clinical settings, where patients then suffer less side effects and a reduced chance for cross reactivity by shutting down too many pathways simultaneously.
Starting with one week of EOT against parental, R1 and R2 cells followed by EOD against R3, R4 cells followed by one week EO+RSL3 against DTP. This treatment series can be repeated from the beginning to enhance its effect and thus turning it into a cyclical treatment. in Our in vitro experiment this series manages to eradicate all cells in the majority of repetitions

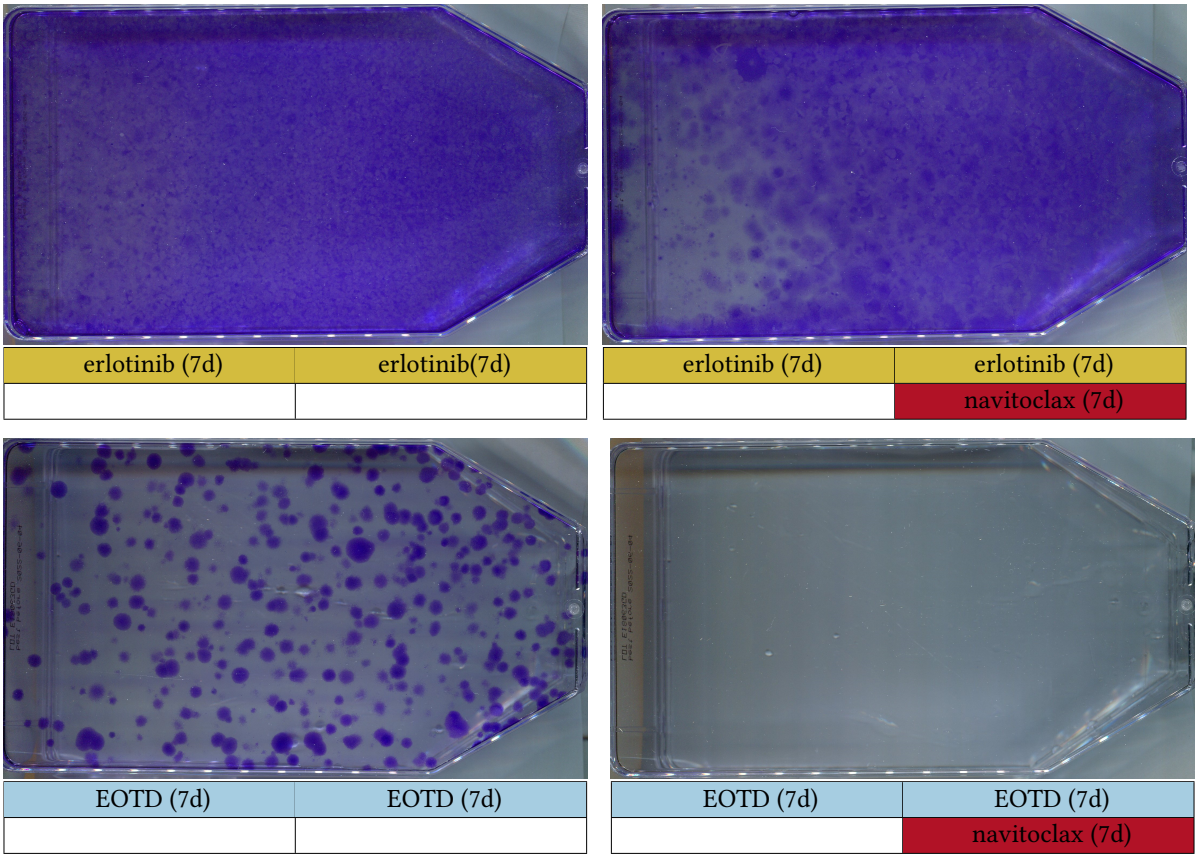

Figure 3.4: Eradicating a large population of PC9 cells with EOTD and navitoclax. PC9 cells were plated in T175 flasks and left untreated until confluency. The flasks were then treated for two weeks with erlotinib (top) or with EOTD (bottom). In the flasks on the right, 1 μM navitoclax was added during the second week. Medium and drug were changed semiweekly to maintain consistent drug exposure and nutrient supply. All flasks were CV stained following a drug holiday of 2 weeks.

and left only $\mathcal{O}(1)$ colonies regrowing after the drug holiday. Despite the great results from the addition of RSL3, it is of no therapeutic use. RSL3 is not *bioavailable*, meaning it can not be absorbed into the human body after consumption. By now, a structural analog of RSL3 has been developed, that is bioavailable [96], and shows tolerable side effects in mouse experiments.
We repeated the experiment with HCC827 cells and obtained the same high efficiency of RSL3 against persisters derived from HCC827 cells, highlighting the promising results and necessity for further research with bioavailable GPX4 inhibitors. Our results are shown in figure 3.5.

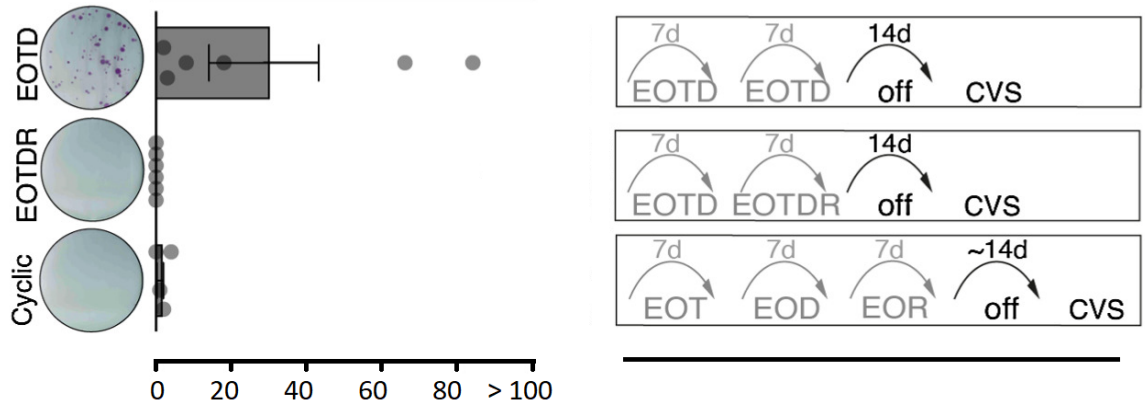

(A) PC9 colony count with treatment scheme

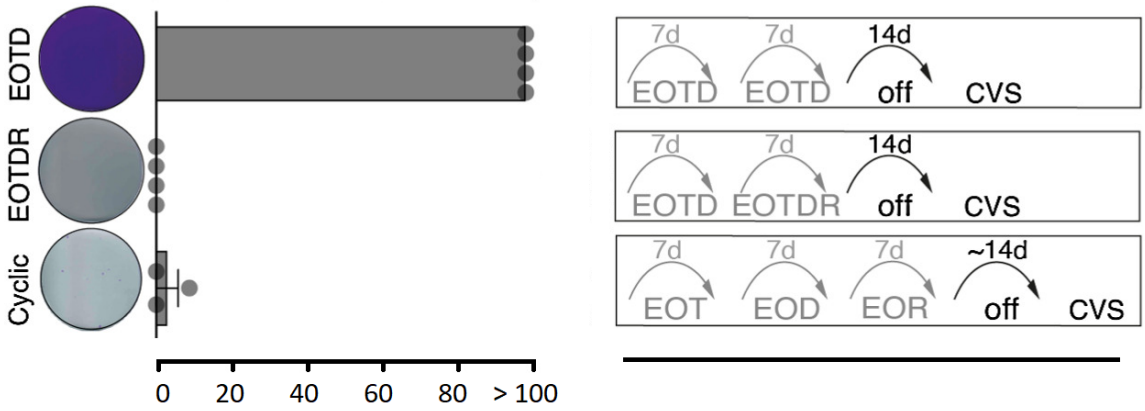

(B) HCC827 colony count with treatment scheme

Figure 3.5: Number of surviving Ex-DTP colonies after indicated treatment
PC9 cells and HCC827 cells are cultivated in 6-well plates and treated as indicated. Following the indicated treatment, the cells were given a two week drug holiday, after which the outgrown ExDTP colonies were CV stained for enhanced visibility. Exemplary scans from the wells are displayed next to the counted numbers of colonies. The number of surviving exEOTD-DTP from HCC827 Cells were so numerous, that they grew to confluency in the wells, hence they are counted as > 100 in the histogram. This experiment was collaboratively planned with the experimental work and visualization conducted by the Brägelmann lab.

3.3 Population Dynamics of Drug Tolerant Persister Cells

3.3.1 Washing Is not the Reason for EOTD Induced Exponential Persister Decay

The number of outgrowing exEOTD-DTP colonies declines exponentially over time, as illustrated in figure 3.3. Several factors might explain this observation. One plausible explanation is that each persister cell may exit its (reversible) drug-tolerant state with a certain probability within a given time interval. If the cells are still exposed to EOTD treatment upon exiting this state, they are unable to survive and die. However, if the cells are in regular growth medium, they re-enter the proliferative phase and form visible colonies. This mechanism would result in an exponential decay of persister cells, where the expected number of remaining persisters as a function of time can be expressed as $N(t) = \mathrm{e}^{-\lambda_{\mathrm{ex}}t}$. where λ_{ex} represents the rate of state exiting.
While this explanation fits the observed data, it is not the only possible reason for the exponential decay. Changes in growth medium, which are necessary for the health of adherent cells like PC9, were performed semiweekly throughout the experiment shown in figure 3.3. Each medium change might introduce additional stress to the cells, thereby influencing their survival or proliferation. Consequently, the number of medium changes is proportional to the passed time, as $n_{\mathrm{wash}} = 2 \times \lfloor t \rfloor$, where time is measured in weeks. If a certain fraction of DTP gets washed away with every medium change and since the numbers of colonies are only counted after integer valued number of weeks we can omit the rounding and obtain for the expected number of DTP as a function of time as

$$N(t) = N_0 \mathrm{e}^{-\lambda_{\mathrm{ex}}t - \lambda_{\mathrm{w}} n_{\mathrm{wash}}} \tag{3.2}$$

$$= N_0 \mathrm{e}^{-(\lambda_{\mathrm{ex}} - 2\lambda_{\mathrm{w}})t} = N_0 \mathrm{e}^{-\lambda_{\mathrm{d}}t}. \tag{3.3}$$

The result is again an exponential decay, where the death rate is a combination of state-exiting rate, washup-rate and washing frequency. Based on the experimental results measured in figure 3.3, it is impossible to determine whether the decay is primarily due to treatment, medium changes, or a combination of both. Medium changes, however, are necessary to maintain drug potency and ensure effective treatment of DTPs. In a separate experiment, visualized in figure 3.6, we demonstrate that the decay rate of persisters is, in fact, independent of washing.
Reducing the number of medium changes could potentially compromise drug efficacy, leading to a higher number of surviving persisters. Conversely, increasing the frequency of medium changes might enhance drug potency, potentially resulting in a lower number of persisters. Both scenarios lend support to the hypothesis that medium changes might influence persister survival. Therefore neither is a suitable experimental design to seperate the influence of a potential washup-rate from the death rate induced by the EOTD drug panel.
To address this, we devised two experimental branches. One branch follows the semiweekly

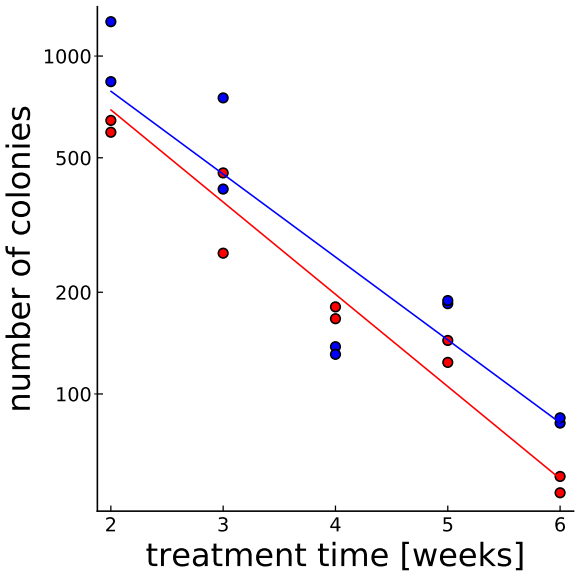

Figure 3.6: Number of outgrown colonies after EOTD treatment with and without fake medium changes

10^6 parental PC9 cells were seeded into T175 cell culture flask. After one day of attachment, they were continuously treated with EOTD for the indicated time. Red curve included the *fake* medium changes, blue only incorporates the regular medium changes. By the end of the treatment, no macroscopic colonies were visible in either flask at any time. The surviving cells were given a two-week drug holiday to allow any remaining cells to proliferate. The outgrown colonies that emerged during this period are CV stained and counted. The plotted exponential curves follow (3.2) and utilize the fitted parameters $\lambda_{\text{ex}} = 0.50$ weeks^{-1} and $\lambda_{\text{w}} = 0.031$ weeks^{-1}.

medium change protocol as previously described, while the other undergoes the same semi-weekly treatment but also includes two additional *fake* medium changes per week. In these fake changes, the medium is collected, centrifuged to separate any persister cells, and the supernatant is returned to the cell culture flask. This process ensures that fresh drugs are not introduced, and the persister cells are continuously exposed to the same treatment medium, eliminating any advantage from newly replenished drugs while maintaining treatment conditions.

With these two branches we have sufficient data, to fit equation (3.2) to the combined dataset and obtain $\lambda_{\text{ex}} = 0.50 \pm 0.03$ weeks^{-1} and $\lambda_{\text{w}} = 0.031 \pm 0.008$ weeks^{-1}. The rate of cells dying due to prolonged treatment time is larger by an order of magnitude than the rate of cells dying due to washings. This implies that the medium changes have only minor effects on the results and we indeed manage to eradicate the cell populations due to effectively treating the cells as opposed to washing them away over time.

3.3.2 Cell Division Shapes Population Dynamics of DTP under EOTD

In the previous section, we explained the observed exponential decay of DTP over time by proposing a constant death rate. This decay is attributed to cells remaining dormant and randomly exiting the persister state, after which they die in the presence of the EOTD treatment. In contrast to that, Hata et al. [87] observed cell division in E-DTP that lead to de novo mutations that could potentially confer resistance against the treatment. In their experiment, cells were locally separated into different wells, and wells containing fast-growing resistant cells were discarded, ensuring only DTPs were studied. The authors attributed the observed slow net growth to a balance between a small cell birth rate λ_b and death rate λ_d of the gefitinib treated DTP, where the two rates were of similar magnitude, but with a slightly larger birth rate. As mutations occur during the DNA duplication during cell division [97], this nonzero birth rate is a key factor to acquire de novo mutations.
We observed similar behavior in our experiments with E-DTP, e.g. see figure 3.8, , where slow growth gradually increased the number of persisters over time. In contrast, no growth was observable in EOTD-DTPs, where cells exhibited a negative net growth rate $\lambda_g = \lambda_b - \lambda_d$, and formerly defined as $-\lambda_{ex}$. While it remains unclear if EOTD-DTPs have a zero birth rate, the exponential decay can be explained by either a zero birth rate combined with a positive death rate or any scenario where $\lambda_b < \lambda_d$. One way to conceptualize this is that cells divide all the time. After each cell division cycle is complete, the cells either die with a certain probability or they divide regularly into two offsprings.
The key difference between a death-only process and a birth-death process lies in the variation of DTP cell numbers within individual colonies. In practical terms, colonies grow into overlapping regions, making it difficult to measure or define local variation after an outgrowth. A better approach would be to analyze spatially separated cells in multi-well plates, as done by Hata et al. [87].
Given an initial population of DTP cells distributed in a multi-well plate. DTP that do not divide but only die at rate $\lambda_g = -\lambda_{ex}$, will only shrink in numbers and only introduce a minor variation in the number of cells per well. In contrast to that, the same initial distribution of DTP in a process that allow for birth and death with the same net growth rate $\lambda_b - \lambda_d = \lambda_g$ will have a completely different distribution of DTP cell numbers after a longer treatment time. The two rates will introduce more variation in the final result, while the expected or mean number of cells still decays exponentially at the same rate λ_g. The extent of this variation increases as the birth and death rates rise while keeping the difference, the net growth rate, constant. A simulation illustrating this phenomenon is shown in figure 3.7. In this simulation an initial distribution of cell numbers in wells was left exposed to either of the two population dynamics, which was calculated using the Gillespie algorithm. The one-rate distribution exhibits minimal variance, maintaining its overall shape while gradually shifting toward zero with time. In contrast, the two-rate distribution shows a more dynamic and complex behaviour during its temporal evolution. While most wells shrink in size—some significantly—a few wells unexpectedly increase their population size despite ongoing treatment.

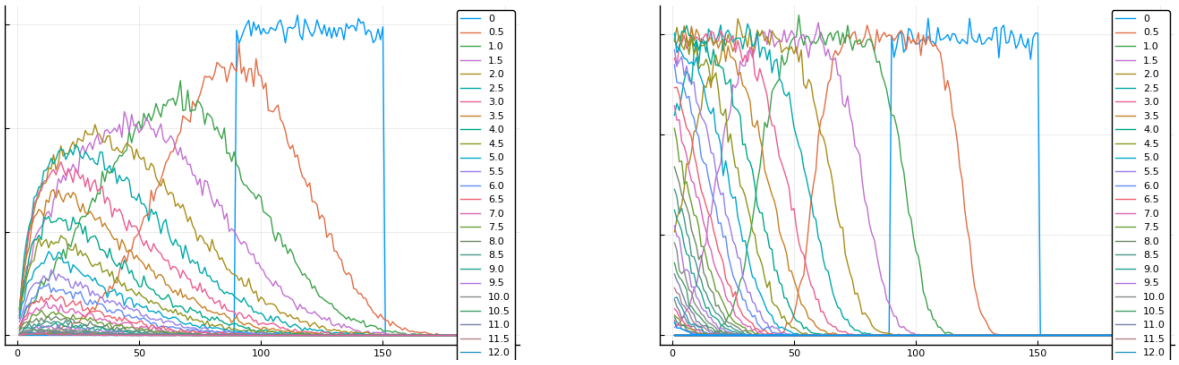

Figure 3.7: Temporal evolution of distributions of DTP with and without cell division

The x-axis represents the colony size, while the y-axis shows the probability of occurrence. The temporal evolution of an initially uniform distribution with noise is simulated using the Gillespie algorithm [98]. The left plot represents a two-rate process, governed by the master equation (3.5), with a birth rate of $\lambda_b = 0.3$ week^{-1} and a death rate of $\lambda_d = 0.9$ week^{-1}. The right plot shows a one-rate, death-only process, as described by the master equation (3.4), with $\lambda_d = 0.6$ week^{-1}. The rates were selected such that the net growth rates of both processes are equivalent, enabling direct comparison of the resulting distributions. The bin for $n = 0$ cells has been excluded.

This growth is simply a result of random fluctuations.
This analysis can be extended to the context of cell culture flasks, where each well can be thought of as representing a tiny section of the flask. In these small sections, the outgrowing Ex-DTPs proliferate into overlapping colonies, eventually losing their distinct boundaries. Over time, this process leads to a distribution where most sectors are empty, a few contain one cell, and a small number houses multiple cells. After a drug holiday, the ex-DTPs begin proliferating: empty sectors remain empty, sectors with one cell form small colonies, and sectors with multiple cells grow into larger colonies of varying sizes. This is precisely what we observed in our EOTD experiment, as depicted in figure 3.2, where the CV-stained colonies span a wide range of sizes.
On the other hand, the size differences can also be attributed to persisters exiting their dormant state earlier than others by chance and therefore getting an exponential advantage in growth.

For a more rigorous analysis of these variations, a stochastic framework is required. We can approach this by constructing the corresponding master equation for the single-rate process

as

$$\frac{\partial \mathscr{P}_n(t)}{\partial t} = \underbrace{(n+1)\lambda_d \mathscr{P}_{n+1}(t)}_{\text{Flow of probability into}\mathscr{P}_n(t)} - \underbrace{n\lambda_d \mathscr{P}_n(t)}_{\text{Flow of probability out of } \mathscr{P}_n(t)}, \tag{3.4}$$

where $\mathscr{P}_n(t)$ describes the probability of an individual well being in the state of being populated by n persister cells at time t, λ_{ex} is the rate of state exiting, which is here the negative of the growth rate for the process. The flow of probability into $\mathscr{P}_n(t)$ is solely consisting of the probability of being in the state with $(n+1)$ cells weighted by cell number and death rate. Similarly, the flow of probability out of $\mathscr{P}_n$ consists solely of the probability of being in that particular state weighted by cell number and state.

In contrast to that, if one incorporates cell birth with a rate λ_{b} as well, the master equation changes to

$$\frac{\partial \mathscr{P}_n(t)}{\partial t} = \underbrace{(n+1)\lambda_d \mathscr{P}_{n+1}(t) + (n-1)\lambda_b \mathscr{P}_{n-1}(t)}_{\text{flow of probability into } \mathscr{P}_n(t)} \underbrace{- n(\lambda_b + \lambda_d)\mathscr{P}_n(t)}_{\text{flow of probability out of } \mathscr{P}_n(t)}. \tag{3.5}$$

The flow of probability into $\mathscr{P}_n$ is now consisting of the two probability neighbouring states of having $(n-1)$ and $(n+1)$ cells, weighted by the respective cell number and the corresponding rate, that connects the states, λ_b, and λ_d respectively. The flow probability out of $\mathscr{P}_n(t)$ still consists of the probability of being in the corresponding state, weighted by cell number but now additional the sum of all rates leading out of the respective state.

The Master equations (3.4),(3.5) are systems of coupled linear equations. Solutions for the probability distribution as well as expectation values can be found in the literature e.g. in [99]. For any given initial probability distribution $\{\mathscr{P}_m(t=0)\}_{m=0}^{\infty}$ and birth and death rates, the temporal evolution can be calculated by transforming the differential equations into a single partial differential equation using the *probability generating function*, solving this partial differential equation using the *method of characteristics* and simplifying the results with standard methodsto arrive at

$$\mathscr{P}_n(t) = \sum_{m=0}^{\infty} P(n,m,t)\mathscr{P}_m(t=0). \tag{3.6}$$

Here $P(n,m,t)$ is the propagator that defines the influence of the probability of being in a certain state with m cells initially on the probability of being in the state with n cells after time t. A linear combination of all initial values with the respective propagators yields the desired result. For the one rate process (3.4) one obtains

$$P^1(n,m,t) = \begin{cases} \binom{m}{n} \mathrm{e}^{-n\lambda_d t}\left(1-\mathrm{e}^{-\lambda_{\text{d}} t}\right)^{m-n} & \text{for } 0 \le n \le m, \\ 0 & \text{else.} \end{cases} \tag{3.7}$$

and the expected number of cells yields

$$\langle n\rangle(t) = \langle m\rangle e^{-\lambda_d t} \tag{3.8}$$

and the variance in cell number yields

$$\mathrm{Var}(n)(t) = \langle m\rangle e^{-\lambda_d t}\left(1 - e^{\lambda_d t}\right) + \mathrm{Var}(m)e^{-2\lambda_d t}. \tag{3.9}$$

both expectation values are related to the expected initial number of cells $\langle m\rangle$ and the initial variance in the starting population $\mathrm{Var}(m)$. The impact of the initial variance decays with a higher exponent than the influence of the stochastic cell deaths.

For the solution of the the two rate birth-death process we define

$$\alpha = \left(\frac{\lambda_d e^{(\lambda_b-\lambda_d)t} - \lambda_d}{\lambda_b e^{(\lambda_b-\lambda_d)t} - \lambda_d}\right), \quad \beta = \left(\frac{\lambda_b e^{(\lambda_b-\lambda_d)t} - \lambda_b}{\lambda_b e^{(\lambda_b-\lambda_d)t} - \lambda_d}\right) \tag{3.10}$$

and the propagator reads

$$P^2(n,m,t) = \begin{cases} \alpha^m & \text{if } n = 0, \\ \alpha^m \beta^n \sum_{j=1}^{\min[m,n]} \binom{m}{j}\binom{n-1}{j-1}\left(\frac{1-\alpha-\beta+\alpha\beta}{\alpha\beta}\right)^j & \text{if } 1 \le n, \end{cases} \tag{3.11}$$

or equivalently in the case $1 \le n$

$$P^2(n,m,t) = m\alpha^m\beta^n\left(\frac{1-\alpha-\beta+\alpha\beta}{\alpha\beta}\right){}_2\mathscr{F}_1\left(1-m, 1-n; 2; \frac{1-\alpha-\beta+\alpha\beta}{\alpha\beta}\right), \tag{3.12}$$

with the Gauss' hypergeometric function ${}_2\mathscr{F}_1\,(a,b;c;x)$. The time-dependent expected number of cells yields

$$\langle n\rangle(t) = \langle m\rangle e^{(\lambda_b-\lambda_d)t} \tag{3.13}$$

and the time dependent variance in cell number yields

$$\mathrm{Var}(n)(t) = \langle m\rangle\frac{(\lambda_b+\lambda_d)}{(\lambda_d-\lambda_b)}e^{(\lambda_b-\lambda_d)t}\left(1 - e^{(\lambda_b-\lambda_d)t}\right) + \mathrm{Var}(m)e^{-2(\lambda_b-\lambda_d)t}. \tag{3.14}$$

The time dependent expectation value again yields an exponential decay with decay rate $\lambda_g = \lambda_b + \lambda_d$ and starting cell number is the expected initial cell number $\langle m\rangle$. The time dependent variance also consists of two terms, one resulting from the initial variance that decays at the fast rate $\propto e^{2(\lambda_b+\lambda_d)t}$, and another term that results from stochastic fluctuations that decays more slowly.
It is clear, that the results for one- and two-rate processes match in the limit $\lambda_b \to 0$. Moreover, for a fair comparison with the same decay rate and therefore the same expected cell number

on both processes λ_g, we note that the fluctuation term in the variances is indeed larger in the two-rate process, by a factor of

$$\frac{\lambda_b + \lambda_d}{\lambda_d - \lambda_b} \geq 1. \tag{3.15}$$

This factor is larger than 1 and equal in the limit $\lambda_b \to 0$, where both processes match. It is larger if both rates are close to each other and diverging in the limit $\lambda_b \to \lambda_d$. However, that divergence is not relevant, as the processes are different in that limit. The one-rate process becomes a fixed state, where nothing changes. The two-rate process allows for cell birth and death and the expected number stays constant over time. However, the variance of cell numbers increases linearly with time [99].
We clearly observe a nonzero decay rate of DTP number under EOTD treatment, as displayed in 3.3. The larger variance in cell number in a birth-death as opposed to a birth-only process can be the explanation for the variance in colony size observed in the DTP treatment experiments: a larger variance in cell number results in a larger variance in starting cell number per surface area in a cell culture flask. That fluctuation manifests in clusters of more than one DTP cell surviving the treatment and thus growing into an overlapping colony, surpassing the size of other colonies outgrown from a single DTP by an order of magnitude.
For treatments, the difference between the two processes has two major impacts. First, cell division allows for de novo mutants developing under treatment and therefore increases the risk for the acquisition of a new resistance mechanism, that has not been present before. Second, is the impact on treatment duration which is necessary. We have estimated an expected treatment duration based on the decay rate and the expected number of cells in chap 3.2.1 as ≈ 23 weeks for a tumor of size 1 cm^3. Estimating a treatment duration based on expectation values alone bares a high risk. Due to stochastic fluctuations, some tumors will consist of longer surviving DTP as others. A better measure for the treatment duration is the maximization of the probability of no surviving persisters. Restricting the initial tumor to contain m DTP allows to solve (3.11) for the necessary time t to treat a tumor to have no surviving persister cells with probability p as

$$t = \frac{\log\left(\frac{\lambda_d(1-\sqrt[m]{p})}{\lambda_d - \lambda_b \sqrt[m]{p}}\right)}{\lambda_b - \lambda_d}. \tag{3.16}$$

Under the assumption that DTP have the same birth rate as wild type cells of $\lambda_b = 5.46$ week^{-1} as measured in table 2.2, we use a death rate of $\lambda_d = 6.31$ week^{-1} which results in a net growth rate of $\lambda_g = -0.78$ week^{-1} as measured in chapter 3.2.1, the same tumor of 1 cm^3 must be continuously treated with EOTD for 35.7 weeks to be eradicated with a probability of $p = 1 - 10^{-5}$.

3.4 Behaviour of Drug Tolerant Persisters under Switched Treatments

Intrigued by the varying numbers of persisters surviving under different treatments, as shown in figure 3.1, and their distinct dynamic behaviour where E-DTPs slowly proliferate while EOTD-DTPs do not, we explored how persisters respond when exposed to the alternative treatment. We seeded two sets of 5×10^5 PC9 cells in six-well plates: one set was treated with erlotinib, while the other was treated with EOTD. After one week, most cells had died, leaving behind only the surviving DTPs, which were visible under the microscope. One replicate of the E-DTPs was subsequently exposed to EOTD for two weeks, while the other remained under erlotinib treatment. Conversely, one replicate of the EOTD-DTPs was switched to erlotinib, with the other remaining on EOTD treatment. The cells that survived erlotinib were tested for the T790M mutation, the resistance mechanism that most commonly develops under erlotinib monotherapy. This test was crucial to ensure that the observed behavior could be reliably attributed to DTP cells rather than the growth of resistant cells.
Examplary images of the results of this experiment are shown in Fig 3.8. We find that under EOTD monotherapy no proliferation was observable after one week or after three weeks. EOTD-DTP under erlotinib treatment slowly proliferated and formed a number of small colonies. Microscopic images confirm, that the cells grow densely packed without distances between cells. We conclude that EOTD-DTP are in general able to divide but hindered by the EOTD treatment to proliferate.
Under erlotinib monotherapy we observe a fine homogeneous film of uniformly distributed surviving persisters formed after one week. after three weeks a similar result got visible, the uniform layer of cells was was denser. E-DTP treated with EOTD for two weeks showed an interesting behaviour. Even though the DTP were continuously treated for two weeks under EOTD, sufficiently many cells survived in close vicinity to be observable without a microscope. Microscopic images further illustrate that there are large enough gaps in between individual cells that could have been populated by other cells bridging the distance but having died throughout the experiment.
The results were consistent over four replicates and showed no presence of the T790M mutation, that would be most likely to appear and is responsible for the R1 cell type 2.4.2. Therefore, we can attribute the results observed here as properties of persisters as opposed to an artefact of resistant cells.
The dynamics observed in this experiment can be explained by a two-rate process, as described in chapter 3.3.2. During erlotinib treatment, the birth rate surpasses the death rate, which explains the proliferation seen in both the erlotinib monotherapy and the EOTD-E branch, where surviving EOTD-DTPs began forming colonies. In contrast, under EOTD, the death rate exceeds the birth rate, leading to a reduction in persister numbers. This limited cell division allows for random fluctuations in local cell density. In certain regions, by chance, cells divide more frequently than they die, forming clusters. These clusters exhibit gaps where cells have died over the course of the treatment. Importantly, the area marked by violet

staining indicates that the absolute number of DTPs was higher in the branch treated with one week of erlotinib compared to the branch followed by two weeks of EOTD, reinforcing the conclusion that cells die under EOTD treatment.

3.5 Summary

Targeted cancer therapy, in its current form, primarily aims at extending progression-free survival rather than achieving a cure. Effective treatment requires not only targeting the main population of wild-type cancer cells but also addressing both pre-existing resistant cells and drug-tolerant persisters, which do not acquire resistance-conferring mutations. This can either happen as polytherapy which is not approved as of now or in a sequential series, which is further discussed in chapter 4.
DTP cells present a particular challenge to targeted therapies because they are not genetically resistant but rather rely on reversible, epigenetic adaptations that allow them to survive under prolonged treatments. Under erlotinib treatment, 21.8% of cells survived, and even with the EOTD combination therapy, around 1.1% of cells persisted.
We identified three promising strategies for DTP eradication:

- Navitoclax treatment: This Bcl-2/Bcl-xL inhibitor quickly eliminated persisters in PC9 cells but was less effective in HCC827 cells, underscoring variability in response across cell lines.
- GPX4 inhibition with RSL3: GPX4 is an upregulated gene in an RNA-seq analysis and inhibiting the approach to inhibit GPX4 successfully eradicated persisters in both PC9 and HCC827 cells.
- Continued EOTD treatment: Sustained exposure to EOTD effectively decayed DTP populations in a consistent exponential manner, with a decay rate estimated at $\lambda = 0.79 \pm 0.17$ weeks^{-1} in PC9 cells. We ruled out that this exponential decay resulted from medium changes and we attribute this solely to the efficacy of the treatment.

Although EOTD effectively reduces the persister population, the question of whether these DTP cells decay solely due to cell death, or through a balance of cell division and death, remains unresolved. While live cell imaging would provide clarity, we did not have access to any live cell imaging equipment during our research. Cell division in DTP under EOTD has an impact on the tumor evolution under treatment, as it increases the variance in surviving DTP number and thus increasing the necessary treatment duration to eradicate the last persister cell with certainty. While the different numbers of surviving persisters under different treatments hints a spectrum of persistence mechanisms exists, we observed similar behaviour of the respective persisters under each treatment combination: slow proliferation under erlotinib and decay under EOTD. Thus, if a spectrum exists, its impact on tumor evolution and treatment efficacy

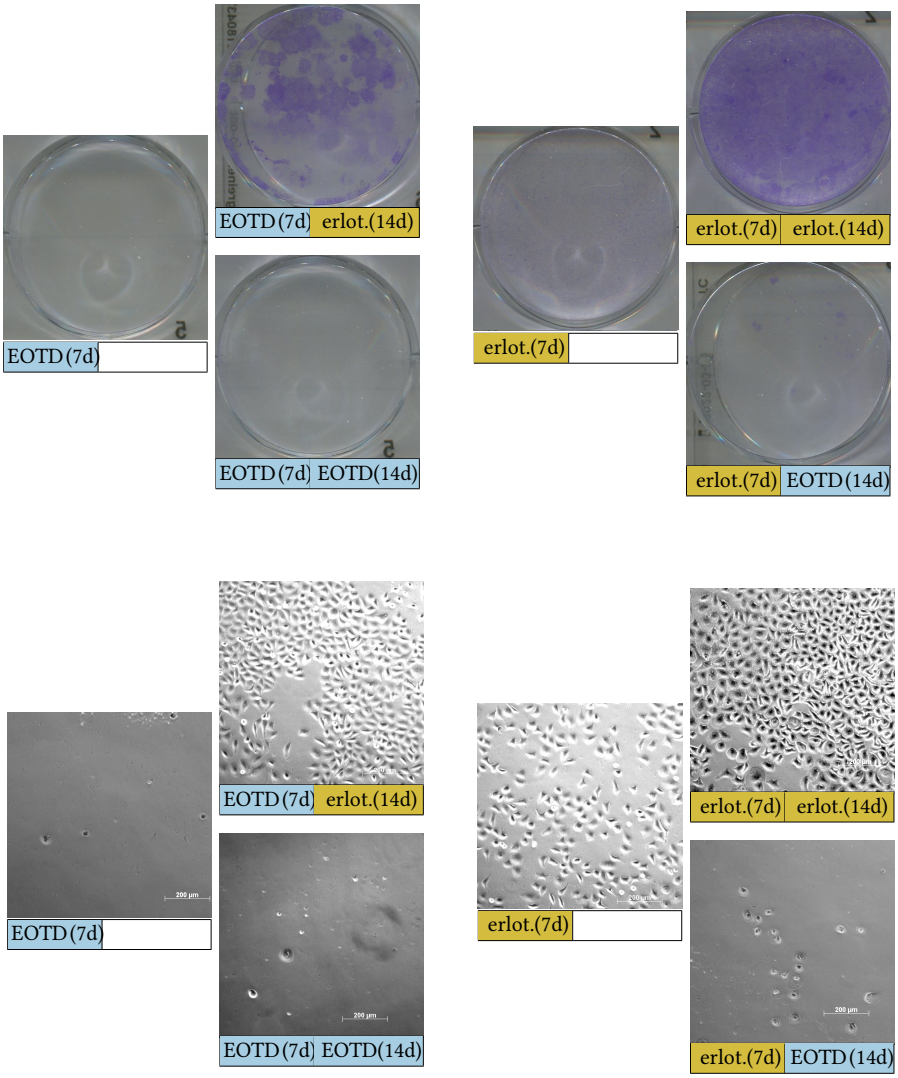

Figure 3.8: Switch of drug-tolerant persisters between erlotinib and EOTD treatment
We plated 7×10^5 cells in regular medium for one day and then treated with EOTD for one week (left) or erlotinib (right). The images shifted to the right display the follow up treatment for two weeks which was either switched to the other treatment or maintained on the same treatment as indicated below each image.
The top row displays CV stains of the dishes and bottom row displays microscopic images for the respective stage of the experiment. All images are representative of four independent experiments. We find that DTP proliferate under erlotinib, but not under EOTD. We checked that populations growing under erlotinib did not contain the mutation EGFR T790M, that is responsible for the resistant variant R1.

is negligible, and based on our further studies on treatment efficiency, we consider them only as one type of persister.
A significant insight is that although DTP cells can theoretically acquire de novo mutations during treatment, their comparatively low numbers reduce the likelihood of developing new resistance mechanisms. However, the endurance of DTPs poses a substantial risk, as prematurely ending treatment could allow these cells to repopulate and potentially contribute to relapse. Based on observed decay rates, a treatment duration of approximately 35.7 weeks is estimated to be necessary to achieve effective tumor eradication for a 1 cm^3 tumor volume under combined therapy, assuming DTPs remain in a dividing state under EOTD.

Chapter 4

Optimizing Targeted Cancer Therapy Schedules

In chapter 2, we identified the spectrum of possible resistance mechanisms in the EGFR-driven NSCLC cell line PC9 and developed a panel of four inhibitors that, when combined, can effectively target both wild-type cells and all potential resistance mechanisms. Moreover, this panel does not only target the genetically altered resistant cell types, it also inhibits proliferation of the epigenetically altered drug tolerant persisters. Initial toxicity testing of the EOTD combination showed no significant cross-toxicity, indicating that such a treatment may be feasible. However, in vitro experiments cannot fully replicate the complexity of in vivo studies or clinical trials, and thus safety for human administration remains uncertain. Some pairwise combinations of these drugs have already been approved for clinical trials, demonstrating tolerable side effects. This includes but is not limited to the combinations erlotinib with dasatinib [100], osimertinib with trametinib [101], osimertinib with tepotinib [102]. We have demonstrated in figure 3.5 that a switching treatment can be feasible to target each resistance mechanism consecutively and eradicate an entire population this way.
In this chapter, we will elaborate that idea and introduce a grid model for the treatment of a heterogeneous tumor consisting of different cell types that respond to different treatments in unique ways. While our experiment ended after three weeks, patients are usually treated for longer periods and heterogeneous tumors might consist of different compositions of cell types. Thus, we incorporate alternating and cyclical repeating treatments in the model. While fixed treatment intervals of a certain length, here $\Delta t = 1$ week are practically easily manageable, they are most certainly not the optimal possible treatment. We define a measure to quantify the expected outcome of a treatment schedule and provide a decision rule for the optimal possible treatment schedule.
The results of this chapter were obtained in collaboration with the student Noah Elbracht [103].

4.1 The Grid Model of Optimal Therapy

A given cell population can contain a variety of mutations and some of these can confer resistances to different therapeutic approaches. In order to completely eradicate the tumor, resistance-targeting treatments must be administered in addition to the standard therapies,

like the EOTD panel for the EGFR driven PC9 cells. While the simultaneous administration of all necessary standard and resistance-targeting medications has been shown to successfully eliminate tumor cells in cell cultures as described in chapters 2 and 3, this approach does not account for the potential impact of combination therapy on healthy cells. Each combination of drugs must be tested for safety and deemed harmless before it can be approved for clinical use. Currently, approvals are generally limited to combinations of two to three drugs.

Despite these limitations, it is still possible to provide patients with a near-optimal therapy by administering medications in an alternating sequence. While we cannot control the number of resistances that may exist prior to treatment, we can reduce the risk of new resistances emerging within the tumor by carefully optimizing the order of drug administration. This leads to the key question of this chapter: how to design an optimal therapy schedule involving drugs acting on different subpopulations

We begin by defining treatments in general. Given are n different species of cancer cells, for example {parental cells, R1, R2, R3, R4} for an $n = 5$ case. We denote the time dependent numbers of each cell type by $N_\mathrm{i}(t)$. Furthermore, we have a panel of possible drugs and or combinations at our hand. Each combination of drugs is labelled as a unique treatment $\mathrm{D_j}$, since different combinations yield different effects on cancer cells. One example with $m = 2$ treatments would be {ED, OT}. We model the action of a certain treatment duration Δt with drug $\mathrm{D_j}$ on cell type N_i with an exponential function as

$$N_\mathrm{i}(t_0 + \Delta t) = N_\mathrm{i}(t_0)\mathrm{e}^{L_\mathrm{ij}\Delta t}. \tag{4.1}$$

The exponential growth rates L_ij that encode the action of treatment $\mathrm{D_j}$ on cell type N_i can be summarized into an (n × m) treatment matrix L. The exponential growth factor L_ij is either a negative value, when the treatment $\mathrm{D_j}$ specifically targets cell type i resulting in an exponential decay of N_i, or conversely it is a positive constant, if the treatment does not target the cell type, leading to exponential growth in N_i. We assume here that the pharmacokinetics of the medications involve immediate effects, without the need for dose accumulation or the effect being dependent on the drug concentration. Conversely, after Δt time the drug loses any effect and the new treatment can be administered without any cross reactivity.
Any effective treatment requires that not only the total number of cells, but also each cell type N_i decays faster during its effective treatment than it grows during all non effective treatments combined. Formally, this is the case if the treatment matrix L allows the treatments to be chosen that any of the equivalent conditions apply

1. $$\exists f_1, f_2 \ldots, f_m \in \mathbb{N}_0 \text{s.th. } N_\mathrm{i}\left(\sum_{j=1}^{m} f_\mathrm{j}\Delta t\right) = N_\mathrm{i}(0)\mathrm{e}^{\sum_{j=1}^{m} L_\mathrm{ij} f_\mathrm{j}} < N_\mathrm{i}(0)\ \forall \mathrm{i} \tag{4.2}$$
2. $$\exists \vec{f} \in \mathbb{N}_0^m \text{ s. th. } L\vec{f} < \vec{0} \quad \text{(elementwise)} \tag{4.3}$$

One could formulate an equivalent condition using Farkas' lemma [104] as

$$\nexists \vec{y} \in \left(\mathbb{R}^n \setminus \mathbb{R}^n_{\leq 0}\right) \text{ s. th. } \vec{y}^T L \leq 0 \quad \text{(elementwise)} \tag{4.4}$$

but this is of little use in practical situations as proving the non existence of such a vector is impractical. The coefficients $\{f_j\}$ indicate how often each respective treatment needs to be administered to achieve the final requirement of $N_i(f\Delta t) < N_i(0)$, with $f := \sum_{j=1}^{m} f_j$ the total number of treatment intervals of length Δt. Note, that the choice of treatment intervals is independent from initial cell number $N_i(0)$ and treatment interval length Δt. Hence, the condition for an effective treatment is only dependent on the treatment matrix L.
After $f\Delta t$ time, or more precisely after administering the drug combination f_1 times D_1, f_2 times D_2, ..., f_m times D_m, the populations N_i can be calculated from (4.1). The final number of cells yields

$$N_i^{\vec{f}}(f\Delta t) = N_i(0) e^{\sum_{j=0}^{m} L_{ij} f_j \Delta t}. \tag{4.5}$$

This expression for the final number of cells depends only on the total number of treatment steps, rather than the entire sequence of administrations. There are in total

$$\frac{\left(\sum_{j=1}^{m} f_j\right)!}{\prod_{j=1}^{m} f_j!} \tag{4.6}$$

possible ways to arrange the treatments and arrive with the cell numbers specified in (4.5). This simplification arises from the multiplicative property of exponential functions, which allows us to combine all the exponents. Therefore, after fixing initial state $N_i(0)$, the growth rate matrix L and treatment interval length Δt, the state of the modelled tumor is fully described by the m integer numbers $\{f_j\}$. These integers can be used as coordinates in an m-dimensional grid. Each of the coordinate axis corresponds to a drug combination D_j, the coordinates correspond to the number of treatment intervals of length Δt of the corresponding drug. The number possibilities to administer the treatment (4.6) corresponds to the possible paths in the grid to connect the origin $(0, \dots, 0)$ to the endpoint $(f_1, \dots, f_m)$. An exemplary grid is displayed in figure 4.1.

4.2 Cost Function for a Therapy Schedule

The number of possibilities to treat a patient with different drugs grows exponentially in the number of treatment intervals, and therefore exponentially in time. Our goal is the minimization of the risk of emergence of new unknown resistance mechanisms that have not been discovered and possibly have no treatment option at our hand to treat them. We attribute a cost to each treatment that will reflect that risk, and finding the treatment path with minimal cost bares minimal risk for new resistances and is the treatment that one should

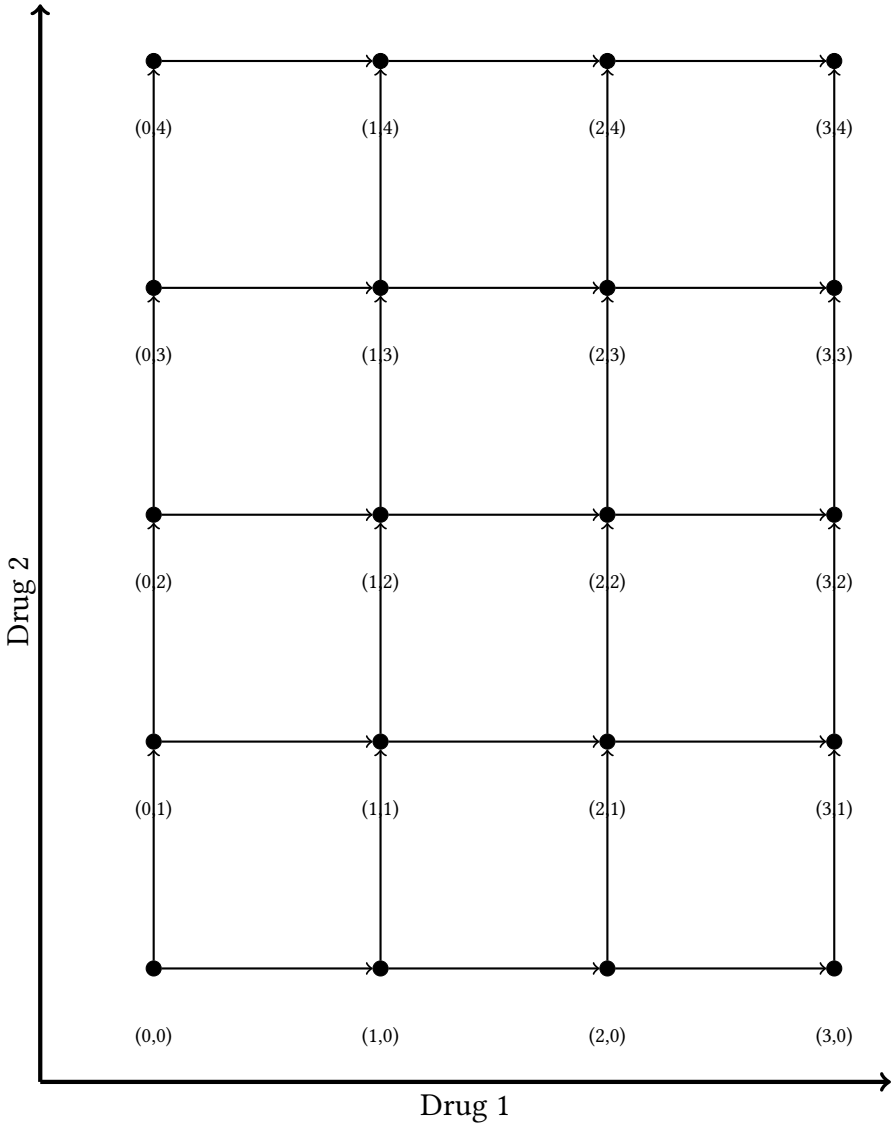

Figure 4.1: Exemplary grid for two drug treatment scheme

Directed graph organized in a grid, representing a tumor treatment model involving a two-drug treatment scheme. The treatment consists of administering drug 1 three times and drug 2 four times, resulting in $\frac{(3+4)!}{3!4!} = 35$ possible treatment sequences. The treatment concludes after seven time intervals $7\Delta t$. Each possible treatment sequence corresponds to a path in the grid, starting from the origin (bottom left) and ending at the treatment completion (top right). Each node in the graph is associated with the cell counts $\{N_i\}$ of all present cell types, reflecting the effects of the corresponding treatments along the path leading to that node. Each possible path ends in the same state $\{N_i^{(3,4)}\}$, but costs can be associated as weights of the edges, allowing the optimal path to be identified as the shortest connection between start and finish.

follow.

New resistances typically originate through mutations that appear during cell division, and the number of divisions at any given time is proportional to the number of cells $N_i(t)$ in a tumor. Therefore, it is desirable for patients to keep the number of tumor cells as low as possible throughout the course of therapy. However, it may be beneficial for patients to temporarily tolerate a higher number of cells if, in doing so, the overall number of cell divisions can be minimized in the long term.

Mathematically, this can be modelled by integrating the total number of cells over the entire treatment period from start $t = 0$ to the finish t_f as

$$K_\gamma = \int_0^{t_f} \mathrm{d}t N(t), \tag{4.7}$$

which is the cost function associated with that particular treatment γ. Here the total number of cells $N(t)$ consists of the individual populations of different phenotypes, $\sum_{i=1}^{n} N_i(t)$. We insert the time dependency of N_i according to the exponential growth or decay in (4.1) that is induced by the respective treatment $D_{j(t)}$ which is present at time t

$$K_\gamma = \int_0^{f\Delta t} \mathrm{d}t \sum_{i=1}^{n} N_i(0) e^{L_{ij(t)}t}. \tag{4.8}$$

Here $j(t)$ denotes the corresponding index for the active treatment D_j at time t. Instead of integrating from 0 to the treatment end $f\Delta t$, we separate the integral into f separate integrals. This has the advantage, that $j(t)$ is constant during each time period. Each integral adds the additional area under the population curve from the interval $t \in [k\Delta t, (k+1)\Delta t]$. During these intervals, all changes in cell numbers are then determined by the function $N_i(t) = N_i(k\Delta t) e^{L_{ij_k}(t-k\Delta t)} \equiv N_i(t') = N_i(k\Delta t) e^{L_{ij_k}(t')}$. We obtain for the cost

$$K_\gamma = \sum_{i=1}^{n} \left(\int_0^{\Delta t} \mathrm{d}t N_i(0) e^{L_{ij_1}t} + \int_0^{\Delta t} \mathrm{d}t N_i(\Delta t) e^{L_{ij_2}t} + \ldots \int_0^{\Delta t} \mathrm{d}t N_i((f-1)\Delta t) e^{L_{ij_f}t} \right) \tag{4.9}$$

$$= \sum_{i=1}^{n} \sum_{k=1}^{f} \int_0^{\Delta t} \mathrm{d}t N_i\left((k-1)\Delta t\right) e^{L_{ij_k}t} \tag{4.10}$$

$$= \sum_{i=1}^{n} N_i(0) \sum_{k=1}^{f} \prod_{l=1}^{k-1} e^{L_{ij_l}\Delta t} \int_0^{\Delta t} \mathrm{d}t\, e^{L_{ij_k}\Delta t}. \tag{4.11}$$

Here we have chosen to shift the time in (4.9) to the primary interval to simplify the exponents and relabel $t' \to t$. This Term reflects the cost that must be minimized over the variables $\{j_k\} \in \{1, \ldots, f_m\}$ which specify the respective treatment for the k^{th} treatment interval to find the optimal treatment plan.

However, while optimizing over the treatment intervals, each previous treatment is known and we can calculate the surviving number of cells per cell type. Utilizing the equation for cell numbers (4.5) yields for the cost

$$K_\gamma = \sum_{i=1}^{n} N_i(0) \sum_{k=1}^{f} e^{\sum_{l=1}^{k-1} L_{ij_l} \Delta t} \int_0^{\Delta t} dt\, e^{L_{ij_k} t} \tag{4.12}$$

$$= \sum_{i=1}^{n} N_i(0) \sum_{k=1}^{f} e^{\sum_{l=1}^{k-1} L_{ij_l} \Delta t} \times \frac{e^{L_{ij_k} \Delta t} - 1}{L_{ij_k}} \,. \tag{4.13}$$

Formally, the best treatment $\gamma = \{j_1, j_2, \dots j_f\}$ is found by minimizing that cost function over all possible choices of $\{j_1, j_2, \dots j_f\}$. .

4.3 Solution Strategies for the Optimal Path

The minimization of the cost function (4.13) with brute force by testing out the entire parameter space of possible treatment schedules is not a desirable strategy for coarse discretizations. The space of all possible treatment schedules scales exponentially with the treatment intervals as as $m^{\frac{t}{\Delta t}}$ and therefore require an exponential runtime. Better solutions algorithm for the optimal treatment schedule that do not require an exponential run time are available by associating the optimizing problem with finding the shortest path in a graph.
Suppose a treatment of f_1 times drug D_1, ..., f_m times drug D_m has been administered, then we can identify the state of the system with a vertex in a grid with coordinates $\vec{f}$ resulting in $N_i^{\vec{f}}$ cells and then we label the accumulated cost of that treatment $K^{\vec{f}}$. Adding one more treatment interval with drug D_j shifts the system to an adjacent vertex at coordinates $\vec{f} + \vec{e}_i$ and yields cell numbers $\left\{N_i^{\vec{f}+\vec{e}_i}\right\}$ and the associated cost

$$K^{\vec{f}+\vec{e}_i} = K^{\vec{f}} + \sum_{i=1}^{n} N_i(0) e^{\sum_{l=1}^{f} L_{ij_l} \Delta t} \times \frac{e^{L_{ij} \Delta t} - 1}{L_{ij}} \tag{4.14}$$

$$= K^{\vec{f}} + \sum_{i=1}^{n} N_i^{\vec{f}} \times \frac{e^{L_{ij} \Delta t} - 1}{L_{ij}} \,. \tag{4.15}$$

We see that the cost difference between the two states $K^{\vec{f}+\vec{e}_i} - K^{\vec{f}}$ only depends on the number of cells of the first state and the growth rates of the chosen treatment. Hence the difference only requires local variables as opposed to the entire history of treatments or respectively the edges in the path. We can utilize this to define the costs associated with an edge in the graph

as the difference of the cost function between ending and starting vertex

$$K^{\vec{f}}(j) \coloneqq K^{\vec{f}+\vec{e}_i} - K^{\vec{f}} = \sum_{i=1}^{n} N_i^{\vec{f}} \times \frac{e^{L_{ij}\Delta t} - 1}{L_{ij}}. \tag{4.16}$$

This definition allows to calculate the cost for a path $\gamma = (j_1, \dots, j_f)$ not only via (4.13), but instead by summing over the costs of all edges within the path:

$$K_\gamma = \sum_{k=1}^{f} K^{\vec{\gamma}_k}(j_k), \tag{4.17}$$

with $\vec{\gamma}_k = \sum_{l=1}^{k-1} \vec{e}_{j_l}$, the vector of coordinates of path γ after k treatment intervals.
With this result the optimal treatment schedule can be determined by finding the shortest path between the origin $\vec{0}$, and final state $\vec{f}$ with the weights per edge defined by (4.16).

4.3.1 Solution with Dynamic Programming

Dynamic programming is commonly applied to optimization problems by breaking down a complex problem into simpler, more manageable subproblems, which is the core characteristic of dynamic programming [105, 106]. Crucially, these subproblems must be similar to each other and should further divide into even smaller subproblems, rather than representing different problems that merely contribute to the overall problem. When the solution to the main problem can be constructed from the solutions to its subproblems, this is formally known as an *optimal substructure* and guarantees that the dynamic programming procedure will find the shortest path in a graph.
Every optimization problem involves a series of decisions that need to be made to minimize costs. A simple criterion for recognizing an optimal substructure is as follows: Suppose you have a solution for an optimization problem consisting of N decisions. If the system is expanded to include an additional decision, only the optimization from step N to step $N + 1$ needs to be carried out, while the total solution can be obtained by combining the two. This characteristic means that there is no need to resolve the entire problem from scratch, which is the primary advantage of dynamic programming. Due to this nested subproblem structure, the function to be optimized is often expressed as a recursive formula starting from the main problem.

There are two primary approaches for solving problems with dynamic programming:

- *Top-down approach*: Starting with the main problem and breaking it down recursively into subproblems, we solve each subproblem once, storing each result. For subsequent steps, only unsolved subproblems are calculated until all are resolved.

- *Bottom-up approach*: Starting with the smallest subproblem and building up to the main problem, each subproblem is solved only once, with previously solved subproblem results readily available for use. Regardless of the chosen approach, dynamic programming evaluates all possible optimizations, ensuring that the optimal solution is found.

Applied to our shortest path problem defined by the weights in (4.16) we set up the recursion relation for the minimal cost of a path from the origin to a point in the grid with coordinates $\vec{f}$ as

$$K_{\min}^{\vec{f}} = \min_{j\in\{1,\dots,m\}} \left\{ K_{\min}^{\vec{f}-\vec{e}_j} + K^{\vec{f}-\vec{e}_j}(j) \right\}, \tag{4.18}$$

which also determines recursively the path by adding a step in j^{th} direction. Negative coordinates are excluded from the minimization and the termination condition reads for the cost of the trivial paths $K_{\min}^{\vec{0}} = 0$. We implement a solution algorithm that follows the chronology of the therapy ("bottom-up" approach). We begin at the origin (0,0) with the initial cell numbers $\{N_i(0)\}$, determine the costs $K^{\vec{f}(j)}$ for all $\prod_{j=1}^{m} f_j$ nodes and all m treatment options. For each point the minimal cost is computed iteratively "bottom-Up" by comparing the minimal cost plus treatment cost for every possible predecessor in accordance to recursion relation (4.18). Furthermore, the used medication to arrive at each point is saved to keep track of the entire treatment history that lead to each state with minimal possible cost. This procedure requires a runtime and memory of $\mathcal{O}(m \times f^m)$, which reflects the scaling of the number of edges in time discretizations f and number of treatments m. The final state $\vec{f} = (f_1, f_2, \dots f_m)^t$ is a required input for the dynamic programming and can be found by fixing a number of treatment intervals f and then minimizing the number of cells over the m-dimensional simplex with size f:

$$\vec{f} = \underset{\vec{f}\in\mathbb{N}_0^m;\|\vec{f}\|_1=f}{\operatorname{argmin}} \left\{ \sum_{i=1}^{n} N_i(0) e^{\sum_{j=1}^{m} L_{ij} f_j \Delta t} \right\} \tag{4.19}$$

We illustrate the result of this algorithm in figure 4.2 for an exemplary system consisting of $n = 2$ cell species $m = 2$ drugs with the parameters for initial population $\vec{N}(0)$ and growth rates L which correspond to half-life and doubling times T as

$$\vec{N}(0) = \begin{pmatrix} 1 \\ 2 \end{pmatrix}, L = \ln(2) \begin{pmatrix} -\frac{5}{6} & \frac{1}{26} \\ \frac{1}{74} & -\frac{10}{21} \end{pmatrix}, T = \begin{pmatrix} -1.2 & 26 \\ 74 & -2.1 \end{pmatrix}. \tag{4.20}$$

In this model system the population of cell type 1 dies with half-life 1.2 days under treatment D_1 while cell type 2 grows with doubling time 74 days. Under a treatment with D_2 cell type 2 decays with half-life 2.1 days while cell type 1 can recover and grows with doubling time 26 days. The growth rates satisfy the conditions (4.2) which means an effective treatment schedule of D_1 and D_2 exists to eradicate all cells.

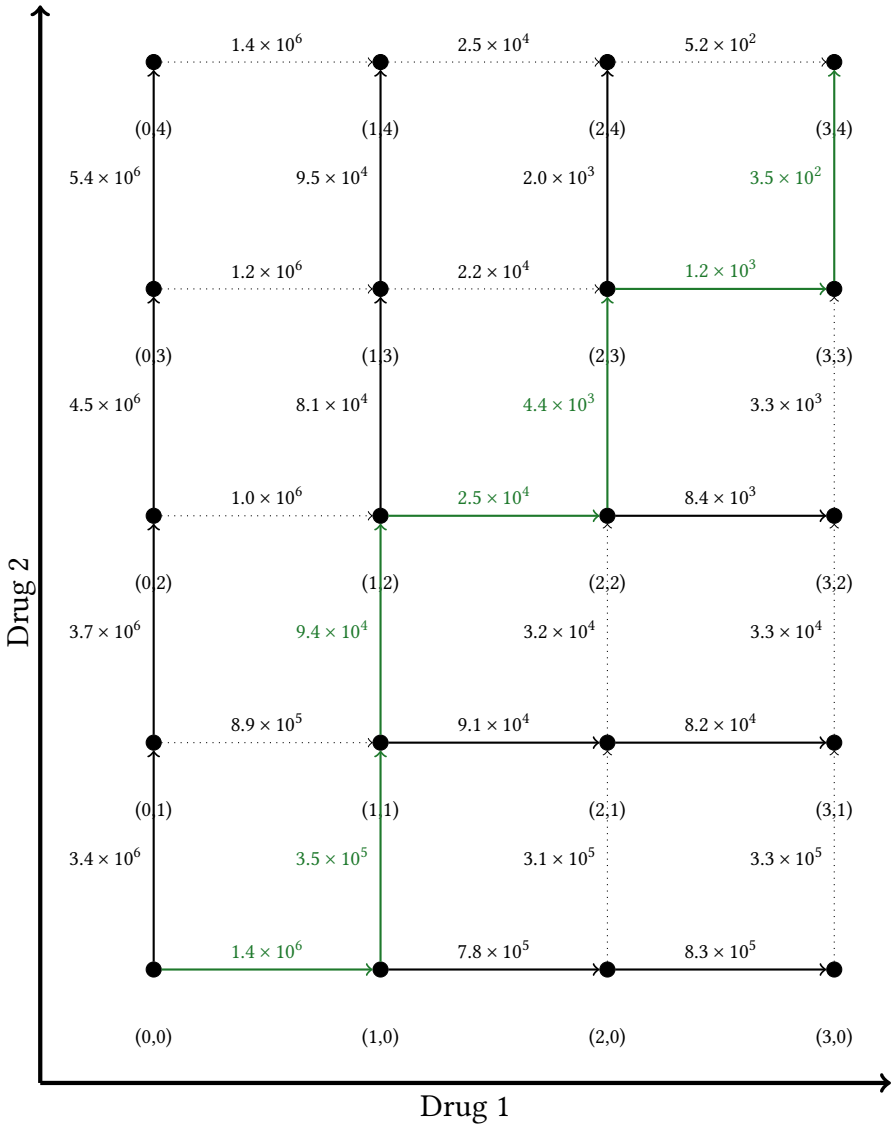

Figure 4.2: Exemplary solution of a two drug treatment scheme with dynamic programming

The exemplary graph from figure 4.1. Each edge is annotated with the associated cost according to (4.16) for an time discretization $\Delta t = 7$ days and exemplary initial population and growth rates specified in (4.20). The shortest path problem connecting the origin $(0, 0)$ to vertex $(3, 4)$ is solved with dynamic programming and bold arrows flowing into a vertex indicate lower total cost compared to any path including a dotted line. The total cost for the shortest path to any vertex can be determined by summing over all costs along bold edges in their reversed direction to the origin. The shortest path to the final vertex is colored in green and indicates the optimal treatment scheme: $\gamma = \{\mathrm{D}_1, \mathrm{D}_2, X_2, X_1, X_2, X_1, X_2\}$.

4.3.2 Solution with a Greedy Algorithm

After determining the optimal path, we proceed to simplify the solution using a streamlined greedy approach. While this method is computationally efficient, it does not inherently guarantee a globally optimal solution. Greedy algorithms tackle optimization problems by making a sequence of decisions, each affecting the objective function, according to a straightforward local decision rule—termed the greedy choice. The term "greedy" refers to the process of selecting the option that yields the most immediate benefit, such as minimizing cost or maximizing gain, without regard to subsequent steps. Although this approach provides a locally optimal solution at each decision point, it may not necessarily yield the overall global optimum.
Applying the greedy approach to the shortest path problem, we set up the greedy decision rule as

$$j^* = \underset{j\in\{1,\dots,m\}}{\operatorname{argmin}} \left\{ K^{\vec{f}}(j) \right\}, \quad K^{\vec{f}+\vec{e}_{j^*}} = K^{\vec{f}} + K^{\vec{f}}(j^*) \tag{4.21}$$

which determines the best next treatment option from a given starting state $\vec{f}$ and the respective cost. Starting from the origin with $K^{\vec{0}} = 0$, iterative repetitions of this decision rule will consecutively construct a path connecting the origin to the final state. Its advantage lies in the local decisions which do not require computing the costs for all possible edges, but only for m edges at each time step. Its runtime scales linear as $\mathcal{O}(mf)$. One major drawback is, that this algorithm does not necessarily determine the globally optimal path but only a local optimal path. This approach corresponds to always minimizing the cell numbers at each time step as opposed to enduring a higher number of cells for a period with the advantage of a lower cell number in the long run.
Unlike dynamic programming, which typically has a predefined endpoint $\vec{f}$, this approach does not inherently specify an ending state. To define the termination point, several strategies can be employed. One possibility is limiting the grid to the according dimensions and once the greedy algorithm approaches the boundaries it will inevitably run into the chosen final state. Alternatively one has the options to fix a final time, determine the treatment intervals as $f = \frac{t}{\Delta t}$ and let the greedy algorithm run and define that as its final state. Alternatively one can use cell number as final criterion, as soon as the total cell number falls below a threshold the algorithm is aborted. The result for a comparison of the greedy implementation compared to the dynamic programming is shown in figure 4.3.

4.4 Optimal Solutions for Two Subpopulations

In the following chapter, we analyze the optimal treatment paths in a two-dimensional framework, considering two distinct cell types and two corresponding drugs for treatment. This

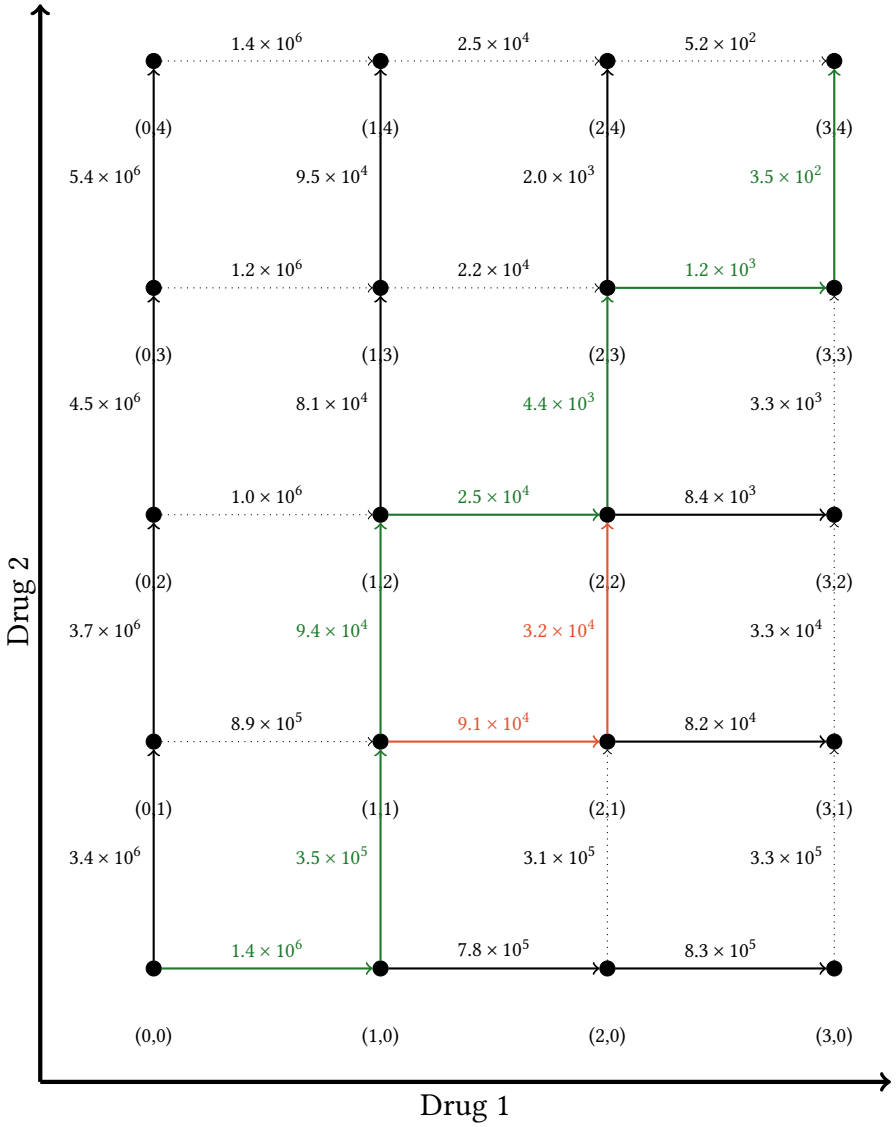

Figure 4.3: Comparison of an exemplary solutions of dynamic programming and greedy heuristic for a two drug treatment scheme

The exemplary graph with the dynamic programming solution from figure 4.2. Each edge is annotated with the associated cost according to (4.16) for an time discretization $\Delta t = 7$ days and exemplary initial population and growth rates specified in (4.20). The shortest path problem connecting the origin $(0, 0)$ to vertex $(3, 4)$ is solved with dynamic programming and bold arrows flowing into a vertex indicate lower total cost compared to any path including a dotted line. The total cost for the shortest path to any vertex can be determined by summing over all costs along bold edges in their reversed direction to the origin.The shortest path determined by dynamic programming to the final vertex is colored in green and indicates the optimal treatment scheme: $\gamma_{\text{opt}} = \{D_1, D_2, D_2, D_1, D_2, D_1, D_2\}$. The greedy solution deviates in one vertex and the respective two edges are colored in orange. The greedy solution for the treatment is given by $\gamma_{\text{greedy}} = \{D_1, D_2, D_1, D_2, D_2, D_1, D_2\}$.

setting is particularly intriguing, as it can simulate a treatment strategy for a tumor that has already undergone initial therapy. In this scenario, the tumor is no longer composed of the original, sensitive cells; instead, it consists of resistant cell types, such as persistent cells and R1-resistant cells.
We will compare the performance of the greedy algorithm and dynamic programming within this framework. By leveraging insights from the greedy algorithm, we aim to further characterize the elements of an optimal treatment plan.

4.4.1 Comparison in Performance of Dynamic and Greedy Approach

The greedy algorithm proves to be computationally more efficient than the dynamic programming. The difference in runtime $\mathcal{O}(mf)$ vs $\mathcal{O}(mf^m)$ is even more distinct in higher grid dimensions or respectively more available treatment options. But what is the cost for choosing the more efficient heuristic? As shown in figure 4.3, the determined path by the greedy heuristic deviates from the optimal path with the lowest cost and bears a higher number of cell divisions and therefore also a higher number of aquired mutations and an enhanced risk to develop a de novo resistance mechanism.
We analyzed the relative cost differences between locally optimal path from the greedy implementation and the global optimal path from the dynamic implementation $\Delta K = \frac{K_{\text{local}} - K_{\text{global}}}{K_{\text{global}}}$ for the same optimization problem in two dimensions for varying time discretizations. The system consists of two cell types and two drugs with parameters specified in (4.20) and the simulation has been continued until the total number of cells dropped to $N = N_1 + N_2 < 1$. The full result is displayed in figure 4.4.
We find that the majority of realizations yields different costs, meaning that the paths determined by dynamic programming and the greedy algorithm deviate. In contrast to that, in all simulations most of the edges of the optimal path match with the edges from the local optimal path determined from the greedy algorithm. Only isolated steps deviate leading to the observed difference in ΔK which results in only minuscule relative difference that ranges between 10^{-2}-10^{-8}. It is noteworthy, that matching costs occur more frequently in the regime of coarser time discretizations. This is of no surprise and there are two reasons for that. A coarser time discretizations means fewer steps in the simulation, which go along with a lower chance to step in a non optimal direction. Furthermore, each step is weighted with an exponentially larger cost, hence making it more unlikely that such a step in the wrong direction occurs.
The orders of magnitude between the relative difference has its origin in the exponential nature of the problem. While cells treated early in the simulation appear in great numbers, they exponentially drop with time or respectively treatment steps. Wrong steps early in the simulation yield a large relative difference, while later missteps yield exponentially smaller cost differences. Moreover, thanks to the exponential nature of the problem, edges far away from the optimal path have a large imbalance in cell numbers. That means treating a dis-

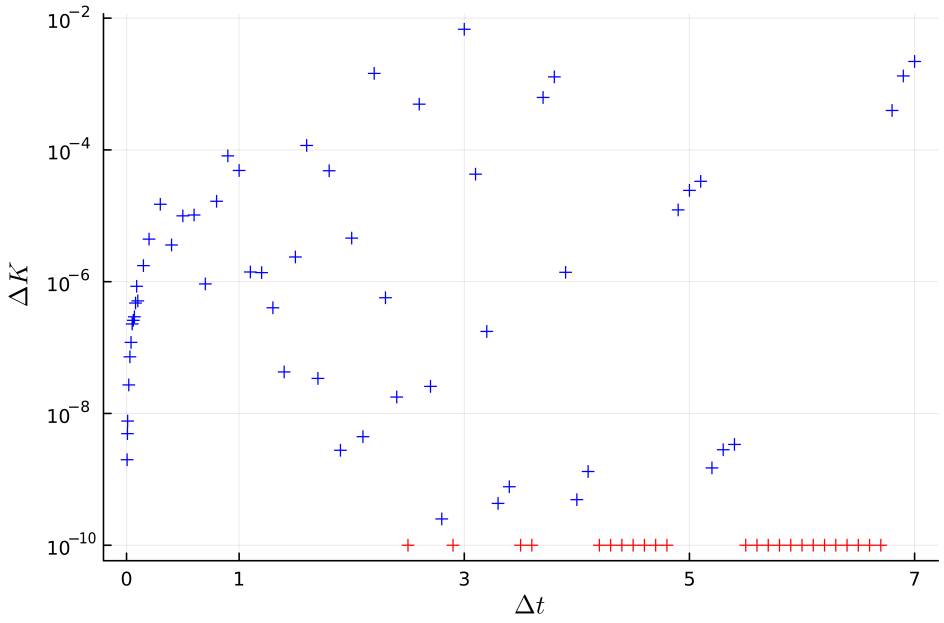

Figure 4.4: Relative difference in performance of greedy and dynamic programming
The treatment path in our grid model with parameters defined in (4.20) has been solved for a global optimum with dynamic programming and locally with a greedy algorithm for varying time discretizations Δt. The relative cost difference between both paths $\Delta K = \frac{K_{\text{local}} - K_{\text{global}}}{K_{\text{global}}}$ is plotted vs. time discretization Δt. Inputs that lead to equal costs and resulted in the same paths, are visualized in red with $\Delta K = 10^{-10}$ for visibility. Thanks to Noah Elbracht for creating this figure [103].

proportionally higher cell number is more effective and will reduce the total number of cells more than its competitor which is lower in cell number. That causes edges leading to the optimal path to be lower in cost as opposed to edges leading further away from the optimal path which are higher in cost. Therefore, the local optimal solution cannot deviate far from the optimal path.
In the limit of small time discretizations, deviations still occur but their effect on the cost is lower resulting in a series of results that appear to converge to zero. We conclude that the local solution provided by the greedy programming is indeed a good approximation for the time-consuming dynamic programming, particularly to investigate the optimal path for small time discretizations.

4.4.2 Greedy Decision Rule

The major decision rule that shapes the optimal path of the therapy schedule is governed by cell numbers, and expected cell number changes within the next treatment interval. In this

chapter we will refine that expression and give a quantitative rule to determine which cell type should be treated against.
If one cell type rises in number compared to the other this makes treating this particular cell type more attractive, given the growth rates support this. For every growth matrix L, given a curative treatment is possible according to the condition in , there is a threshold where the ratio of $\frac{N_1}{N_2}$ grows so large under continued treatment against species 2 that a switch to treatment 1 is favourable. The point when this switch becomes more favourable is precisely quantified by $K^{\vec{f}}(1)$ and $K^{\vec{f}}(2)$. We set them equal and solve for the ratio of cell numbers per species as

$$K^{\vec{f}}(1) = \sum_{i=1}^{2} N_i^{\vec{f}} \times \frac{e^{L_{i1}\Delta t} - 1}{L_{i1}} \stackrel{!}{=} \sum_{i=1}^{2} N_i^{\vec{f}} \times \frac{e^{L_{i2}\Delta t} - 1}{L_{i1}} = K^{\vec{f}}(2) \tag{4.22}$$

$$\Rightarrow \frac{N_1^{\vec{f}}}{N_2^{\vec{f}}} = \frac{\frac{e^{L_{22}\Delta t}-1}{L_{22}} - \frac{e^{L_{21}\Delta t}-1}{L_{21}}}{\frac{e^{L_{11}\Delta t}-1}{L_{11}} - \frac{e^{L_{12}\Delta t}-1}{L_{12}}} =: r_{12}(\Delta t). \tag{4.23}$$

Note that the greedy ratio $r_{12}(\Delta t)$ is independent of the position on the grid, meaning it does not depend on the treatment history that led to the current state under analysis. This ratio now serves as a decision criterion for the greedy algorithm, relying solely on cell counts and system parameters. At the end of each treatment interval, the algorithm can either make decisions based on the rule specified in equation (4.19), or it may follow the alternative rules outlined below:

- If the ratio of cell numbers $\frac{N_1}{N_2} > r_{12}(\Delta t)$ then treat against species 1
- If the ratio of cell numbers $\frac{N_1}{N_2} < r_{12}(\Delta t)$ then treat against species 2

While this is only a trivial alteration of the rule, it becomes interesting in the limit of infinitesimal time discretizations, or continuous time

$$r_0 := \lim_{\Delta t \to 0} r_{12}(\Delta t) = \frac{L_{22} - L_{21}}{L_{11} - L_{12}}\,. \tag{4.24}$$

This result implies that whenever species 1 becomes dominant, it should be targeted for treatment. Similarly, species 2 should be treated if it becomes dominant. In continuous time, these transitions occur infinitely often. Consequently, the strategy aims to maintain the relative proportions of the species at a stable level, specifically at the ratio r_0.

4.4.3 Population and Treatment Dynamics

In any practical in vivo treatment scenario, there will be finite discretization times Δt. While directly comparing the cell ratio to the greedy ratio may not yield the precise decision rule

needed to achieve the optimal path, it provides an approximation that is close enough to offer intuitive insight into the system dynamics. The species undergoing treatment will experience exponential decay, while the untreated species will simultaneously recover and grow exponentially. This continues until the cell ratio surpasses the greedy threshold $r_{12}(\Delta t)$.

This process creates a seemingly repeating sawtooth pattern, which persists until the expected alternating pattern is suddenly disrupted. Cell numbers from such a simulation, using the system parameters given in equation (4.20), are shown in Figure 4.5b.

Initially, there is a phase where the starting conditions favor treatment against one cell type over multiple consecutive periods. Following this phase, a regular sequence of alternating treatment choices emerges, during which the cell counts of each species oscillate in a sawtooth pattern. The total cell population is influenced by both rising and falling terms, resulting in a subtle but noticeable zigzag pattern. Because the treatment choice is based on the ratio of cell counts and switches when the imbalance crosses the greedy threshold, each species and the overall cell count decay at the same effective rate λ_{eff} over time. Based on constant cell ratios we can further quantify the observations made in 4.5b.
Given a -possibly infinitely- long treatment pattern $f\Delta t$ that consists of a share of η drug 1 and respectively a share of $(1-\eta)$ drug 2 but results in the same ratio of cells after its application, then we can equalize the cell ratios to obtain

$$\frac{N_1(t=0)}{N_2(t=0)} \stackrel{!}{=} \frac{N_1(f\Delta t)}{N_2(f\Delta t)} = \frac{N_1(0)\mathrm{e}^{f\Delta t(\eta L_{11}+(1-\eta)L_{12}}}{N_2(0)\mathrm{e}^{f\Delta t(\eta L_{21}+(1-\eta)L_{22}}}. \tag{4.25}$$

Cell numbers and treatment length cancel out and we are left with an equation defining the share for each treatment as

$$\Rightarrow \quad 1 = \mathrm{e}^{\eta L_{11}+(1-\eta)L_{12}-(\eta L_{21}-(1-\eta)L_{22}} \tag{4.26}$$

$$\Rightarrow \quad \eta = \frac{L_{22}-L_{12}}{\sigma}, \quad (1-\eta) = \frac{L_{11}-L_{21}}{\sigma} \tag{4.27}$$

$$\text{with} \quad \sigma = L_{11}-L_{12}-L_{21}+L_{22}. \tag{4.28}$$

After an initializing treatment to reach the according cell ratios for the first time, the optimal path tries to realize a treatment schedule which divides into a share of η for treatment 1 and $(1-\eta)$ for treatment 2. in an infinitely long treatment these fractions can be perfectly realized. However in finite treatment durations, it is usually impossible to perfectly approximate the rational (or even real) numbers η by the ratio of treatments $\frac{f_1}{f}, \frac{f_2}{f}$.
This type of problem is ever-present and is brought to our attention every four years. The Earth takes approximately 365.24219 days to orbit the sun. When dividing the calendar into years of 365 days and leap years of 366 days, a periodic pattern emerges: three regular years

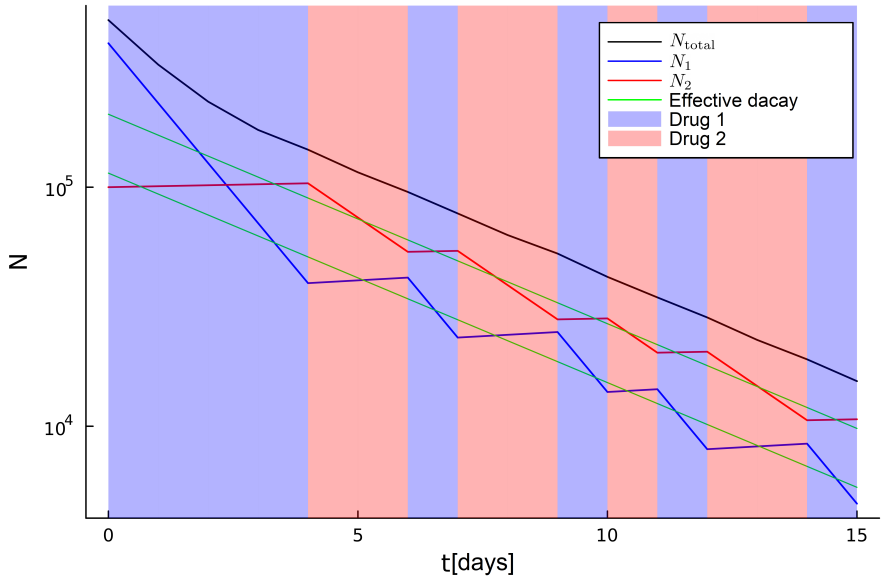

(A) Initial 15 days under the optimal treatment

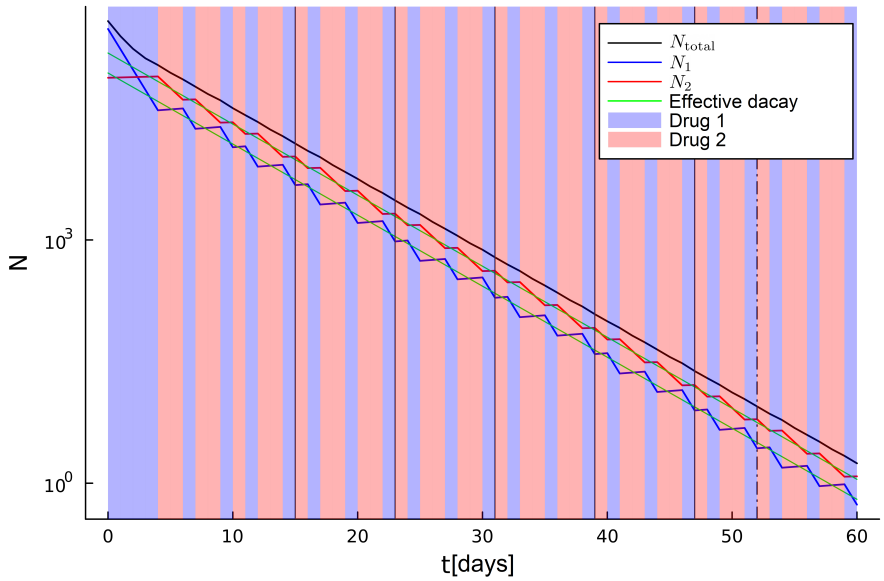

(B) Full 60 days treatment under the optimal treatment

Figure 4.5: Population dynamics of a two species system under the optimal treatment

The figure shows the cell counts of both species (blue and red) in a two-species system under the optimal treatment plan derived using dynamic programming (see 4.3.1) and their sum as the total cell count in black.The cell counts for each species following the effective rate, λ_{eff} are plotted in green. The background shading in blue and red represents the active drug targeting the corresponding cell type. The top plot focuses on the initial 15 days of treatment, while the bottom plot displays the full 60-day period. Vertical black lines indicate the repeating pattern of an 8-day cycle, that resets after 52 intervals. Thanks to Noah Elbracht for the creation of this figure [103].

followed by a leap year. This continues until the accumulated inaccuracies from approximating a rational number (365.24219) with natural numbers become too large. At that point, we adjust the cycle by skipping a leap year every 100 years, breaking the usual pattern to correct for the discrepancy.
Precisely such a thing happens in figure 4.5b. Between day 16 and 48 we see four repeating patterns of length 8 with sequence (D2,D1,D2,D2,D1,D2,D2,D1), which has a small perturbation in its 5^{th} cycle. Such a repeating sequence results in a share of drug 1 administered of $\frac{3}{8}$ which is very close to the ideal value with the rates inserted $\eta \approx 0.378$.
We can further quantify the effective exponential decay observed in figure 4.5. As any finite time treatment tries to approximate the shares η and $(1-\eta)$ we just need to weight the growth rates for any cell type with the shares of their treatment to arrive at the effective rate as

$$\lambda_{\text{eff}} = L_{\text{i}1}\eta + L_{\text{i}2}(1-\eta) = \frac{L_{11}L_{22} - L_{12}L_{21}}{\sigma} = \frac{\det(L)}{\sigma}. \tag{4.29}$$

This decay rate represents the effective reduction in both individual cell types and the total cell population. Initially, an overabundance of species 1 makes it optimal to administer its corresponding drug over four consecutive periods. During this initial phase, focusing exclusively on species 1 results in a higher decay rate, as the significantly lower population of species 2 means that its growth has minimal impact on the total cell count. As a result, the total decay rate is initially dominated by species 1 under its respective treatment. Over time, as the population of species 2 begins to grow and reach comparable levels, the overall decay rate gradually aligns with the effective rate. This transition marks the beginning of alternating treatment cycles, as the system adjusts to maintain the balance between both species.

This elegant and straightforward result highlights the true power of this model. By precisely fine-tuning the treatment intervals for each drug, it enables an optimal approach for treating a given tumor under specific model assumptions. Any deviation from the optimal treatment sequence described in equation (4.27) results in a reduced decay rate for at least one cell type. Due to the exponential nature of cancer cell growth, even a slight reduction in the decay rate can significantly increase the total number of cell divisions, raising the risk of mutations that confer drug resistance.
Furthermore, a faster decay rate implies that the treatment can be completed sooner, which offers substantial benefits. A shorter treatment duration minimizes the patient's exposure to potentially harmful side effects and reduces the overall costs for both the patient and the healthcare system. For comparison, the effective decay rate in the optimal path shown in figure 4.5 yields $\lambda_{\text{eff}} \approx -0.2$. That rate can be compared to a naive case of treatment equal partitioned treatment intervals, that results in one species dominating the population and the other dying out. The overall decay rate for the population then assumes the value $\lambda \approx -0.16$, which is is approximately 20% smaller than λ_{eff} and thus requiring a 20% longer therapy to achieve the same result.
This optimized approach thus not only enhances treatment efficiency but also contributes to patient well-being and financial sustainability.

4.5 Conclusion

Summary

In Chapter 4, we develop a model to optimize the treatment of heterogeneous cancer populations under varied treatment schedules. This model incorporates a cost metric, which is based on the cumulative cell population over the treatment duration, aiming to reduce the risk of evolving new resistance mechanisms and minimize the tumor burden on the patient. This cost metric provides a tool to compare different treatment schedules by minimizing the total cancer cell count over time. Additionally, alternative cost metrics could weigh distinct cell types differently if they contribute disproportionately to patient morbidity or have elevated mutation rates.
To solve this model, we identify treatment schedules by paths on a weighted, directed rectangular graph. We introduce two solution strategies to find the shortest path and thus the optimal treatment schedule. The computational more demanding using dynamic programming in polynomial runtime as $\mathcal{O}(m \times f^m)$, which utilizes the optimal substructure of the model and always yields the shortest paths. And an approximation using a greedy heuristic, which yields very close results near the shortest paths in linear runtime as $\mathcal{O}(mf)$. Notably, as the time interval Δt becomes infinitesimally small, the two solutions converge.
As long as the condition for a curative treatment in (4.2) is met, the model can predict an optimal path. If the condition is not met, a curative treatment is not possible and the model can still be utilized to find a treatment schedule that minimizes cell numbers throughout the treatment or respectively prolongs the treatment as long as possible. Based on the treatment matrix L we can estimate the shares of treatment durations for each drug in an alternating schedule and this can then be incorporated with Δt into repeating treatment cycles. This further allows to estimate the effective decay rate λ_{eff}. The effective decay rate reflects the true strength of this model, as a the optimal selection of treatments in a changing schedule will eradicate an overall tumor quicker then any other naive guess, such as uniform treatment intervals for each drug.

Discussion

While promising, this model has limitations, primarily the absence of pharmacokinetics in its design. The model assumes immediate drug potency and an instant loss of effect upon discontinuation. In reality, drugs often require time to achieve peak concentration [107] and continue to exert effects even after cessation. This simplification in the model thus favors rapid treatment switches as quick as Δt permits, and its predicted results will thus deviate the more from real results in the regime of small Δt.

Additionally, accurate application of this model relies on known growth and decay rates for each cancer cell type under each treatment option. This includes not only the primary cancer

cells and their resistant variants but also the drug-tolerant persister, which are critical to account for due to their role in long-term survival under prolonged therapy.

Chapter 5

Conclusion and Outlook

Hidden genomic factors play a crucial role in tumor evolution under targeted therapy, and understanding these factors is essential. Knowledge of specific driver genes enables the development of targeted therapies that inhibit these critical pathways, effectively striking at the cancer's Achilles' heel. However, from this point forward, pre-existing resistance mutations and epigenetic persistence mechanisms become key factors in shaping tumor evolution. If all possible resistance and persistence mechanisms are known, tumor evolution becomes predictable, allowing targeted measures against these cell populations.

In this thesis, we studied the evolution of cancer cells under targeted therapy from both experimental and theoretical perspectives. We analyzed resistance mechanisms in PC9 cells treated with EGFR inhibition therapy using erlotinib. Thus, expanded the already existing spectrum of three identified resistance mechanisms the EGFR T790M gatekeeper mutation, the NRAS Q61R mutation, focal amplification of HGF by another resistance mechanism that results from an overexpression of WWTR1 (see chapter 2.4) and is responsible for the Resistance in R4 and is sensitive to dasatinib and dactolisib. A combination of four drugs—erlotinib, osimertinib, trametinib, and dasatinib—successfully targets both wild-type and resistant cells, with no fifth resistance type emerging in populations treated with EOTD. Estimates of mutation and death rates, along with measurements of birth rates for each resistant variant, allowed us to predict the expected number of pre-existing mutants in a cancer cell population (see chapter 2.5). Each isolated resistant cell line displayed a stable resistance mechanism, with no reversion to the parental phenotype.

This stability distinguishes resistant cells from drug tolerant persisters. Through epigenetic modifications, DTPs can withstand targeted cancer therapies and, upon cessation of treatment, revert to their highly proliferative wild-type state. Under treatment, DTPs either grow slowly with erlotinib or decay exponentially under EOTD. An experiment involving *mock* medium changes confirmed that the exponential decay observed with EOTD was due to the treatment's efficacy, rather than washing off the persister cells (see figure 3.6). Besides combined EOTD treatment, we identified two vulnerabilities of DTPs: inhibiting anti-apoptotic proteins effectively treats DTPs in PC9 cells but is ineffective in HCC827 cells, while inhibiting the

anti-ferroptotic protein GPX4 successfully eradicates DTPs across multiple cell lines(see chapter 3.2).
The birth and death processes shape the evolution of both cancer cells and DTPs, with birth-death dynamics increasing the variance in cell populations compared to a death-only process with the same net growth rate. This variance in DTP numbers is critical for therapy, as targeted treatment must continue until the last resistant or persistent cell is eradicated (see chapter 3.3.2). Otherwise, prematurely ending treatment could allow surviving cells to proliferate and lead to tumor relapse.

Understanding the mechanisms underlying cancer evolution enables the design of targeted therapies tailored to specific tumors. Such therapies may involve polytherapy like EOTD, where feasible, or an alternating schedule of smaller combinations targeting resistant cells and DTPs separately. An effective therapy schedule aims to target the heterogeneous population as efficiently as possible while minimizing the risk of de novo mutation acquisition. We proposed a general model for evaluating the costs associated with different therapy schedules. Minimizing the cost function across possible schedules can be approached as a shortest-path problem on a weighted rectangular graph. With dynamic programming or a greedy heuristic, combined with comprehensive information on drug efficacy for each cell type and estimates on their initial population sizes, we can identify optimal therapy schedules. The results indicate that treatment intervals should be adjusted based on drug efficacy to achieve the best outcomes in minimal time. Further analysis and reliable quantitative predictions for therapeutic predictions, show the limitations of this general model and illustrate where further research is needed.

Prospects for optimizing cancer therapy schedules through modeling

An alternating targeted therapy schedule that addresses resistant cells would represent a significant improvement over current therapies, where a single drug targeting the cancer driver is administered until a macroscopic tumor relapses. The next logical step is to simulate and optimize a patient's therapy schedule before prescribing drugs. A model that predicts such a therapy schedule should include the pharmacokinetics of the drugs to account for the time until the drug becomes effective and the time until it loses effect.

Furthermore, drugs have varying potency in every patient, and thus precise modeling is only possible to a limited extent. Therefore, the determined optimal therapy schedule will inevitably differ from the actual optimal schedule for an individual patient. Regular check-ups with an oncologist can help reduce the difference between both schedules. If an imbalance in cell numbers compared to the expected optimal ratio is detected, the estimated rates for the drug treatment matrix should be updated. One way to do this is to replace fixed values for the rates with probability distributions, using experience from previous patients as prior knowledge, and use Bayes' theorem to update them with measurements from check-ups to

further refine the distributions around the true values for any given patient.
While the grid model aims to reduce the probability of de novo mutations leading to potentially untreatable resistance mechanisms, it cannot eliminate this risk entirely. To address this, a potential addition could be incorporating a chemotherapy cycle into the therapy schedule. This chemotherapy cycle should aim to target cancer cells nonspecifically, including any cells with new mutations leading to untreatable resistance mechanisms.

Beyond these adaptations to the grid model, we are further refining and assessing EGFR-driven cancer cell responses to test and benchmark the grid model's performance in vitro and to evaluate its effectiveness.

GLOSSARY

Adenocarcinoma A type of cancer that forms in the glandular cells of epithelial tissue, which are responsible for secreting mucus or other fluids. Adenocarcinoma can occur in various organs, such as the lungs, colon, breast, and pancreas. It is one of the most common types of cancer and typically develops in tissues that line or cover internal organs.

(Gene) amplification A process by which the number of copies of a particular gene is increased in a cell. This can lead to the overexpression of the gene, often resulting in an abnormal increase in the production of its protein product. Gene amplification is frequently observed in cancer cells, where it can drive tumor growth and resistance to therapies by enhancing the expression of oncogenes.

Apoptosis A process of programmed cell death in multicellular organisms. It is a controlled mechanism by which cells self-destruct when they are no longer needed or are damaged.

Bcl-2 A protein that regulates cell death (apoptosis), playing a role in cell survival. Inhibition of Bcl-2 has been explored as a strategy to eliminate persister cells in cancer treatment. Bcl-2 inhibition with navitoclax effectively eradicates EOTD Persister.

BCR-ABL A fusion gene resulting from a translocation between chromosomes 9 and 22, creating an abnormal tyrosine kinase that drives chronic myeloid leukemia (CML). It is targeted by drugs like imatinib and dasatinib.

CML (chronic myeloid leukemia) A type of cancer that affects the bone marrow and blood, characterized by the overproduction of myeloid cells. It is driven by the BCR-ABL fusion gene.

Cellular receptor A protein found on the surface or inside of a cell that binds to specific molecules (ligands), such as hormones, neurotransmitters, or drugs. Upon binding, the receptor triggers a series of intracellular signals that regulate various cellular processes, including growth, differentiation, and metabolism.

Crystal violet (CV) stain A common histological stain used to visualize cells by binding to DNA and proteins. It is often used for staining adherent cells in cell culture, providing a clear contrast for microscopy and scans of macroscopic cell clusters.

Dasatinib A tyrosine kinase inhibitor that targets BCR-ABL, SRC family kinases, and c-KIT, used in the treatment of chronic myeloid leukemia (CML) and acute lymphoblastic leukemia (ALL). Moreover, it is used to treat R3 and R4.

Dactolisib A dual inhibitor of PI3K and mTOR pathways, involved in regulating cell growth and survival, used to treat R4.

Driver (mutation, gene) A genetic change crucial for the growth and survival of cancer cells. These drivers can be mutations in genes that regulate key cellular processes, such as signaling pathways, or involve gene amplifications that lead to increased cell division. Molecular drivers are central to cancer progression, often acting as targets for specific treatments aimed at halting the underlying mechanisms that fuel tumor growth.

Drug tolerant persister cells (DTPs) A subpopulation of cancer cells that survive targeted therapy without having acquired genetic mutations that confer resistance. These cells can eventually revert to a drug-sensitive state and are characterized by their epigenetic alterations.

Dynamic programming An algorithmic technique used to solve optimization problems by breaking them down into simpler subproblems. In the context of this thesis, it is used to determine the optimal treatment paths for cancer therapies.

EGFR (Epidermal growth factor receptor) A receptor tyrosine kinase that, when activated by its ligand EGF, triggers cellular signaling pathways involved in cell growth, proliferation, and survival. Mutations in EGFR can lead to uncontrolled cell growth and result in cancer.

Epigenetic changes Heritable changes in gene expression that do not involve changes to the underlying DNA sequence. Epigenetic alterations are implicated in the survival of DTPs.

EOTD A combination of drugs: Erlotinib, Osimertinib, Trametinib, and Dasatinib—used to combat drug resistance in cancer cells, particularly in the context of drug-tolerant persisters.

Erlotinib A tyrosine kinase inhibitor (TKI) used to target EGFR in cancers such as NSCLC. It binds to the EGFR kinase domain and prevents activation of the downstream signaling pathways.

ErbB family A group of receptor tyrosine kinases that includes EGFR/ErbB1, HER2/ErbB2, HER3/ErbB3, and HER4/ErbB4. These receptors play a critical role in the regulation of cell growth and differentiation.

Ferroptosis A form of regulated cell death characterized by the accumulation of lipid peroxides. It is different from apoptosis and is implicated in cancer cell death mechanisms.

GPX4 (glutathione peroxidase 4) An enzyme that protects cells from oxidative stress and lipid peroxidation. It is involved in the survival of drug-tolerant persisters in cancer therapy. Its Inhibition with RSL3 effectively treats EOTD persisters.

Growth factor A signaling protein that stimulates cell growth, proliferation, and differentiation by binding to specific cellular receptors. Growth factors play essential roles in processes like tissue repair, embryonic development, and immune response. Examples include epidermal growth factor (EGF) and hepatocyte growth Factor (HGF).

Greedy heuristic A heuristic approach to solving problems by making a locally optimal choice at each step. It is faster than dynamic programming but may not yield a globally optimal solution.

HCC827 A human non-small cell lung cancer (NSCLC) cell line harboring an activating mutation in the EGFR gene. HCC827 is commonly used in cancer research to study the efficacy of EGFR-targeted therapies and the development of drug resistance.

HGF (hepatocyte growth factor) A protein that stimulates cell growth, movement, and differentiation by binding to the MET receptor. It is involved in the resistance of cancer cells to EGFR inhibitors.

Iterative exhaustion A strategy described in the thesis for isolating and identifying multiple resistance mechanisms in a sequential manner by repeatedly exposing cells to treatment and selecting for resistant clones.

(Protein) kinase An enzyme that catalyzes the transfer of a phosphate group from a donor molecule, like ATP, to specific proteins. This process, known as phosphorylation, often induces a conformational change in the target protein, activating or regulating its function. Protein kinases play a key role in cell signaling, controlling various cellular processes such as growth, division, and metabolism.

MAPK (mitogen-activated protein kinase) pathway Another key signaling pathway that regulates cell division, differentiation, and survival. It is activated by growth factors like EGFR and is implicated in cancer progression.

MEK (mitogen-activated protein kinase kinase) A key enzyme in the MAPK signaling pathway and possible way of resistance mechanism against EGFR treatment.

MET (mesenchymal-epithelial transition factor) A receptor tyrosine kinase that binds to its ligand, hepatocyte growth factor (HGF), to activate signaling pathways involved in cell growth, survival, and migration. A focal amplification of MET is the resistance driver for R3.

Metastasis The process by which cancer cells spread from the original (primary) tumor to other parts of the body, forming secondary tumors. These metastases consist of cells that are similar to the primary tumor, meaning if lung cancer spreads to the liver, the metastatic cells in the liver are lung cancer cells, not liver cells. Metastasis is a key

characteristic of malignant tumors and is often associated with more advanced stages of cancer.

Mutation Rate The probability of a mutation occurring in a single nucleotide of the DNA per cell division.

Neoplasm An abnormal growth of tissue caused by uncontrolled cell division. Neoplasms can be benign (non-cancerous) or malignant (cancerous). Malignant neoplasms, or tumors, have the potential to invade surrounding tissues and metastasize to distant parts of the body. Neoplasms are commonly referred to as tumors and are often categorized by the type of cells they originate from.

NSCLC (non-small cell lung cancer) The most common type of lung cancer, often driven by mutations in genes like EGFR. It represents a major focus of targeted cancer therapies.

Oncogene A gene that, when mutated or overexpressed, has the potential to cause normal cells to become cancerous is called proto-oncogene. After the alteration it is denoted as oncogene.

Osimertinib A third-generation EGFR inhibitor designed to target both the original EGFR mutations and the T790M resistance mutation in non-small cell lung cancer. Used to treat R1, R2, R3, R4 cells.

Overexpression The process by which a gene is expressed at higher than normal levels, resulting in an excess of its corresponding protein. Overexpression can occur due to gene amplification, mutations in regulatory regions, or other alterations in cellular mechanisms. In cancer, overexpression of certain genes, such as oncogenes, can lead to uncontrolled cell growth and proliferation, contributing to tumor development and progression.

Passage A process in cell culture where cells are seeded, allowed to expand, and then split into new vessels once the population reaches confluence. This cycle ensures the continuous growth and maintenance of the cell line by preventing overcrowding and depletion of nutrients.

PC9 A specific type of non-small cell lung cancer (NSCLC) cell line used in research to study EGFR mutations and drug resistance mechanisms. The main model organism in this thesis.

Phosphorylation A biochemical process in which a phosphate group is added to a molecule, typically a protein. This modification is often catalyzed by enzymes called kinases and can activate or deactivate a protein's function through conformal changes. Phosphorylation plays a key role in regulating cellular activities such as metabolism, cell signaling, and division.

PI3K/AKT/mTOR pathway A signaling pathway that regulates cell growth, proliferation, survival, and metabolism. Dysregulation of this pathway is commonly associated with cancer and is a target for many cancer therapies.

Resistance mechanism A genetic or epigenetic alteration that allows cancer cells to survive treatment with drugs that were initially effective. Resistance mechanisms can be pre-existing or acquired during therapy.

Senescence Cellular state where cells stop dividing permanently but remain metabolically active. Triggered by stressors like DNA damage, it serves as a cancer defense by halting the proliferation of damaged cells.

SRC kinases A family of non-receptor tyrosine kinases involved in regulating various cellular processes, including growth, differentiation, and survival.

Tepotinib A MET inhibitor used to target cancer cells with MET amplification or overexpression, which can contribute to resistance to EGFR inhibitors. Used to treat R3 and R4 cells.

Trametinib A MEK inhibitor that targets the MEK1 and MEK2 enzymes, part of the MAPK pathway, used to treat R2, R3, R4 cells

Tumor heterogeneity The presence of genetically diverse cancer cells within the same tumor, which complicates treatment as different subpopulations may respond differently to therapies.

Whole exome sequencing A genomic technique that sequences all protein-coding regions (exons) of the genome. These exons make up about 1-2% of the genome. Thus, being much cheaper compared to sequencing the entire genome. Whole exome sequencing is used to identify genetic variants associated with diseases, and determine the resistance mechanism of cancer cells surviving their respective treatment.

List of Figures

List of Tables

Bibliography

[1] S. Mukherjee, *The Emperor of All Maladies: A Biography of Cancer* (Scribner, 2010), ISBN: 9781439181713.

[2] I. for Health Metrics and E. (IHME), *Global Burden of Disease: Cancers*, https://ourworldindata.org/grapher/leading-cause-of-death, With minor processing by Our World in Data, Seattle, United States, 2024.

[3] R. A. Weinberg, *The Biology of Cancer*, 3rd (W. W. Norton & Company, 2023), ISBN: 9780393887655.

[4] P. C. Nowell, "The Clonal Evolution of Tumor Cell Populations," Science **194**, 23 (1976) DOI: 10.1126/science.959840.

[5] L. Sobin, M. Gospodarowicz, and C. Wittekind, *TNM Classification of Malignant Tumours*, Uicc International Union Against Cancer (John Wiley & Sons, 2009), ISBN: 9781444332414.

[6] S. Salvatori, I. Marafini, F. Laudisi, G. Monteleone, and C. Stolfi, "Helicobacter pylori and Gastric Cancer: Pathogenetic Mechanisms," International Journal of Molecular Sciences **24**, DOI: 10.3390/ijms24032895, ISSN: 1422-0067 (2023) DOI: 10.3390/ijms24032895.

[7] E. Pešut, A. Đukić, L. Lulić, J. Skelin, I. Šimić, N. Milutin Gašperov, V. Tomaić, I. Sabol, and M. Grce, "Human Papillomaviruses-Associated Cancers: An Update of Current Knowledge," Viruses **13**, DOI: 10.3390/v13112234, ISSN: 1999-4915 (2021) DOI: 10.3390/v13112234.

[8] W. Ill et al., "Lung adenocarcinoma promotion by air pollutants," Nature **616**, 159 (2023) DOI: 10.1038/s41586-023-05874-3.

[9] J. Ngeow and C. Eng, "Precision medicine in heritable cancer: when somatic tumour testing and germline mutations meet," npj Genomic Medicine **1**, 15006 (2016) DOI: 10.1038/npjgenmed.2015.6.

[10] F. Lalloo and D. G. Evans, "Familial Breast Cancer," Clinical Genetics **82**, 105 (2012) DOI: https://doi.org/10.1111/j.1399-0004.2012.01859.x.

[11] O. M. Valencia, S. E. Samuel, R. K. Viscusi, T. S. Riall, L. A. Neumayer, and H. Aziz, "The Role of Genetic Testing in Patients With Breast Cancer: A Review," JAMA Surgery **152**, 589, ISSN: 2168-6254 (2017) DOI: 10.1001/jamasurg.2017.0552.

[12] T. Sawicki, M. Ruszkowska, A. Danielewicz, E. Niedźwiedzka, T. Arłukowicz, and K. E. Przybyłowicz, "A Review of Colorectal Cancer in Terms of Epidemiology, Risk Factors, Development, Symptoms and Diagnosis," Cancers **13**, DOI: 10.3390/cancers13092025, ISSN: 2072-6694 (2021) DOI: 10.3390/cancers13092025.

[13] A. Leiter, R. R. Veluswamy, and J. P. Wisnivesky, "The global burden of lung cancer: current status and future trends," Nature Reviews Clinical Oncology **20**, 624 (2023) DOI: 10.1038/s41571-023-00798-3.

[14] D. Hanahan and R. A. Weinberg, "The Hallmarks of Cancer," Cell **100**, 57, ISSN: 0092-8674 (2000) DOI: https://doi.org/10.1016/S0092-8674(00)81683-9.

[15] D. Hanahan and R. A. Weinberg, "Hallmarks of Cancer: The Next Generation," Cell **144**, 646, ISSN: 0092-8674 (2011) DOI: https://doi.org/10.1016/j.cell.2011.02.013.

[16] O. Warburg and S. Minami, "Versuche an überlebendem Carcinomgewebe," Klinische Wochenzeitschrift **2**, 776 (1923).

[17] O. Warburg, F. Wind, and E. Negelein, "The Metabolism of Tumors in the Body," Journal of General Physiology **8**, 519 (1927) DOI: 10.1085/jgp.8.6.519.

[18] M. G. Vander Heiden, L. C. Cantley, and C. B. Thompson, "Understanding the Warburg effect: the metabolic requirements of cell proliferation," Science **324**, 1029 (2009) DOI: 10.1126/science.1160809.

[19] L. Sompayrac, *How the Immune System Works*, The How it Works Series (Wiley, 2019), ISBN: 9781119542124.

[20] Y. Zhang and Z. Zhang, "The history and advances in cancer immunotherapy: understanding the characteristics of tumor-infiltrating immune cells and their therapeutic implications," Cellular & Molecular Immunology **17**, 807 (2020) DOI: 10.1038/s41423-020-0488-6.

[21] E. Mortaz, P. Tabarsi, D. Mansouri, A. Khosravi, J. Garssen, A. Velayati, and I. M. Adcock, "Cancers Related to Immunodeficiencies: Update and Perspectives," Frontiers in Immunology **7**, 365 (2016) DOI: 10.3389/fimmu.2016.00365.

[22] S. I. Grivennikov, F. R. Greten, and M. Karin, "Immunity, Inflammation, and Cancer," Cell **140**, 883, ISSN: 0092-8674 (2010) DOI: https://doi.org/10.1016/j.cell.2010.01.025.

[23] S. Negrini, V. G. Gorgoulis, and T. D. Halazonetis, "Genomic instability — an evolving hallmark of cancer," Nature Reviews Molecular Cell Biology **11**, 220 (2010) DOI: 10.1038/nrm2858.

[24] L. Falzone, S. Salomone, and M. Libra, "Evolution of Cancer Pharmacological Treatments at the Turn of the Third Millennium," Frontiers in Pharmacology **9**, 1300 (2018) DOI: 10.3389/fphar.2018.01300.

[25] P. Curie and M. Curie, "Sur la radioactivité provoquée par les rayons de Bécquerel," Comp. Rendus Acad. Sci. **129**, 714 (1899).

[26] E. H. Grubbe, "Priority in the therapeutic use of X-rays," Radiology **21**, 156 (1933).

[27] T. Ohno, "Particle radiotherapy with carbon ion beams," EPMA Journal **4**, 9 (2013) DOI: 10.1186/1878-5085-4-9.

[28] R. R. Wilson, "Radiological Use of Fast Protons," Radiology **47**, 487, ISSN: 0033-8419 (1946) DOI: 10.1148/47.5.487.

[29] L. Zhong, Y. Li, L. Xiong, W. Wang, M. Wu, T. Yuan, W. Yang, C. Tian, Z. Miao, T. Wang, and S. Yang, "Small molecules in targeted cancer therapy: advances, challenges, and future perspectives," Signal Transduction and Targeted Therapy **6**, 201 (2021) DOI: 10.1038/s41392-021-00572-w.

[30] I. B. Weinstein, "Addiction to Oncogenes–the Achilles Heel of Cancer," Science **297**, 63 (2002) DOI: 10.1126/science.1073096.

[31] N. Wagle, C. Emery, M. F. Berger, M. J. Davis, A. Sawyer, P. Pochanard, S. M. Kehoe, C. M. Johannessen, L. E. Macconaill, W. C. Hahn, M. Meyerson, and L. A. Garraway, "Dissecting therapeutic resistance to RAF inhibition in melanoma by tumor genomic profiling," Journal of Clinical Oncology **29**, Erratum in: J Clin Oncol. 2024 Mar 10;42(8):976. doi: 10.1200/JCO.24.00017, 3085 (2011) DOI: 10.1200/JCO.2010.33.2312.

[32] A. B. Turke, K. Zejnullahu, Y.-L. Wu, Y. Song, D. Dias-Santagata, E. Lifshits, L. Toschi, A. Rogers, T. Mok, L. Sequist, N. I. Lindeman, C. Murphy, S. Akhavanfard, B. Y. Yeap, Y. Xiao, M. Capelletti, A. J. Iafrate, C. Lee, J. G. Christensen, J. A. Engelman, and P. A. Jänne, "Preexistence and Clonal Selection of MET Amplification in EGFR Mutant NSCLC," Cancer Cell **17**, 77, ISSN: 1535-6108 (2010) DOI: https://doi.org/10.1016/j.ccr.2009.11.022.

[33] P. Nowell, "Discovery of the Philadelphia chromosome: a personal perspective," Journal of Clinical Investigation **117**, 2033 (2007) DOI: 10.1172/JCI31771.

[34] N. Heisterkamp, J. R. Stephenson, J. Groffen, P. F. Hansen, A. de Klein, C. R. Bartram, and G. C. Grosveld, "Localization of the c-abl oncogene adjacent to a translocation break point in chronic myelocytic leukaemia," Nature **306**, 239 (1983).

[35] J. Groffen, J. R. Stephenson, N. Heisterkamp, A. de Klein, C. R. Bartram, and G. Grosveld, "Philadelphia chromosomal breakpoints are clustered within a limited region, bcr, on chromosome 22," Cell **36**, 93, ISSN: 0092-8674 (1984) DOI: https://doi.org/10.1016/0092-8674(84)90077-1.

[36] T. G. Lugo, A.-M. Pendergast, A. J. Muller, and O. N. Witte, "Tyrosine Kinase Activity and Transformation Potency of *bcr-abl* Oncogene Products," Science **247**, 1079 (1990) DOI: 10.1126/science.2408149.

[37] E. Buchdunger, J. Zimmermann, H. Mett, T. Meyer, M. Müller, B. J. Druker, and N. B. Lydon, "Inhibition of the Abl protein-tyrosine kinase in vitro and in vivo by a 2-phenylaminopyrimidine derivative," Cancer research **56**, 100 (1996).

[38] T. Schindler, W. Bornmann, P. Pellicena, W. T. Miller, B. Clarkson, and J. Kuriyan, "Structural Mechanism for STI-571 Inhibition of Abelson Tyrosine Kinase," Science **289**, 1938 (2000) DOI: 10.1126/science.289.5486.1938.

[39] P. Cohen, "Protein kinases — the major drug targets of the twenty-first century?" Nature Reviews Drug Discovery **1**, 309 (2002) DOI: 10.1038/nrd773.

[40] N. Iqbal and N. Iqbal, "Imatinib: a breakthrough of targeted therapy in cancer," Chemotherapy Research and Practice **2014**, Epub 2014 May 19, 357027 (2014) DOI: 10.1155/2014/357027.

[41] M. Agrawal, R. J. Garg, J. Cortes, and A. Quintás-Cardama, "Tyrosine Kinase Inhibitors: The First Decade," Current Hematologic Malignancy Reports **5**, 70 (2010) DOI: 10.1007/s11899-010-0045-y.

[42] J. Senapati, K. Sasaki, G. C. Issa, J. H. Lipton, J. P. Radich, E. Jabbour, and H. M. Kantarjian, "Management of chronic myeloid leukemia in 2023 – common ground and common sense," Blood Cancer Journal **13**, 58 (2023) DOI: 10.1038/s41408-023-00823-9.

[43] D. M. Pardoll, "The blockade of immune checkpoints in cancer immunotherapy," Nature Reviews Cancer **12**, 252 (2012) DOI: 10.1038/nrc3239.

[44] R. Yao, C. Xie, and X. Xia, "Recent progress in mRNA cancer vaccines," Human Vaccines & Immunotherapeutics **20**, Epub 2024 Jan 28, 2307187 (2024) DOI: 10.1080/21645515.2024.2307187.

[45] E. Blass and P. Ott, "Advances in the development of personalized neoantigen-based therapeutic cancer vaccines," Nature Reviews Clinical Oncology **18**, 215 (2021) DOI: 10.1038/s41571-020-00460-2.

[46] L. Rojas et al., "Personalized RNA neoantigen vaccines stimulate T cells in pancreatic cancer," Nature **618**, Epub 2023 May 10, 144 (2023) DOI: 10.1038/s41586-023-06063-y.

[47] L. Hayflick and P. Moorhead, "The serial cultivation of human diploid cell strains," Experimental Cell Research **25**, 585, ISSN: 0014-4827 (1961) DOI: https://doi.org/10.1016/0014-4827(61)90192-6.

[48] R. Skloot, *The Immortal Life of Henrietta Lacks* (Picador, London, England, 2024), ISBN: 9781509877027.

[49] S. Schmitz, *Der Experimentator: Zellkultur*, 4th ed., Experimentator (Springer Spektrum Berlin, Heidelberg, 2020), ISBN: 978-3-662-58950-2, DOI: 10.1007/978-3-662-58951-9.

[50] S. M. Mennen, C. Alhambra, C. L. Allen, M. Barberis, S. Berritt, T. A. Brandt, A. D. Campbell, J. Castañón, A. H. Cherney, M. Christensen, D. B. Damon, J. Eugenio de Diego, S. García-Cerrada, P. García-Losada, R. Haro, J. Janey, D. C. Leitch, L. Li, F. Liu, P. C. Lobben, D. W. C. MacMillan, J. Magano, E. McInturff, S. Monfette, R. J. Post, D. Schultz, B. J. Sitter, J. M. Stevens, I. I. Strambeanu, J. Twilton, K. Wang, and M. A. Zajac, "The Evolution of High-Throughput Experimentation in Pharmaceutical Development and Perspectives on the Future," Organic Process Research & Development **23**, 1213 (2019) DOI: 10.1021/acs.oprd.9b00140.

[51] H. Satam, K. Joshi, U. Mangrolia, S. Waghoo, G. Zaidi, S. Rawool, R. P. Thakare, S. Banday, A. K. Mishra, G. Das, and S. K. Malonia, "Next-Generation Sequencing Technology: Current Trends and Advancements," Biology **12**, DOI: 10.3390/biology12070997, ISSN: 2079-7737 (2023) DOI: 10.3390/biology12070997.

[52] A. Ullrich and J. Schlessinger, "Signal transduction by receptors with tyrosine kinase activity," Cell **61**, 203, ISSN: 0092-8674 (1990) DOI: https://doi.org/10.1016/0092-8674(90)90801-K.

[53] Y. Yarden, "The EGFR family and its ligands in human cancer: signalling mechanisms and therapeutic opportunities," European Journal of Cancer **37**, 3, ISSN: 0959-8049 (2001) DOI: https://doi.org/10.1016/S0959-8049(01)00230-1.

[54] Yarden, Y. and Sliwkowski, M., "Untangling the erbb signalling network," Nature Reviews Molecular Cell Biology **2**, 127 (2001) DOI: 10.1038/35052073.

[55] C. Braicu, M. Buse, C. Busuioc, R. Drula, D. Gulei, L. Raduly, A. Rusu, A. Irimie, A. G. Atanasov, O. Slaby, C. Ionescu, and I. Berindan-Neagoe, "A Comprehensive Review on MAPK: A Promising Therapeutic Target in Cancer," Cancers **11**, DOI: 10.3390/cancers11101618, ISSN: 2072-6694 (2019) DOI: 10.3390/cancers11101618.

[56] A. Glaviano, A. Foo, H. Lam, K. Yap, W. Jacot, R. Jones, H. Eng, M. Nair, P. Makvandi, B. Geoerger, M. Kulke, R. Baird, J. Prabhu, D. Carbone, C. Pecoraro, D. Teh, G. Sethi, V. Cavalieri, K. Lin, N. Javidi-Sharifi, E. Toska, M. Davids, J. Brown, P. Diana, J. Stebbing, D. Fruman, and A. Kumar, "PI3K/AKT/mTOR signaling transduction pathway and targeted therapies in cancer," Molecular Cancer **22**, 138 (2023) DOI: 10.1186/s12943-023-01827-6.

[57] O. Khajuria and N. Sharma, "Epigenetic targeting for lung cancer treatment via CRISPR/Cas9 technology," Advances in Cancer Biology - Metastasis **3**, 100012, ISSN: 2667-3940 (2021) DOI: https://doi.org/10.1016/j.adcanc.2021.100012.

[58] T. Arao, H. Fukumoto, M. Takeda, T. Tamura, N. Saijo, and K. Nishio, "Small in-frame deletion in the epidermal growth factor receptor as a target for ZD6474," Cancer Research **64**, 9101 (2004).

[59] T. J. Lynch, D. W. Bell, R. Sordella, S. Gurubhagavatula, R. A. Okimoto, B. W. Brannigan, P. L. Harris, S. M. Haserlat, J. G. Supko, F. G. Haluska, D. N. Louis, D. C. Christiani, J. Settleman, and D. A. Haber, "Activating Mutations in the Epidermal Growth Factor Receptor Underlying Responsiveness of Non–Small-Cell Lung Cancer to Gefitinib," New England Journal of Medicine **350**, 2129 (2004) DOI: 10.1056/NEJMoa040938.

[60] J. G. Paez, P. A. Jänne, J. C. Lee, S. Tracy, H. Greulich, S. Gabriel, P. Herman, F. J. Kaye, N. Lindeman, T. J. Boggon, K. Naoki, H. Sasaki, Y. Fujii, M. J. Eck, W. R. Sellers, B. E. Johnson, and M. Meyerson, "EGFR Mutations in Lung Cancer: Correlation with Clinical Response to Gefitinib Therapy," Science **304**, 1497 (2004) DOI: 10.1126/science.1099314.

[61] M. Lynch, "Rate, molecular spectrum, and consequences of human mutation," Proceedings of the National Academy of Sciences of the United States of America **107**, 961 (2010) DOI: 10.1073/pnas.0912629107.

[62] S. Kobayashi, T. J. Boggon, T. Dayaram, P. A. Jänne, O. Kocher, M. Meyerson, B. E. Johnson, M. J. Eck, D. G. Tenen, and B. Halmos, " EGFR Mutation and Resistance of Non–Small-Cell Lung Cancer to Gefitinib," New England Journal of Medicine **352**, 786 (2005) DOI: 10.1056/NEJMoa044238.

[63] W. Pao, V. A. Miller, K. A. Politi, G. J. Riely, R. Somwar, M. F. Zakowski, M. G. Kris, and H. Varmus, "Acquired Resistance of Lung Adenocarcinomas to Gefitinib or Erlotinib Is Associated with a Second Mutation in the EGFR Kinase Domain," PLOS Medicine **2**, null (2005) DOI: 10.1371/journal.pmed.0020073.

[64] D. A. E. Cross, S. E. Ashton, S. Ghiorghiu, C. Eberlein, C. A. Nebhan, P. J. Spitzler, J. P. Orme, M. R. V. Finlay, R. A. Ward, M. J. Mellor, G. Hughes, A. Rahi, V. N. Jacobs, M. R. Brewer, E. Ichihara, J. Sun, H. Jin, P. Ballard, K. Al-Kadhimi, R. Rowlinson, T. Klinowska, G. H. P. Richmond, M. Cantarini, D.-W. Kim, M. R. Ranson, and W. Pao, "AZD9291, an irreversible EGFR TKI, overcomes T790M-mediated resistance to EGFR inhibitors in lung cancer," Cancer Discovery **4**, 1046 (2014) DOI: 10.1158/2159-8290.CD-14-0337.

[65] E. Hodis, I. R. Watson, G. V. Kryukov, S. T. Arold, M. Imielinski, J. P. Theurillat, E. Nickerson, D. Auclair, L. Li, C. Place, D. Dicara, A. H. Ramos, M. S. Lawrence, K. Cibulskis, A. Sivachenko, D. Voet, G. Saksena, N. Stransky, R. C. Onofrio, W. Winckler, K. Ardlie, N. Wagle, J. Wargo, K. Chong, D. L. Morton, K. Stemke-Hale, G. Chen, M. Noble, M. Meyerson, J. E. Ladbury, M. A. Davies, J. E. Gershenwald, S. N. Wagner, D. S. Hoon, D. Schadendorf, E. S. Lander, S. B. Gabriel, G. Getz, L. A. Garraway, and L. Chin, "A landscape of driver mutations in melanoma," Cell **150**, 251 (2012) DOI: 10.1016/j.cell.2012.06.024.

[66] M. H. Huang, J. H. Lee, Y. J. Chang, H. H. Tsai, Y. L. Lin, A. M. Lin, and J. C. Yang, "MEK inhibitors reverse resistance in epidermal growth factor receptor mutation lung cancer cells with acquired resistance to gefitinib," Molecular Oncology **7**, 112 (2013) DOI: 10.1016/j.molonc.2012.09.002.

[67] D. B. Solit, L. A. Garraway, C. A. Pratilas, A. Sawai, G. Getz, A. Basso, Q. Ye, J. M. Lobo, Y. She, I. Osman, T. R. Golub, J. Sebolt-Leopold, W. R. Sellers, and N. Rosen, "BRAF mutation predicts sensitivity to MEK inhibition," Nature **439**, 358 (2006) DOI: 10.1038/nature04304.

[68] J. A. Engelman, K. Zejnullahu, T. Mitsudomi, Y. Song, C. Hyland, J. O. Park, N. Lindeman, C.-M. Gale, X. Zhao, J. Christensen, T. Kosaka, A. J. Holmes, A. M. Rogers, F. Cappuzzo, T. Mok, C. Lee, B. E. Johnson, L. C. Cantley, and P. A. Jänne, "MET Amplification Leads to Gefitinib Resistance in Lung Cancer by Activating ERBB3 Signaling," Science **316**, 1039 (2007) DOI: 10.1126/science.1141478.

[69] M. Lindauer and A. Hochhaus, "Dasatinib," Recent Results in Cancer Research **201**, 27 (2014) DOI: 10.1007/978-3-642-54490-3_2.

[70] G. Martin, "The hunting of the Src," Nature Reviews Molecular Cell Biology **2**, 467 (2001) DOI: 10.1038/35073094.

[71] F. Lo Sardo, S. Strano, and G. Blandino, "YAP and TAZ in Lung Cancer: Oncogenic Role and Clinical Targeting," Cancers **10**, DOI: 10.3390/cancers10050137, ISSN: 2072-6694 (2018) DOI: 10.3390/cancers10050137.

[72] M. Pfeifer, J. Brammeld, S. Price, J. Pilling, D. Bhavsar, A. Farcas, J. Bateson, A. Sundarrajan, R. Miragaia, N. Guan, S. Arnold, L. Tariq, M. Grondine, S. Talbot, M. Guerriero, D. O'Neill, J. Young, C. Company, S. Dunn, H. Thorpe, M. Martin, K. Maratea, D. Barrell, M. Ahdesmaki, J. Mettetal, F. G. Centre, J. Brownell, and U. McDermott, "Genome-wide CRISPR screens identify the YAP/TEAD axis as a driver of persister cells in EGFR mutant lung cancer," Communications Biology **7**, 497 (2024) DOI: 10.1038/s42003-024-06190-w.

[73] K. J. Kurppa, Y. Liu, C. To, T. Zhang, M. Fan, A. Vajdi, E. H. Knelson, Y. Xie, K. Lim, P. Cejas, A. Portell, P. H. Lizotte, S. B. Ficarro, S. Li, T. Chen, H. M. Haikala, H. Wang, M. Bahcall, Y. Gao, S. Shalhout, S. Boettcher, B. H. Shin, T. Thai, M. K. Wilkens, M. L. Tillgren, M. Mushajiang, M. Xu, J. Choi, A. A. Bertram, B. L. Ebert, R. Beroukhim, P. Bandopadhayay, M. M. Awad, P. C. Gokhale, P. T. Kirschmeier, J. A. Marto, F. D. Camargo, R. Haq, C. P. Paweletz, K. K. Wong, D. A. Barbie, H. W. Long, N. S. Gray, and P. A. Jänne, "Treatment-Induced Tumor Dormancy through YAP-Mediated Transcriptional Reprogramming of the Apoptotic Pathway," Cancer Cell **37**, 104 (2020) DOI: 10.1016/j.ccell.2019.12.006.

[74] J. M. Lamar, Y. Xiao, E. Norton, Z. G. Jiang, G. M. Gerhard, S. Kooner, J. S. A. Warren, and R. O. Hynes, "SRC tyrosine kinase activates the YAP/TAZ axis and thereby drives tumor growth and metastasis," Journal of Biological Chemistry **294**, 2302 (2019) DOI: 10.1074/jbc.RA118.004364.

[75] N. Müller, C. Lorenz, J. Ostendorp, F. S. Heisel, U. P. Friese, M. Cartolano, D. Plenker, H. Tumbrink, A. Heimsoeth, P. Baedeker, J. Weiss, S. Ortiz-Cuaran, R. Büttner, M. Peifer, R. K. Thomas, M. L. Sos, J. Berg, and J. Brägelmann, "Characterizing Evolutionary Dynamics Reveals Strategies to Exhaust the Spectrum of Subclonal Resistance in EGFR-Mutant Lung Cancer," Cancer Research **83**, 2471, ISSN: 0008-5472 (2023) DOI: 10.1158/0008-5472.CAN-22-2605.

[76] E. M. Levine, Y. Becker, C. W. Boone, and H. Eagle, "CONTACT INHIBITION, MACROMOLECULAR SYNTHESIS, AND POLYRIBOSOMES IN CULTURED HUMAN DIPLOID FIBROBLASTS," Proceedings of the National Academy of Sciences **53**, 350 (1965) DOI: 10.1073/pnas.53.2.350.

[77] M. Watabe, A. Nagafuchi, S. Tsukita, and M. Takeichi, "Induction of polarized cell-cell association and retardation of growth by activation of the E-cadherin-catenin adhesion system in a dispersed carcinoma line.," Journal of Cell Biology **127**, 247, ISSN: 0021-9525 (1994) DOI: 10.1083/jcb.127.1.247.

[78] T. Payen, J. Trédaniel, L. Moreau, S. Larivé, J. Le Treut, C. Nocent, S. Hominal, V. Grangeon, J.-L. Bizec, O. Molinier, and D. Debieuvre, "Real world data of efficacy and safety of erlotinib as first-line TKI treatment in EGFR mutation-positive advanced non-small cell lung cancer: Results from the EGFR-2013-CPHG study," Respiratory Medicine and Research **80**, 100795, ISSN: 2590-0412 (2021) DOI: https://doi.org/10.1016/j.resmer.2020.100795.

[79] L. van der Maaten and G. Hinton, "Visualizing Data using t-SNE," Journal of Machine Learning Research **9**, 2579 (2008).

[80] M. J. Hangauer, V. S. Viswanathan, M. J. Ryan, D. Bole, J. K. Eaton, A. Matov, J. Galeas, H. D. Dhruv, M. E. Berens, S. L. Schreiber, F. McCormick, and M. T. McManus, "Drug-tolerant persister cancer cells are vulnerable to GPX4 inhibition," Nature **551**, 247 (2017) DOI: 10.1038/nature24297.

[81] H. F. Cabanos and A. N. Hata, "Emerging Insights into Targeted Therapy-Tolerant Persister Cells in Cancer," Cancers **13**, DOI: 10.3390/cancers13112666, ISSN: 2072-6694 (2021) DOI: 10.3390/cancers13112666.

[82] N. Müller, J. Brägelmann, C. Lorenz, U. P. Michel, D. Plenker, S. Ortiz-Cuaran, J. Weiss, R. Büttner, M. Peifer, R. K. Thomas, M. L. Sos, and J. Berg, "In vitro model for resistance in oncogene-dependent tumors at the limit of radiological detectability," bioRxiv, DOI: 10.1101/756593 (2019) DOI: 10.1101/756593.

[83] M. Ducasse and M. A. Brown, "Epigenetic aberrations and cancer," Molecular Cancer **5**, 60 (2006) DOI: 10.1186/1476-4598-5-60.

[84] D. Mancarella and C. Plass, "Epigenetic signatures in cancer: proper controls, current challenges and the potential for clinical translation," Genome Medicine **13**, 23 (2021) DOI: 10.1186/s13073-021-00837-7.

[85] S. V. Sharma, D. Y. Lee, B. Li, M. P. Quinlan, F. Takahashi, S. Maheswaran, U. McDermott, N. Azizian, L. Zou, M. A. Fischbach, K. K. Wong, K. Brandstetter, B. Wittner, S. Ramaswamy, M. Classon, and J. Settleman, "A chromatin-mediated reversible drug-tolerant state in cancer cell subpopulations," Cell **141**, 69 (2010) DOI: 10.1016/j.cell.2010.02.027.

[86] M. Russo, M. Chen, E. Mariella, H. Peng, S. K. Rehman, E. Sancho, A. Sogari, T. S. Toh, N. Q. Balaban, E. Batlle, R. Bernards, M. J. Garnett, M. Hangauer, E. Leucci, J.-C. Marine, C. A. O'Brien, Y. Oren, E. E. Patton, C. Robert, S. M. Rosenberg, S. Shen, and A. Bardelli, "Cancer drug-tolerant persister cells: from biological questions to clinical opportunities," Nature Reviews Cancer **24**, 694 (2024) DOI: 10.1038/s41568-024-00737-z.

[87] A. Hata, M. J. Niederst, H. L. Archibald, M. Gomez-Caraballo, F. M. Siddiqui, H. E. Mulvey, Y. E. Maruvka, F. Ji, H.-e. C. Bhang, V. K. Radhakrishna, G. Siravegna, H. Hu, S. Raoof, E. Lockerman, A. Kalsy, D. Lee, C. L. Keating, D. A. Ruddy, L. J. Damon, A. S. Crystal, C. Costa, Z. Piotrowska, A. Bardelli, A. J. Iafrate, R. I. Sadreyev, F. Stegmeier, G. Getz, L. V. Sequist, A. C. Faber, and J. A. Engelman, "Tumor cells can follow distinct evolutionary paths to become resistant to epidermal growth factor receptor inhibition," Nature Medicine **22**, 262 (2016) DOI: 10.1038/nm.4040.

[88] M. Ramirez, S. Rajaram, R. J. Steininger, D. Osipchuk, M. A. Roth, L. S. Morinishi, L. Evans, W. Ji, C.-H. Hsu, K. Thurley, S. Wei, A. Zhou, P. R. Koduru, B. A. Posner, L. F. Wu, and S. J. Altschuler, "Diverse drug-resistance mechanisms can emerge from drug-tolerant cancer persister cells," Nature Communications **7**, 10690 (2016) DOI: 10.1038/ncomms10690.

[89] J. Huang, L. Meng, B. Yang, S. Sun, Z. Luo, and H. Chen, "Safety Profile of Epidermal Growth Factor Receptor Tyrosine Kinase Inhibitors: A Disproportionality Analysis of FDA Adverse Event Reporting System," Scientific Reports **10**, 4803 (2020) DOI: 10.1038/s41598-020-61571-5.

[90] S. J. Welsh and P. G. Corrie, "Management of BRAF and MEK inhibitor toxicities in patients with metastatic melanoma," Therapeutic Advances in Medical Oncology **7**, 122 (2015) DOI: 10.1177/1758834014566428.

[91] Z. Nekoukar, M. Moghimi, and E. Salehifar, "A narrative review on adverse effects of dasatinib with a focus on pharmacotherapy of dasatinib-induced pulmonary toxicities," Blood Research **56**, 229 (2021) DOI: 10.5045/br.2021.2021117.

[92] A. W. Tolcher, P. LoRusso, J. Arzt, T. A. Busman, G. Lian, N. S. Rudersdorf, C. A. Vanderwal, W. Kirschbrown, K. D. Holen, and L. S. Rosen, "Safety, efficacy, and pharmacokinetics of navitoclax (ABT-263) in combination with erlotinib in patients with advanced solid tumors," Cancer Chemotherapy and Pharmacology **76**, 1025 (2015) DOI: 10.1007/s00280-015-2883-8.

[93] E. M. Bertino, R. D. Gentzler, S. Clifford, J. Kolesar, A. Muzikansky, E. B. Haura, Z. Piotrowska, D. R. Camidge, T. E. Stinchcombe, C. Hann, J. Malhotra, L. C. Villaruz, C. P. Paweletz, C. L. Lau, L. Sholl, N. Takebe, J. A. Moscow, G. I. Shapiro, P. A. Jänne, and G. R. Oxnard, "Phase IB Study of Osimertinib in Combination with Navitoclax in EGFR-mutant NSCLC Following Resistance to Initial EGFR Therapy (ETCTN 9903)," Clinical Cancer Research **27**, 1604 (2021) DOI: 10.1158/1078-0432.CCR-20-4084.

[94] R. B. Corcoran, K. T. Do, J. E. Kim, J. M. Cleary, A. R. Parikh, O. O. Yeku, N. Xiong, C. D. Weekes, J. Veneris, L. G. Ahronian, G. Mauri, J. Tian, B. L. Norden, A. G. Michel, E. E. Van Seventer, G. Siravegna, K. Camphausen, G. Chi, I. J. Fetter, J. S. Brugge, H. Chen, N. Takebe, R. T. Penson, D. Juric, K. T. Flaherty, R. J. Sullivan, J. W. Clark, R. S. Heist, U. A. Matulonis, J. F. Liu, and G. I. Shapiro, "Phase I/II Study of Combined BCL-xL and MEK Inhibition with Navitoclax and Trametinib in KRAS or NRAS Mutant Advanced Solid Tumors," Clinical Cancer Research **30**, 1739 (2024) DOI: 10.1158/1078-0432.CCR-23-3135.

[95] X. Jiang, B. R. Stockwell, and M. Conrad, "Ferroptosis: mechanisms, biology and role in disease," Nature Reviews Molecular Cell Biology **22**, 266 (2021) DOI: 10.1038/s41580-020-00324-8.

[96] J. T. Randolph, M. J. O'Connor, F. Han, C. W. Hutchins, Y. A. Siu, M. Cho, Y. Zheng, J. A. Hickson, J. L. Markley, V. Manaves, M. Algire, K. A. Baker, A. M. Chapman, S. M. Gopalakrishnan, S. C. Panchal, K. Foster-Duke, D. F. Stolarik, A. Kempf-Grote, D. Dammeier, S. Fossey, Q. Sun, C. Sun, Y. Shen, M. J. Dart, W. M. Kati, A. Lai, A. J. Firestone, and M. E. Kort, "Discovery of a Potent Chloroacetamide GPX4 Inhibitor with Bioavailability to Enable Target Engagement in Mice, a Potential Tool Compound for Inducing Ferroptosis In Vivo," Journal of Medicinal Chemistry **66**, PMID: 36877935, 3852 (2023) DOI: 10.1021/acs.jmedchem.2c01415.

[97] B. Alberts, A. Johnson, J. Lewis, M. Raff, K. Roberts, and P. Walter, *Molecular Biology of the Cell*, 4th (Garland Science, New York, 2002).

[98] D. T. Gillespie, "Exact stochastic simulation of coupled chemical reactions," The Journal of Physical Chemistry **81**, 2340 (1977) DOI: 10.1021/j100540a008.

[99] N. T. J. Bailey, *The Elements of Stochastic Processes with Applications to the Natural Sciences* (John Wiley & Sons, 1991), ISBN: 978-0-471-52368-0.

[100] K. A. Gold, J. J. Lee, N. Harun, X. Tang, J. Price, J. D. Kawedia, H. T. Tran, J. J. Erasmus, G. R. Blumenschein, W. N. William, I. I. Wistuba, and F. M. Johnson, "A phase I/II study combining erlotinib and dasatinib for non-small cell lung cancer," Oncologist **19**, 1040 (2014) DOI: 10.1634/theoncologist.2014-0228.

[101] M. F. S. A. Ribeiro, F. H. Knebel, F. Bettoni, R. Saddi, K. P. Sacardo, F. S. N. A. Canedo, J. V. M. Alessi, A. K. Shimada, J. F. G. Marin, A. A. Camargo, and A. Katz, "Impressive response to dabrafenib, trametinib, and osimertinib in a metastatic EGFR-mutant/BRAF V600E lung adenocarcinoma patient," npj Precision Oncology **5**, 5 (2021) DOI: 10.1038/s41698-021-00149-4.

[102] E. F. Smit, C. Dooms, J. Raskin, E. Nadal, L. M. Tho, X. Le, J. Mazieres, S. Hin, M. Morise, V. W. Zhu, D. Tan, K. H. Holmberg, B. Ellers-Lenz, S. Adrian, S. Brutlach, K. M. Schumacher, N. Karachaliou, and Y. L. Wu, "INSIGHT 2: a phase II study of tepotinib plus osimertinib in MET-amplified NSCLC and first-line osimertinib resistance," Future Oncology **18**, 1039 (2022) DOI: 10.2217/fon-2021-1406.

[103] N. Elbracht, "Die Dynamik resistenter Tumorzellen und ihr optimaler Therapiezyklus," Unpublished bachelor thesis, 2023.

[104] M. Bazaraa, J. Jarvis, and H. Sherali, *Linear Programming and Network Flows* (Wiley-Interscience, 2004).

[105] D. Bertsekas, *Dynamic Programming and Optimal Control: Volume I*, Athena Scientific optimization and computation series (Athena Scientific, 2012), ISBN: 9781886529434.

[106] D. Bertsekas, *Dynamic Programming and Optimal Control*, Athena Scientific optimization and computation series v. 2 (Athena Scientific, 2007), ISBN: 9781886529083.

[107] E. Calvo, C. Walko, E. C. Dees, and B. Valenzuela, "Pharmacogenomics, Pharmacokinetics, and Pharmacodynamics in the Era of Targeted Therapies," American Society of Clinical Oncology Educational Book, PMID: 27249721, e175 (2016) DOI: 10.1200/EDBK_159061.

[108] Michel, Ulrich and Kliesch, Martin and Kueng, Richard and Gross, David, "Comments on "improving compressed sensing with the diamond norm"–saturation of the norm inequalities between diamond and nuclear norm," IEEE Transactions on Information Theory **64**, 7443 (2018) DOI: 10.1109/TIT.2018.2861887.